Technische Universität Wien

Martina Marchetti-Deschmann

DIPLOMARBEIT

HYPHENATION OF nES GEMMA WITH OFFLINE MALDI MS ANALYSIS

Ausgeführt am

Institute für Chemische Technologien und Analytik

der Technische Universität Wien

unter der Anleitung von

Assistant Prof. Mag.rer.nat. Dr.rer.nat. Victor U. Weiss

Univ.Prof. Mag.pharm. Dr.rer.nat. Günter Allmaier

with the support of

Associate Prof. Mag.rer.nat. Dr.rer.nat. Martina Marchetti-Deschmann

durch

Katja Balantič, BSc.

Seilerstätte 2, 1010 Wien

Katja Balantič

Wien, Mai 2019

Acknowledgment

I would like to thank assist.prof.dr. Victor U. Weiss and uni.prof.dr. Günter Allmaier for giving me the opportunity to work on my master's thesis under their supervision and guidance. I would also like to thank ao.prof. dr. Martina Marchetti-Deschmann for all of her help and support.

Special thanks to dr. Ernst Pittenauer for teaching me how to operate and acquire data on MALDI MS and for his help and time during my research work.

Furthermore, I would like to thank ao.prof.dr. Gernot Friedbacher for his work on AFM measurements.

A big thank you also goes to all of my colleagues at the working group for their help and insight.

Finally yet importantly, I would like to thank my family and friends for their support.

My studies at TU Wien were funded by the Ad-Futura scholarship and Lukas Knaffel´sche Privatstiftung scholarship

for my mom Irena and dad Andrej

with love

I. ABSTRACT

Liposomes are spherical vesicles consisting of at least one lipid bilayer with the unique ability to encapsulate various cargo materials. Consequently, liposomes can be used as nano-carriers in pharmaceutical or medical applications and must be characterized in order to understand their drug delivery properties. On the other hand, very low-density lipoprotein (VLDL) particles are nanoparticles formed by lipids and proteins. They play an important role in the transport of fats and cholesterol through the human body. Size based characterization and separation of liposomes and VLDLs can be achieved using gas-phase electrophoretic mobility molecular analysis (GEMMA) with the help of a nano-electrospray (nES) charge-reduction source. Separation is based on high-laminar sheath flow and orthogonal, tunable electric field which enables the size separation of single-charged analytes based on their electrophoretic mobility diameter (EMD) corresponding to the diameter of the spherical particles. What is more, if the voltage is kept at a constant value, only particles of a pre-selected EMD pass through the instrument and can be collected for subsequent particle analysis employing orthogonal methods such as mass spectrometric characterization using Matrix Assisted Laser Desorption/Ionization (MALDI) mass spectrometry. Via this novel offline hyphenation liposomes as well as VLDLs will be targeted via MS after size-selection. Separation of lipid compounds out of complex mixtures will be demonstrated.

II. ZUSAMMENFASSUNG

Liposomen sind kugelförmige Vesikel, die aus mindestens einer Lipiddoppelschicht bestehen und die einzigartige Fähigkeit besitzen, verschiedene Ladungen zu verkapseln und zu transportieren. Folglich können Liposomen als Trägermaterialien im Nanometerbereich für pharmazeutische oder medizinische Anwendungen verwendet werden. Um ihre Arzneimittelabgabeeigenschaften zu verstehen, hat jedoch in weiterer Folge ihre Charakterisierung zu erfolgen. Auch VLDL-Partikel (Very Low Density Lipoprotein) sind aus Lipiden und Proteinen gebildete Nanopartikel. Sie spielen eine wichtige Rolle beim Transport von Fetten und Cholesterin durch den menschlichen Körper. Die größenbasierte Charakterisierung und Trennung von Liposomen und VLDL kann mithilfe von Elektrophorese in der Gasphase (GEMMA Instrument) basierend auf einer Nano-Elektrospray (nES) Quelle mit nachfolgender Ladungsreduktion erfolgen. Die Trennung basiert auf einem hochlaminaren Luftstrom und einem orthogonalen, variablen elektrischen Feld, das die Größentrennung von einfach geladenen Analyten basierend auf deren Electrophoretic Mobility Diameter (EMD), der dem Durchmesser der kugelförmigen Teilchen entspricht, ermöglicht. Wenn die Spannung zudem auf einem konstanten Wert gehalten wird, können nur Partikel mit einem bestimmten EMD das Instrument passieren und können für die nachfolgende Partikelanalyse mit orthogonalen Methoden, wie z. B. die massenspektrometrische Charakterisierung, mit Hilfe von Matrix Assisted Laser Desorption / Ionization (MALDI), gesammelt werden. Anhand von Liposomen und VLDL wird diese neuartige Offline-Kopplung mit massenspektrometrischer Charakterisierung gezeigt werden.

III. CONTENTS

1. INTRODUCTION

Hyphenation of analytical techniques has enabled improved separation and detection of various compounds, consequently resulting in better quantification and qualification of unknown substances from very complex mixtures. Hyphenation is usually carried out between a separation method, for example a chromatographic or electrophoretic separation and another analytical technique, such as mass spectroscopy (1). Electrophoretic instruments separate chemical compounds out of mixtures, while spectrometric instruments identify said compounds and enable their quantification.

Through research and from natural resources more and more complex mixtures are developed and used. Thus, hyphenation of different analytical methods, to analyse these mixtures has received ever-increasing attention. Hyphenation can very well be used in medical research and drug discovery where fast and accurate determination of molecular and pharmacokinetics properties is highly desirable (1).

One of the more popular novel drug delivery systems nowadays are liposomal drug carriers.

Liposomes are very versatile which makes them perfect candidates for many therapeutic applications in gene therapy, cancer therapy and immunology. However, their functions and stability are not yet fully explained. Consequently their use in the field of medicine is still somehow limited (2). What is more, liposomes can also be used in other fields of science, for example in cosmetic and pharmaceutical industry and in food and farming industry, which further increases the need for their detailed characterization.

In order to achieve better understanding of how liposomes work as molecule delivery systems hyphenation of different analytical instruments can be used, to better analyse and explain their structure and pharmacokinetic properties.

Furthermore, also other analytes should be targeted via such an approach. Very complex structures are produced in the human body (e.g. the very-low density lipoproteins, VLDLs), giving us another challenge to use hyphenation of a separation method and a detection method to better understand and analyse compounds produced by human cells.

1.1. Aim of the work

Hyphenation of two different analytical methods, gas-phase electrophoretic mobility analysis and matrix assisted laser desorption/ionization mass spectrometry, brings together the best of both, which means that better and more detailed results can be obtained. In the following work, an electrophoretic separation method was joined offline with a spectrometric detection method, to better characterize liposomes as carriers and analyse VLDLs. The aim was to show how size separation of particles is possible before mass spectrometric analysis. This would enable besides information gained after gas-phase electrophoresis to size separate and thus purify analytes of complex mixtures before detection of the desired compounds with a mass spectrometer.

A gas-phase electrophoretic instrument named nano-electrospray (nES) gas-phase electrophoretic molecular mobility analyser (GEMMA) was used, separating particles based on their size in an applied electric field. Liposomes were analysed to visualize their size distribution and afterwards collected for offline mass spectrometric analysis. The same process was carried out with very low-density lipoproteins. Since mass spectrometric analysis of composite compounds has proved quite challenging, a size selective separation beforehand is a possible solution. With a hyphenation of

two different analytical techniques, we obtain more information about the analyte. In our case, not only information on particle size and size distribution was obtained but also particle characterization with mass spectrometry was possible.

1.2. Liposomes and lipoprotein-particles

1.2.1. Lipid molecules

Lipids are one of the most important molecules found in human bodies. What is more, they are found in all biological organisms and are vital to the life on Earth. Their primary function is to form biological cells and cell compartments, due to their unique chemical properties. Lipids are amphiphilic molecules, which means that they consist of a non-polar or hydrophobic part and a polar or hydrophilic part. The hydrophobic part does not interact well with water and polar solvents. The opposite is true for the hydrophilic part, which is best soluble in polar solvents. These structural phenomena make lipids one of the most useful and abundant molecules in biological tissues. It was also shown that evolutionary advantages exist as to way lipids have such complex structures. One of them is the fundamental biological law stating that "structure is mechanically a cause for function", which means that structural molecules play the key role in the way our body functions (3). Since living organisms are made out of cells it is no wonder that molecules that build cells are complex and possess unique chemical properties.

Lipid is a general term for different molecules such as fatty acids, monoglycerides, diglycerides, triglycerides, waxes, sterols, vitamins and phospholipids (4). They have a lot of varying functions. Besides the already mentioned structural function, they also act as molecules for storage of energy, mainly triglycerides, and as signalling molecules in biological pathways (5). In this work, phospholipids and cholesterol were used, since they are the key structural components of cell membranes.

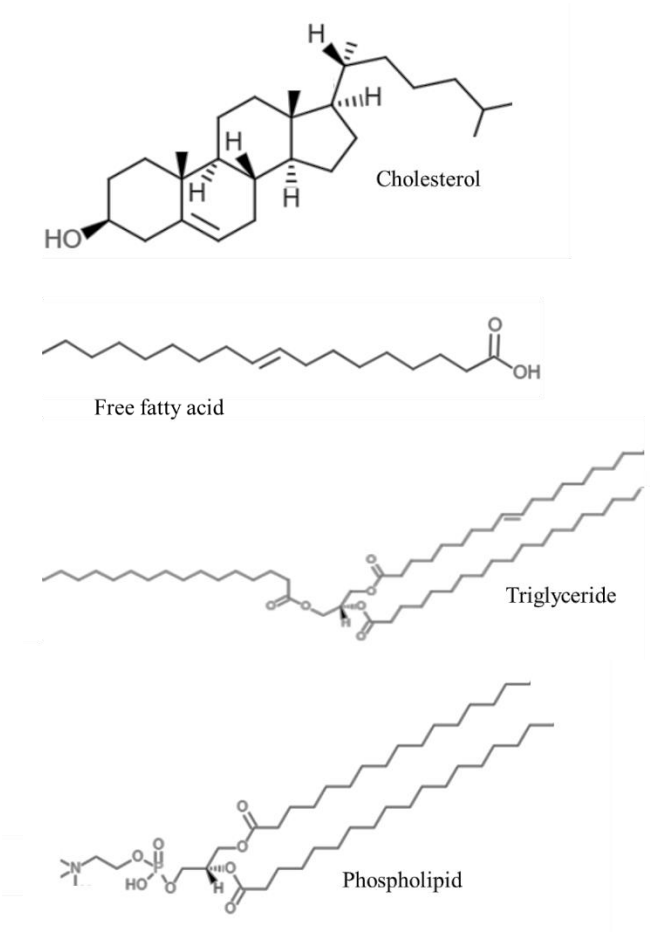

Figure 1: Different types of lipid molecules

Cholesterol is a type of lipid molecule, called sterol. It is an essential structural part of cell membranes. However, its structure is different from the phospholipid one. Cholesterol is made out of four fused hydrocarbon rings with a hydrocarbon tail on one end of the steroid and a hydroxyl group linked to the other end (5). It is synthesized in human body and it plays an important role in membrane fluidity.

1.2.1.1. Phospholipid molecules

As mentioned before, lipids or phospholipids to be more precise have an important structural role since they build biological cell membranes. Phospholipids have a well-known structure. They consist of two fatty acid chains and a phosphate group, joined together by an alcohol called glycerol. There is a large variety of different phospholipids, with different fatty acids, such as saturated or unsaturated fatty acid chains with different numbers of double bonds and with different chain lengths. What is more, different molecules can attach to the phosphate head group which results in an even larger diversity of phospholipid molecules (6). The most common modifications to the phosphate group is an addition of a choline or an ethanolamine molecule. In the following work, phosphocholine lipids as well as phosphoethanolamine lipids were used.

Phospholipids form cell membranes because of their amphiphilic nature. To form such bilayer structures, hydrophilic lipid heads face the external aqueous environment. With this, hydrophobic lipid tails are shielded from the polar environment in the lipid bilayer. Towards the interior of the cell, another layer of lipids is oriented in such a way that hydrophobic tails are joint with the tails of the lipids from the outermost layer and the hydrophilic heads are oriented towards the interior

of the cell. To sum up, due to hydrophobic interactions the hydrophobic tails line up to one another, with the hydrophilic heads on each side facing the aqueous environment. In such a way a structural lipid bilayer is formed which turns out to be a thermodynamically stable state, since hydrophilic lipid parts mix with the aqueous environment while the hydrophobic parts are shielded and protected from the same aqueous environment (6). What is more, lipids are able to form a variety of different structures apart from lipid bilayers. They can form micelles, where there is no interior aqueous space, just the hydrophobic tails lining against one another, lipid bilayers and lipid monolayers. The closest *in vitro* approximation to a biological cell is a structure formed by phospholipids called liposome.

1.2.2. Liposomes

Due to the lipids amphiphilic nature so called liposomes, i.e. vesicles can be formed, which can be large or small, unilamellar or multilamellar. Liposomes are formed by self-organization of lipids which occurs because of their chemical structure, as mentioned above (7). Therefore, liposomes are spherical vesicles in dispersion consisting of phospholipid molecules, with an aqueous core.

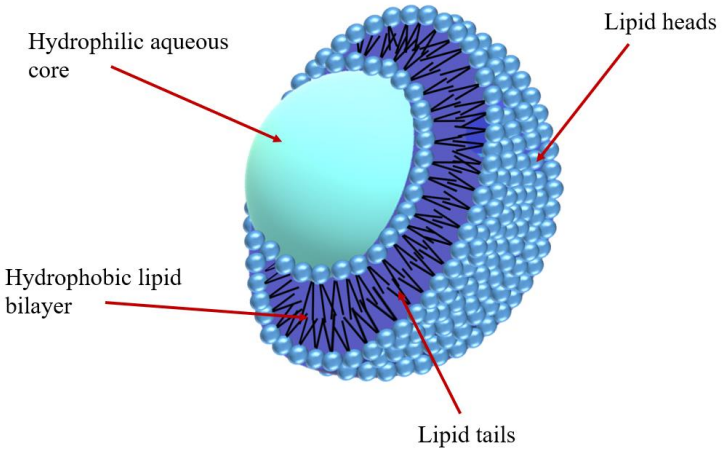

Figure 2: Liposome with a hydrophilic core surrounded by a lipid bilayer membrane

In order for liposomes to form, the lipids need to be dissolved in a polar, aqueous solution. This enables the process of lipid bilayer formation, where some of the aqueous solution is encapsulated in the interior of the liposome. There are many reasons that favour the self-assembly of liposomes. Firstly, the unfavourable interaction between hydrophobic and hydrophilic parts can be minimized with folding into closed vesicles. Consequently, the large difference in free energy is reduced with formation of spherical vesicles. pH also plays an important role in formation and stability of liposomal vesicles. At neutral pH fatty acid carboxyl ions have better electrostatic interactions which makes liposomes more stable, compared to acidic environments. Temperature also plays an important role in liposome formation. All lipids have a specific transition temperature at which they transit from gel phase to liquid crystalline phase. Liposome can be formed spontaneously only when the environment temperature is higher than the transition temperature of the employed lipids (2).

There are several different methods for liposome preparation. All methods have some basic steps in common. First, the lipids are thoroughly mixed in an organic solvent and then dried. After that, the lipids are dispersed in an aqueous solution.

The most common liposome preparation techniques are mechanical dispersion methods, solvent dispersion methods and detergent removal methods. Some of the methods are listed below (8):

→ Hydration method: a mechanical dispersion method - dispersion of dried lipid films with intensive mechanical mixing
→ Sonication method: a mechanical dispersion method - disruption of lipid dispersions with sonic energy
→ Ethanol or ether injection method: a solvent dispersion method - lipids dissolved in an organic solvent are gradually injected to an aqueous solution

With these methods, different liposome structures can be formed.

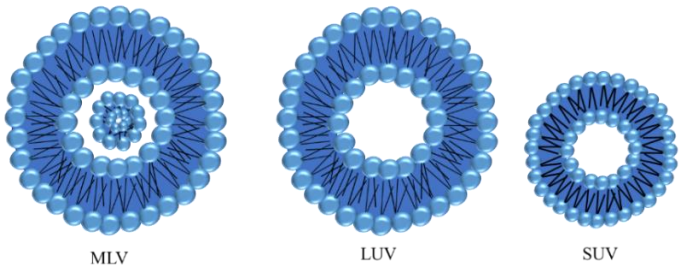

Figure 3: Different forms of liposome structure, multilamellar vesicle (MLV), large unilamellar vesicle (LUV) and small unilamellar vesicle (SUV)

Unilamellar liposomes can be produced, that have a single lipid bilayer which results in a very large core, where polar compounds can be stored. Multilamellar liposomes on the other hand consist of several lipid bilayers and a small core in the middle so they are mostly used to load hydrophobic molecules. Unilamellar liposomes can also be divided into subclasses according to their size into small unilamellar vesicles (SUV, 50 nm – 100 nm) and large unilamellar veiscles (LUV, 100 nm – 150 nm) (9). Following dispersion, the size of prepared liposomes can additionally be reduced either with sonication or mechanical energy (extrusion).

Since liposomes are made out of self-assembled phospholipid bilayers which have a high biocompatibility, they resemble cell membranes in their structure and function. The first spherical, closed lipid bilayer was described in 1965 by Alec Bangham and his colleagues at the Agricultural Research Institute in Babraham, Cambridge, UK. Their work described diffusion of ions across swollen phospholipids. They discovered that such diffusion across phospholipid membranes is very similar to that one across biological cell membranes. It was also written that liposomes can form spontaneously when lipids are mixed in aqueous solutions (10).

Later on, Gregory Gregoriadis from the Centre for Drug Delivery Research, University of London, UK discovered that these spherical vesicles could actually encapsulate different hydrophilic drugs very efficiently. He also stated the importance of drug delivery systems that can deliver the drug selectively and in controlled manner to the site where they are needed. Liposomes fulfil these requirements, since they can encapsulate drug molecules and are biologically inert, which means that there should not be any reaction occurring with the carrier in the human body. Liposomes injected into living animals showed that the release of molecules encapsulated in the liposomes was controlled as well as directed to the specific site in the animal body. In his study there was no loss of structural integrity of the liposomes in the blood (11).

1.2.1.2. Liposomes as drug delivery systems

The first tests using liposomes as drug delivery systems in vivo were done with anti-cancer drug cytosine arabinoside in mice with leukaemia. The study showed that survival of tumour bearing mice treated with liposomal drug carriers was higher. Furthermore, the influence of cholesterol concentration in lipid bilayers was also demonstrated. Liposomes with low cholesterol

concentration released more drugs than those prepared with higher cholesterol concentrations (12). Consequently, high cholesterol levels in liposomal drug carriers are better for prolonged drug encapsulation and more sustained hydrophilic cargo release.

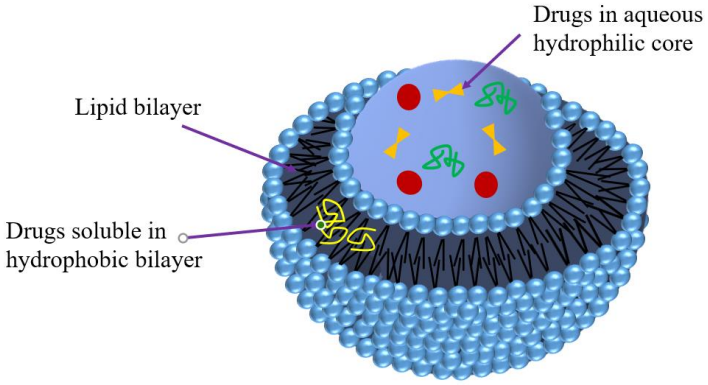

Figure 4: Liposome for drug delivery with hydrophilic molecules loaded into the hydrophilic core and hydrophobic molecules loaded into the hydrophobic membrane

Nowadays, liposomes are made from natural, non-toxic and biodegradable lipid molecules and can very well encapsulate hydrophilic molecules into their lumen or hydrophobic molecules into their membrane (7). All drug delivery systems aim to carry a respective drug to the specific place of action and control the rate of the drug release as needed. Furthermore, with liposomal drug systems intracellular drug delivery can be achieved as well as receptor-mediated endocytosis of liposomes, triggered release and delivery of nucleic acids (13). The focus of the liposomal development is prolonging the stability of the liposomal drug carriers and achieving the maximum drug release at the desired site. If liposomes are aimed to reach a specific tissue then antibody derivatives are inserted into the vesicle bilayer. When they reach the target cell, immunoglobulin molecules destabilize the vesicle and the encapsulated content is released at this site of action (2). There are four main steps of drug delivery when it comes to liposomal carriers. First, the liposomal vesicle with encapsulated drug molecules reaches the target cell and becomes adsorbed to the cell membrane. After that, endocytosis occurs which is the engulfment of the liposomal drug carrier to the interior of the cell. (13).

There are many different methods how to achieve the encapsulation of the drug into the liposome. Passive and active loading techniques are known. Passive loading methods include all techniques where the lipid and drug are mixed in an aqueous buffer, thus achieving encapsulation while the liposomes are being formed. During active encapsulation, drugs are loaded into the liposomes after they are already formed. This can be done with charged drug molecules and a pH gradient between the exterior and interior of the liposome (8).

Liposomal drug carriers have to remain stable throughout manufacturing steps, delivery and storage. When liposomes are formed, they come in different sizes. During storage, they can aggregate in order to form more thermodynamically favourable structures. This can cause leakage of drugs encapsulated in the liposomes. That is why size distribution and morphology are two very important factors when assessing the stability of drug carriers (13).

Cholesterol plays an important role in the stabilization of liposomes, but its concentration cannot exceed 50%, since higher cholesterol concentrations destabilize lipid bilayers and molecules would not be encapsulated efficiently. Furthermore, saturated phospholipids yield more stable vesicles since they are less prone to peroxidation (2).

Liposomes as drug delivery systems are more bio-compatible, less toxic and have an increased permeability across cell membranes when compared to existing therapeutic formulations. The release of the drugs can be triggered either externally, with the use of an ultrasound and heating of

the body part for example, or internally through specific properties found at the disease site such as a difference in pH value (13). With this, liposomes are able to release the encapsulated drugs through time, when prolonged drug concentration is needed in the blood. Usually drugs need to be taken regularly to maintain a sufficient concentration in the blood, with liposomal drug carriers this is no longer needed, since they can be formulated in such a way that drug concentration keeps constant over a longer period of time. Liposomes also protect drugs from chemical and immunological breakdown, since drugs are shielded in the liposomal core (14).

Nowadays, an improved liposome preparation called PEGylation, has been introduced which increases the pharmacokinetic and pharmacodynamic properties of therapeutic delivery molecules such as liposomes. PEGylation is an attachment of a polymer polyethylene glycol to the lipid molecules of the liposome. With this, chemical and structural properties of the liposome are changed to increase the encapsulation of the therapeutic drug inside the liposome and the stability of the vesicles.

55 years have passed from the first idea of a liposome used as a drug delivery system and finally liposomes have a more approved and recognized position in the clinical use. However, further classification and understanding of the lipid and liposomal functions is of great importance to develop new applications and approaches to prevent, diagnose and cure different diseases (6). Selected approved liposomal drug delivery systems are listed below (9):

Lipid composition	Drug	Product name	Production company	Treatment
HSPC, PEG 2000 –DPSE cholesterol	Doxorubicin	Doxil	Sequus Pharmaceuticals	Metastatic breast cancer
DSPC, cholesterol	Daunorubicin	DaunoXome	NeXstar Pharmaceuticals	Blood cancer
DOPC, DPPG, cholesterol	Cytarabine	Depocyt	SkyPharma Inc.	Neoplastic meningitis and lymphomatous meningitis
Egg sphingomyelin and cholesterol	Vincristine sulfate	Marqibo	Talon Therapeutics Inc.	Acute lymphoblastic leukemia

Table 1: Selected treatments with liposomal drug carriers

Of course, there are also disadvantages to the use of liposomes as drug delivery systems. The main disadvantages are very high production costs. Furthermore, the purification and sterilization of liposomes is a complicated process, since they are sensitive to high temperatures. The best sterilization option is filtration. Liposomes also do not have a long shelf life and stability. This can be increased with drying and freezing the liposomes with the encapsulated drugs. To minimize chemical peroxidation, only highest quality solvents can be used in liposome preparation and liposomes are then stored in inert gas, for example nitrogen. Furthermore, all manufacturing processes should be done in a deoxygenated environment (15). Main advantages and disadvantages of liposomes used as drug delivery systems are listed in the table below (8):

Advantages	Disadvantages
Liposomes increase efficiency of drugs as pharmaceutically active compounds are concentrated on their site of action. Hence, lower overall drug concentration needs to be administered	Low concentration of encapsulated drugs (Low encapsulation efficiency)
Liposome increase stability of drugs via encapsulation	Short half-life of liposomes per se
Liposomes are non-toxic, biocompatible and completely biodegradable	Sometimes phospholipids undergo oxidation and hydrolysis-like reactions altering the original lipid material
Liposomes reduce the toxicity of the encapsulated drug as it travels through the circulatory system	Drug leakage during circulation and fusion of encapsulated drug/ molecules as undesired by-products
Liposomes help reduce the exposure of sensitive tissues to toxic drugs	Production cost is high
Flexibility to couple with site-specific ligands to achieve active targeting	

Table 2: Advantages and disadvantages of liposomal drug carriers

In addition to assembling cellular membranes, phospholipids also give structure to lipoproteins. Lipoproteins are spherical vesicles that consist of lipids and proteins, with a main task to transport hydrophobic triglycerides through the hydrophilic blood (16).

1.2.3. Lipoprotein particles

Lipoprotein particles are vesicles consisting of lipids and proteins. The structural aspect of such a vesicle is based on phospholipids, which form an enclosed lipid monolayer in such a way that hydrophilic head groups of the phospholipids are facing the external aqueous environment while the hydrophobic fatty acid tails are centred in the middle of the vesicle (16). In such a way, hydrophobic fats, such as triacylglycerol can be transported through the hydrophilic blood. The protein part consists of apolipoproteins, which are embedded in the lipid monolayer. Proteins stabilize the whole vesicle and determine its function in the body (17). To sum up, lipoprotein particles play an important role in our body as they emulsify hydrophobic lipid molecules and thus enabled them to be transported through the hydrophilic fluids such as blood, cerebrospinal fluid and lymph.

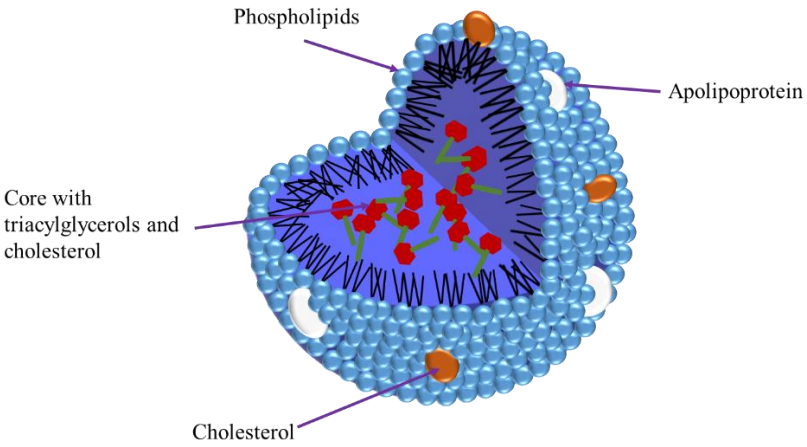

Figure 5: Schematic structure of lipoprotein particles

Different apolipoproteins attached to the phospholipid vesicles give different functions to lipoprotein particles. Apolipoproteins have four major roles. Firstly, they aid in structural arrangement of the phospholipid vesicle. They can act as ligands for different lipoprotein receptors, help in the formation of the whole lipoprotein particles and act as enzyme cofactors activating or inhibiting enzyme reactions. There are seven classes of apolipoproteins which differ in structure based on the amino acids present and size which corresponds to the number of amino acids that form the α-helix or β-sheet (16):

→ Apolipoprotein A
→ Apolipoprotein B
→ Apolipoprotein C
→ Apolipoprotein D
→ Apolipoprotein E
→ Apolipoprotein H
→ Apolipoprotein L

The variety of different apolipoproteins gives rise to different lipoprotein particles. They all generally consist of phospholipids forming the vesicles, apolipoproteins attached to the vesicle membrane and fats, such as triglycerides and sterols packed in the hydrophobic core of the vesicles. Lipoprotein particles differ based on size, lipid content and apolipoprotein class and are listed below (16):

→ Chylomicrons: the largest and most tightly packed lipoprotein particles. Their main function is to transport the fat and cholesterol that we ingest in a phospholipid-protein vesicle. This vesicle then diffuses from the small intestine to the circulatory system. There they flow to the capillaries inside the muscles and other body parts where energy is needed. At these sites, fats are digested, and then cholesterol travels further to the liver where it is metabolized.
→ Very low-density lipoproteins (VLDL): Vesicles with low density and a high content of triglycerides. They consist of proteins, fats and cholesterol and are synthesized in the liver. These vesicles carry fats and cholesterols produced by the liver to other body tissues via a metabolic pathway with many intermediate products.
→ Intermediate density lipoprotein (IDL): it is an intermediate product of VLDL metabolism.
→ Low-density lipoprotein (LDL): the last product of VLDL metabolism, which consists mainly of cholesterols after fat digestion.

→ High-density lipoprotein (HDL): theses vesicles have the highest density due to their high protein to lipid ratio. HDL carries the cholesterol away from the tissue to the liver, so it is often referred to as 'good cholesterol', since it lowers the concentration of cholesterol in the blood.

The main difference of the above-mentioned lipoprotein particles is their density, which changes due to the varying fat content of the vesicles and consequently their size. The following table presents lipoprotein particles based on their size. The data is applicable for young, healthy subjects and it is an average across individuals studied (16):

Lipoprotein particle	Particle diameter	Particle density
Chylomicron	75 – 1200 nm	<0.93 g/ml
VLDL	30 – 80 nm	0.93 – 1.006 g/ml
IDL	25 – 35 nm	1.006 – 1.019 g/ml
LDL	18 – 25 nm	1.019 – 1.063 g/ml
HDL	5 – 12 nm	>1.063 g/ml

Table 3: Lipoprotein particle properties

All lipoproteins have a low density compared to extracellular water. The higher the fat content in the vesicle the lower is the density of the lipoprotein particle. Lipoprotein particles play an important role in our health. A high content of VLDLs, LDLs and triglycerides in our body leads to increased risk of heart diseases and arteriosclerosis. On the other hand, HDLs remove the cholesterol from the blood circulation. So they reduce cholesterol levels and consequently lower the risk of cardiovascular diseases (18).

The lipoprotein particle pathway starts in the intestine where lipids, such as fats and cholesterol we ingest are encapsulated into chylomicrons. After that, particles are carried through the circulation system to the muscles and fat tissue where there are metabolized and free fatty acids are released. Based on these compounds chylomicron remnants are formed, which travel to the liver and are digested here. The second possible pathway of lipoprotein particles starts inside our body, more specifically in the liver. Here very low-density lipoproteins particles are formed which encapsulate and carry triglycerides synthesized by our body to muscles and fat tissue. Here, free fatty acids are released and an intermediate-density lipoprotein particle is formed that now encapsulates cholesterol only. IDL is further metabolized to form low-density lipoprotein particles, which are again taken up by the liver, where cholesterol can be digested. To sum up, lipoprotein particles play a very important role in the transport of lipids we ingest from the small intestine to the liver and in the transport of the lipids synthesized in the liver to peripheral tissue (16).

1.2.1.3. Very low-density lipoprotein (VLDL) particles

In the following work, very low-density lipoprotein (VLDL) particles were used. VLDLs are secreted by the hepatocytes of the liver, and as mentioned before they carry triglycerides synthesized in our body, to the peripheral tissue where energy is needed. Triglycerides are very energy-rich molecules and are indispensable for the normal function of our body. However they

are hydrophobic, which hinders their movement through the aqueous body fluids like blood (19). To overcome this problem, lipoprotein particles are used since they are able to shield the hydrophobic energy molecules in their core.

Concentration of lipoprotein particles in plasma is strongly related to an increased risk of cardiovascular diseases. However, a method to measure the concentration of different lipoprotein particles is not yet standardized. Consequently, a gas-phase electrophoretic mobility analysis was applied (see below) to analyse distribution and concentration of lipoprotein particles (20). Gas-electrophoretic mobility analysis proves quite beneficial for lipoprotein particle classification since it measures its size. Consequently, a specific lipoprotein particle can be determined and the number of particles present at each specific size, which gives us particle concentration values.

1.3. Electrophoresis as a separation method

Electrophoresis is a separation method, where charged particles are separated under the influence of a uniform electric field, based on the differences of particles' migration speeds. Most common is the movement of particles through a fluid or gel, with the electric field applied by two electrodes on each end of the fluid filled space. Charged particles are thus driven by the applied electric potential between the two electrodes. With this separation technique, molecules can be separated base on their size, shape and number of charges. In the simplest case, negatively charged ions or particles, move towards the positively charged anode, while positively charged ions or particles, move towards the negatively charged cathode (21).

The fundamental principle of electrophoresis can be described using physics. The migration speed of the charged particles depends on the size of the particle, number of charges it carries, the value of applied voltage and the medium used to facilitate the movement of particles. Basically, the speed difference of particles is a function of many variables. During electrophoresis, an electric force is exerted on a particle. This force is equal to the charge of the particle q and the electric field E (21):

$$F_e = q \times E \tag{1}$$

When the charged particles start to move in the applied electric field, an opposite drag or friction force becomes exerted on the particles as well. The friction force can be written as:

$$F_d = f \times v \tag{2}$$

Where f is the friction coefficient and v is the velocity of the particle.

The electrophoretic mobility of the particle is then defined as:

$$\mu = \frac{v}{E} \tag{3}$$

After a short time period, the electric force equals to the friction force as particles are instantaneously accelerated to velocity v. Therefore, the resultant force is zero and each particle moves based on their size, charge and the separation medium (21).

1.3.1. Gas-phase electrophoresis

In gas-phase electrophoresis the employed separation medium is a gas or gas mixture. As mentioned before, electrophoresis is an analytical separation method, where particles are separated based on their size and charge in the applied electric field. In gas-phase electrophoresis, the particles are single-charged and they move at varying speeds in air, due to their different electrophoretic mobilities. Single-charged particles are let into the tube under the flow of gas. The applied electric field, induced by electrodes, drives the particles through the tube at different speeds to the detector. This method thus enables the separation of the analyte as well as their detection based on the time it takes them to reach the detector. Gas electrophoretic separation can be done in a drift tube or in a differential mobility analyser (21).

In order to separate particles only based on their size, single-charged particles need to be obtained from the sample solution. At first, radioactive nickel-63 was used to ionize the sample. This means that only gas-phase samples could be applied to the gas-phase electrophoresis. Later, electrospray ionization was adapted to gas-phase electrophoresis which means that today liquid samples can be analysed as well, with the predisposition that volatile solvents are used to dissolve analytes. The

carrier liquid evaporates fast and does not reach the analyser (22). The electrospray generator is an instrument that disperses the liquid to aerosol with the use of an electric field. It is similar to electrospray ionization, since it produces charged particles, however finally there is a difference in the charge of the particles. Electrospray ionization produces multiple-charged ions, while the electrospray aerosol generator produces single-charged particles. For the electrospray aerosol generator, the liquid sample is usually fed to the electrospray with the use of a capillary. At the end tip of the capillary, the liquid forms a so-called Taylor cone, which emits the liquid just through its tip. The application of high voltage to the capillary tip leads to the formation of small, charged liquid droplets. In contrast to electrospray ionization, where the repulsion of the electrostatic forces in the droplet becomes stronger than the surface tension holding it together, since the droplet is becoming smaller and electrostatic repulsions increase to the point of droplet explosion and formation of many smaller droplets, which are much more stable (23), the electrospray aerosol generator produces single-charged particles (see below). In the end, we wish to obtain ions or dried single-charged particles. Apart from the fact that the sample buffer has to be volatile thus prepared e.g. from an organic solvent, compounds that increase the electric conductivity of water can also be added to the fluid sample, for example acetic acid or ammonium acetate. Ideally, the applied electrolyte exhibits also slight buffering capacities. To sum up, electrospray creates small highly charged droplets by feeding the sample solution through the capillary in an electric field. In comparison, an electrospray aerosol generator leads to single-charged particles. After the electrospray process, dried charged particles flow to the separation tube where an applied electric field separates charged particles based on either their size and charge or their size alone.

1.3.2. Gas-phase electrophoretic mobility molecular analysis

In the following work a nano-electrospray (nES) gas-phase electrophoretic mobility molecular analyser (GEMMA) was used. It is similar to the gas electrophoresis principles described above with slight alterations. The nES GEMMA instrument consists of an electrospray aerosol generator, a differential mobility analyser and a condensation particle counter.

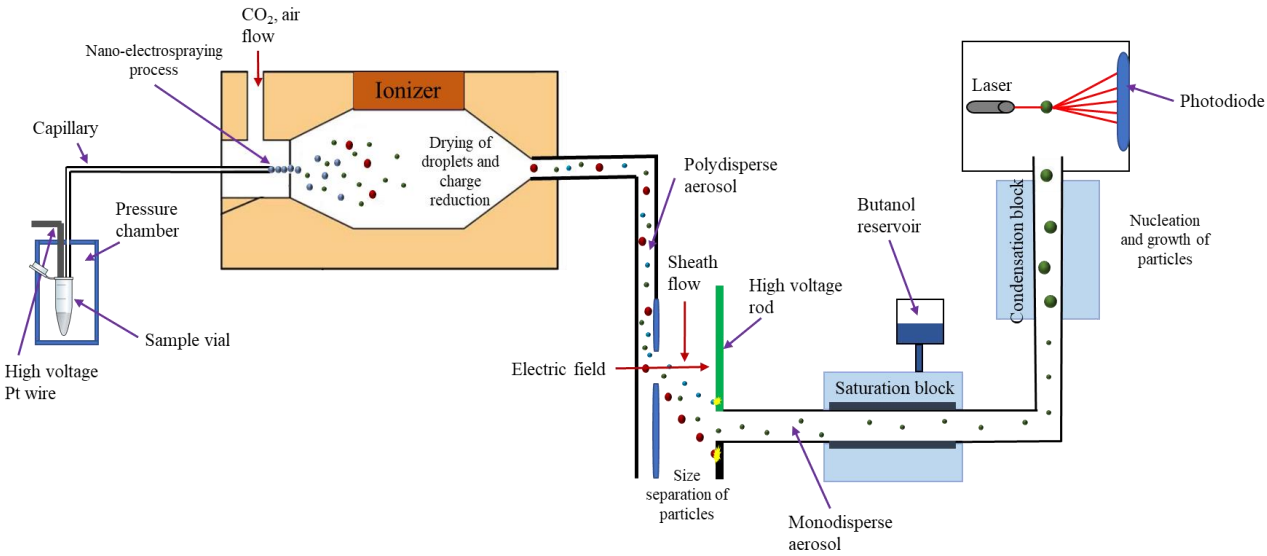

Figure 6: Schematic diagram of nES GEMMA

Therefore, a nES GEMMA is a set of different instruments used to separate molecules and particles based on their electrophoretic mobility in the gas-phase. The principle of how instruments joined together work is that particles of known size and charge behave in a very predictable manner when

flowing in a gas flow and being subjected to an electric field. As a separation method it was first described in 1996 by Stanley Kaufman and his collages at University of North Carolina, Chapel Hill, NC, USA. They studied the electrophoretic mobility of globular proteins (24).

1.3.2.1. Nano-electrospray aerosol generator

The nES aerosol generator generates primary droplets of around 150 µm in size. The liquid sample is fed to the electrospray generator through a capillary. The sample solution moves through the capillary due to an applied pressure difference, an electric field and a sheath flow at the capillary tip. Hence, a Taylor cone at the tip of the capillary is formed. Charged droplets containing both the solutes and solvent break off from the Taylor cone and travel toward the nearest grounded surface which results in a formation of several smaller droplets as drying of droplets occurs in the gas-phase (25). Filtered air and carbon dioxide aid in the evaporation of the remaining liquid. Subsequently, dried particles pass through an ionizer and are neutralized. Neutralization occurs in the ionization chamber either by a radioactive source (e.g. Polonium, 210), a soft X-Ray charger or a corona discharge device.

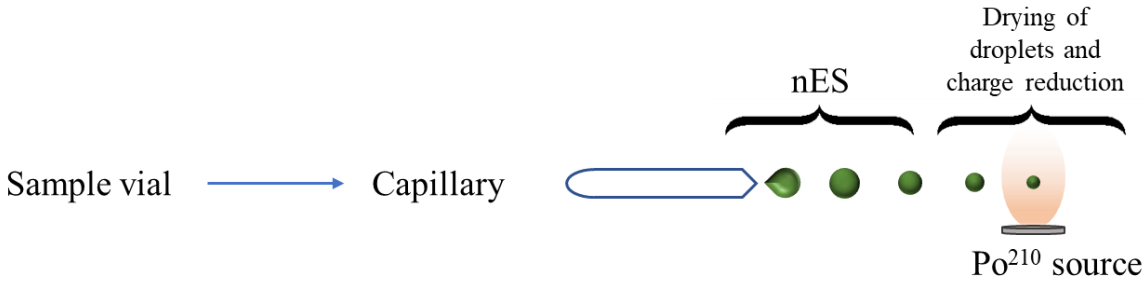

Figure 7: Schematic principle of work for nES aerosol generator

Most of the generated aerosol particles become neutral, and only a small fraction of particles become single-charged and can continue to the particle analyser (26). Particles then flow to the particle classifier; a nano differential mobility analyser was used in the following work.

1.3.2.2. Electrostatic classifier

The nano differential mobility analyser (nDMA) separates the polydisperse aerosol introduced at its inlet. Finally, a monodisperse aerosol is obtained at the outlet. Particles entering the differential mobility analyser are separated based on their electrophoretic molecular mobility, by application of a laminar gas flow and an orthogonal electric field in a cylindrical shaped tube (26). As mentioned before, particles electrophoretic mobility is proportional to the number of charges on the particle and inversely proportional to particle size. As the particle charge equals one after charge equilibration, in the case of spherical particles, the electrophoretic mobility (EM) diameter corresponds to the analyte size. The nDMA consists of two cylindrical electrodes. When an electric voltage is applied, charged particles are deviated from their flow path imposed by a high laminar sheath flow. This deviation is based on their size or EM diameter. This enables the separation of particles, since due to different electrical mobilities of the particles only certain charged molecules will be able to reach the outlet slit of the nDMA to be counted or detected.

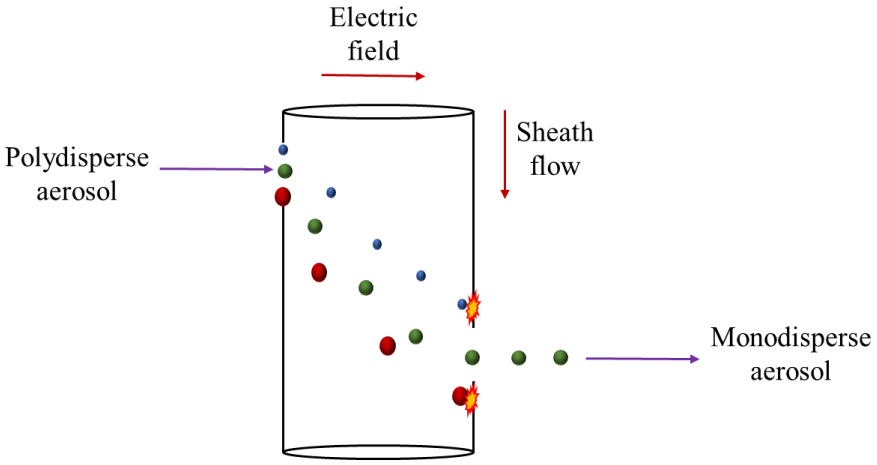

Figure 8: Schematic principle of work for nDMA

The nES GEMMA instrument can work in two different modes. It can either have a constant voltage and consequently only monodisperse particles will exit the nDMA. On the other hand, the voltage can be varied and the size distribution of the polydisperse particles will be obtained with the use of the correct particle detector, for example a condensation particle counter (27). At the outlet of the nDMA particles are still suspended in air, so apart from detecting them with a use of a particle counter, we can also collect the particles and analyse them separately with orthogonal methods.

1.3.2.3. Ultrafine condensation particle counter

The condensation particle counter (CPC) is a device that detects and counts particles in air by enlarging them in a supersaturated environment of n-butanol or water. Particles as small as three nm in diameter can be detected. As particles flow to the CPC, the liquid in the instrument, for example n-butanol condenses on the particles, thus using them as nucleation centres, which enables them to grow in size to about one micrometre. They are then large enough to be detected by a beam of focussed laser light, based on scattering.

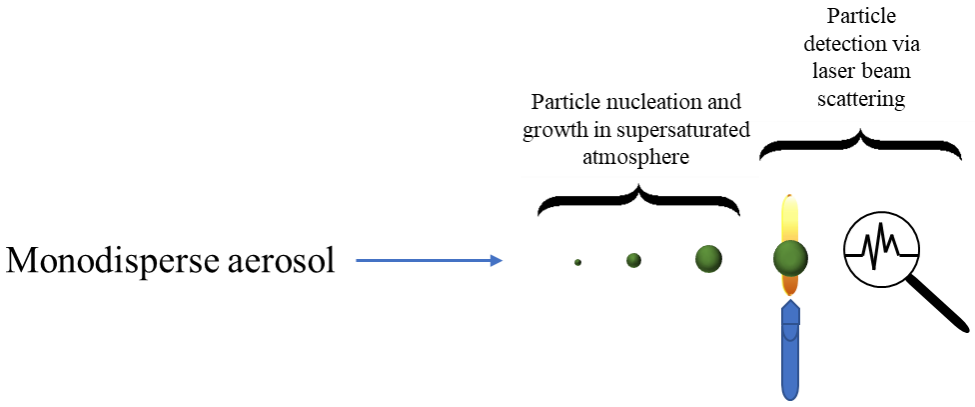

Figure 9: Schematic principle of work for CPC

The flashes of particles passing through a beam of light can be detected, counted and as result particle size or size distributions are obtained (28). Three principles are used to enlarge aerosol particles (29):

→ Adiabatic process

→ Mixing of hot and cold gases
→ Thermophoresis

The most often used technique is thermophoresis. Supersaturation in the CPC is usually around 100% to 200%, due to the fact, that greater vapour concentration is needed for spherical surfaces. However, the supersaturation level must be low enough to prevent spontaneous formation of clusters, which would give false particle counts. Monodisperse particles flow through a porous material, which is usually heated to create enough vapour. After that humified particles reach an area with cooler air where condensation and consequently growth of droplets occurs (29).

To sum up, nES GEMMA is a series of instruments which enable the separation of particles in the gas-phase that carry a single charge based on their electrophoretic mobility diameter. The nES source creates an aerosol out of the sample solution. After drying, the particles undergo charge reduction in a bipolar atmosphere induced e.g. by a radioactive source. Mainly neutral and singly-charged particles are formed which then flow to the differential mobility analyser where they are separated with the use of a laminar sheath flow and an orthogonal applied electric field. Finally, particles are detected and counted using a condensation particle counter. This technique has been used for characterization of liposomes in the past, as both vesicle size and size distribution can be obtained with the measurements. This proves very useful as liposomes are more and more often used as drug carriers. Consequently, their pharmacodynamic properties must be very well known and defined (26).

1.3. Atomic Force Microscopy

Atomic force microscopy (AFM) is a very high-resolution microscopy technique that enables the visualization of objects in the nanometre scale. It is a type of scanning probe microscopy commonly used in biology, since biological structures can be observed in their native state under ambient conditions. What is more, biological samples are not damaged during the process and can be visualized in buffer solutions (30). With AFM, whole cells can be imaged, as well as their components and smaller molecules such as liposomes. Hence, a better understanding of nanometre scale biological systems was obtained with the development of AFM. What is more, interaction between biological molecules can be visualized as well (31).

The resolution of the AFM is more than 100 times better than the optical diffraction limit. AFM uses a mechanical probe to touch and scan the surface of the sample in order to gather information. Scanning of the sample is very precise due to the use of piezoelectric elements, which bring the tip in contact with the sample and moves it in three dimensions, x, y and z. In order to keep the sample undamaged and unchanged, a feedback loop is used to control the force between the probe tip and the sample with a voltage applied to the z piezo element. The input parameter of this feedback loop that adjusts the voltage is the movement of a cantilever, which is constantly changed as the tip scans the sample, thus generating an electrical current caused by tunnelling electrons across the gap between the sample and the tip. The output signal is the distance in the z direction between the tip and the sample. The feedback thus adjusts the height of the tip so that the deflection of the cantilever remains approximately constant as the x and y piezo elements scan the sample in lateral direction (32).

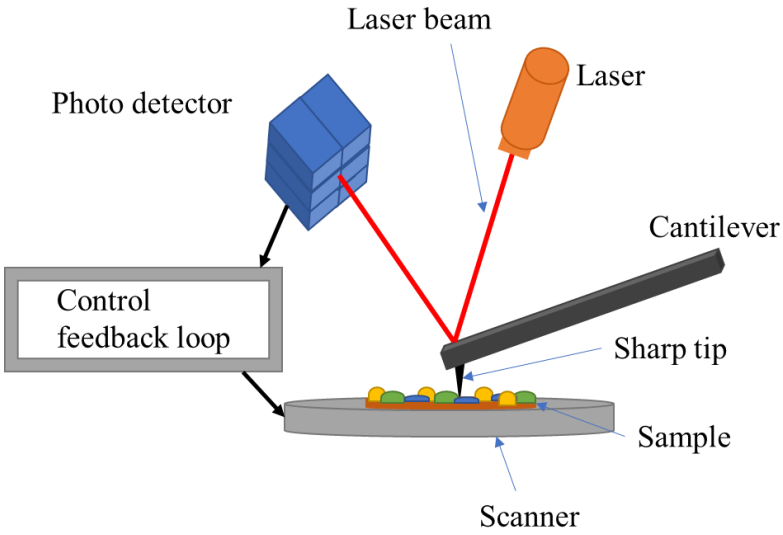

Figure 10: Schematic presentation of AFM working principle

While the sample surface is being scanned, the difference in the height of the tip or the deflection of the cantilever is recorder and stored. This data can then be plotted to form an image of the sample surface. Each position on the image represents an x-y position of the sample, while the obtained signal gives the image its colour (33). AFM is an extraordinary method since it enables visualization of non-conductive samples; consequently, it is used for imaging of biological samples, which are usually not conducting electrons.

AFM can run measurements in three different modes, which differ in the interaction of the tip with the sample (30):

→ Contact mode
→ Tapping mode
→ Non-contact mode

In contact mode, the tip of the mechanical probe touches the sample as the scan is in process. Tapping mode is an intermediate option, where tip is in direct contact to the sample only at discrete times. In the non-contact mode, the tip is brought close to the sample and the force interactions are studied during the scan, but the tip never really touches the sample (30).

Nowadays, tapping mode is the most commonly used AFM technique. The main problem with AFM is trying to get the tip close enough to the sample to detect short-range forces, while preventing the tip to damage the surface. That is why tapping mode is extremely useful, since the tip oscillates up and down, meaning it cannot stick to the sample surface. A small piezo element enables the oscillation of the probe tip and the oscillation amplitude is constant if there is no interaction between the tip and the sample. When the tip comes close to the sample surface, different interactions occur. Consequently, the amplitude of the oscillation changes and this can be interpreted and presented as an image. An image is therefore produced by tracking the force arising from the contact between the probe tip and the sample surface. What is more, due to the mechanism of work in tapping mode, the sample is less damaged compared to contact mode measurements. In tapping mode, the probe tip touches the sample only in downward movement, thus decreasing the friction forces and contact time (34).

For this work, a Nano Scope 8 scanning probe microscope was used. The microscope was operated in tapping mode, since it is gentle enough for visualization of the liposomes. What is more, after the visualization of the samples, liposomes were intact and could be further analysed.

1.4. Mass Spectrometry

Mass spectrometry (MS) is an analytical technique measuring the mass to charge (m/z) ratio of charged particles, either ions or molecules. The first MS instrument was described in the 1900s, but it had very limited use. After that, different ionization techniques were developed, such as electrospray ionization, which greatly improved and increased the function of MS. Furthermore, in 1980 a new ionization technique was developed, named matrix assisted laser desorption/ionization (MALDI), which even further increased the use of MS in biological sciences (35). Every mass spectrometer roughly consists of three main parts; the ion source, a mass analyser and a detector. In the first part, gas-phase charged particles are created, that continue their flow to the mass analyser, where they are separated based on their mass to charge ratio. In the end, particles are detected usually by an electrical change occurring on the detector device.

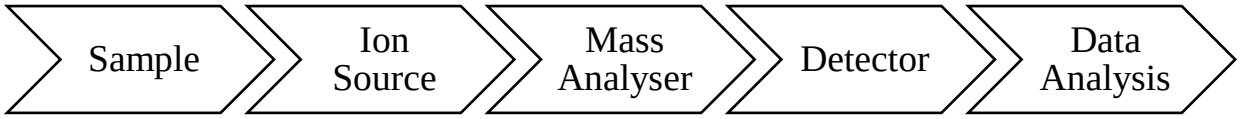

In order to separate and analyse samples with mass spectrometry the sample needs to be ionized to produce gas-phase charged particles or ions (36). This means that a force needs to be exerted on the sample which would cause it to lose an electron, lose a proton, gain a proton or similar species such as a sodium ion, etc. The protonation of a molecule to obtain a charged particle would have the following mechanism:

$$M + H^+ \rightarrow [M + H]^+ \quad (4)$$

If electrons are used for the ionization the mechanism of obtaining charged molecules would be the following (36):

$$M + e^- \rightarrow M^{\cdot +} + 2e^- \quad (5)$$

Mass spectrometric measurements are usually carried out in high vacuum so that generated ions do not collide with other gaseous molecules. Collisions would change the path of the ions which would in turn fail to reach the detector. Furthermore, collisions can also produce unwanted reactions which can result in a more complex spectrum (36).

1.4.2. Ion Source

In order for mass spectrometry instruments to work, the sample has to enter the ion source first, where ions are generated. Different ionization techniques exist and each one of them has its own advantages and disadvantages. When choosing the right ion source for a respective analyte, special considerations must be put to the chemical properties of the sample and the energy transfer during the ionization process, since some ionization techniques produce large amounts of energy, which can cause analyte fragmentation. There is a number of soft ionization techniques, which generate only ions of the molecular species (36). What is more, some ionization techniques are only applicable for gas-phase ionization, which means that the sample itself must be volatile. Main ionization methods are electron capture, electron ejection, protonation, deprotonation, ionization of a neutral molecule or transfer of charged species (33).

The most common ionization techniques are (36):

- → Electron ionization
- → Chemical ionization
- → Thermospray ionization
- → Field ionization
- → Electrospray ionization
- → Plasma desorption ionization
- → Matrix assisted laser desorption/ionization
- → Laser desorption ionization
- → Atmospheric pressure ionization
- → Secondary ion mass spectrometry

For the following work the matrix assisted laser desorption/ionization (MALDI) ionization technique was used. This method was first introduced in 1988 by Michael Karas and Franz Hillenkamp (37). Although, in 1985 a Japanese engineer Koichi Tanaka, already described soft ionization technique used for ionization of proteins. Since then it has become a very popular method to generate ions from large, non-volatile molecules (36). The most important difference to other techniques is the use of a desorption/ionization matrix leading to a soft molecule ionization.

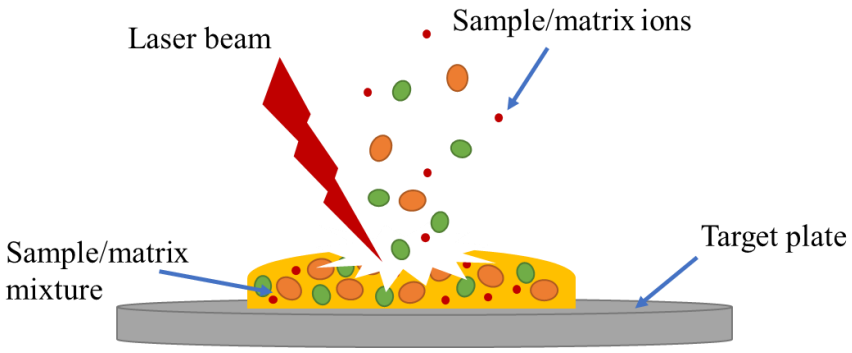

Figure 11: Schematic presentation of the MALDI ionization method

Ionization with the MALDI method is carried out in two steps. First, the compound we wish to analyse is mixed with a solution of organic molecules called the matrix. The ratio between the sample and the matrix can vary and is crucial. Then, the mixture is applied on a target plate and all of the liquid solvents used for the preparation of sample and matrix mixture must evaporated before the target plate is introduced to the ionization chamber of the instrument, leaving only the recrystallized matrix with analyte molecules embedded into it. Thus, the matrix and the analyte are co-crystallized. On the target plate small dots can be seen, and when enlarged under a light microscope, we can see, that tiny crystals are formed and our analyte is embedded in the solid crystals of the matrix. Secondly, the target plate is inserted into the high vacuum ion source of the mass spectrometer. Here big chunks of the solid crystals are ablated by a laser. This heats up the matrix crystals by accumulation of high quantities of energy, which causes sublimation of the matrix crystals. Therefore, the matrix expands into the gas-phase. Consequently, the analyte is transferred to the gas-phase as well. Ion formation then occurs either in the solid phase or gas-phase via a proton transfer (36). Therefore, the ionized matrix induces ionization of the analyte molecules, with minimal fragmentation, by protonation or deprotonation in the hot plume of ablated gases (38). These ions in the gas-phase are then accelerated to the mass analyser. To sum up, the matrix assists in desorption and ionization of the analyte. During the ionization process a neutral molecule M can receive a charge when a proton H^+ is added to form $[M+H]^+$ or removed to form $[M-H]^-$. Also sodium or similar ions can bind to the analyte molecule during the ionization

process to yield a $[M+Na]^+$ type of charged particles. What is more, with MALDI we can create single-charged ions or multiply charged ions ($[M+nH]^{n+}$) depending on the nature of the matrix, the laser intensity and the voltage used (36).

In order to excite the matrix and consequently the analyte, a high-energy laser must be used. Most common are UV lasers even though IR lasers can also be used for MALDI ionization processes. Standardly, N_2 lasers are used, with the wavelength of λ=337 nm, furthermore Nd:YAG lasers can also be used (35).

Due to different chemical properties of the sample, a variety of MALDI matrices exists, which are optimized for the use with a specific analyte. The main chemical property of the matrix has to be its ability to absorb laser energy and to transfer it to the analyte. In the table below, the most common matrices and the type of analytes they are optimal for are presented (36):

Matrix	Abbreviation	Type of analyte
Trihydroxyacetophenone	THAP	Carbohydrates
α-Cyano-4-hydroxycinnamic acid	CHCA	Peptides, proteins
3,5-Dimethoxy-4-hydroxycinnamic acid (sinapic)	SA	Peptides, proteins
2,5-Dihydroxybenzoic acid (gentisic)	DHB	Peptides, proteins, carbohydrates
Dithranol	DIT	Lipids

Table 4: MALDI-MS matrices

A liquid solution of the above listed molecules is made with an organic solvent like methanol, or with a mixture of an organic solvent and highly purified water. Occasionally, trifluoroacetic acid is added to the matrix to adjust the pH of the solution to aid in the protonation process of the ion source to produce $[M+H]^+$ ions. The choice of the right matrix takes into consideration the chemical and molecular structure aspects of the compounds and matrix (38).

MALDI is more sensitive and softer than other laser ionization techniques. The concentration of matrix molecules is usually higher than analyte concentration, which means that analyte molecules are separated from each other in the crystal form which prevents the formation of clusters which would inhibit the generation of molecular ions. The matrix also absorbs the majority of laser energy and thus decreases the damage to the analyte. MALDI is also more universal than the other laser ionization techniques, for example it is not necessary to adjust the wavelength of the laser to match the absorption frequency of each analyte because it is the matrix that initially absorbs the laser pulse. MALDI sources use pulsed lasers to desorb and ionize the analyte, which means that ions are produced in discrete times. Consequently, a mass analyser working in pulsed mode such as a time-of-flight (TOF) mass analyser is perfectly suitable to be used with MALDI (36).

1.4.3. Mass analyser

To start at the beginning, after the ions are formed in the ion source, they are transferred to the mass analyser, where they are separated based on their mass to charge ratio. There are several different principles and techniques for ion separation based on the m/z ratio. However, all mass

analysers have some aspects in common, for example they all use static or dynamic electric and magnetic fields for the separation process. The basic difference is in how the electric and magnetic fields are used to achieve separation. Mass analysers can also be classified based on their properties such as use of continuous or pulsed fields, low or high kinetic energy and ion beam or ion trapping mechanisms (36).

Types of analysers used in mass spectrometry (36):

- → Quadrupole
- → Ion trap
- → Time of flight
- → Electric sector
- → Magnetic sector

The main performance characteristics of a mass analyser are its mass range limit, scan speed, transmission of ions, mass accuracy and resolution. The mass range limit tells us the mass to charge ratio values, which can be measured with the mass analyser. The scan speed tells us how fast an analysis is carried out. The transmission of ions tells us how many of the ions entering the mass analyser actually reach the detector. The mass accuracy tells us how accurate are the m/z ratios produced by the mass analyser. Last but not least, the resolution of the mass analyser is its ability to separate or resolve two ions with a very small m/z ratio difference (36).

A comparison of different types of mass analysers is given in the following table (36):

	Mass limit	Resolution	Accuracy	Ion sampling
Quadrupole	4000	2000	100 ppm	Continuous
Ion trap	6000	4000	100 ppm	Pulsed
TOF	>1 000 000	5000	100 - 200 ppm	Pulsed
TOF - reflectron	10 000	20 000	5-10 ppm	Pulsed
Magnetic	20 000	>=100 000	<10 ppm	Continuous

Table 5: Different types of mass analysers and their performance characteristics

In the following work, a time-of-flight (TOF) mass analyser was used. As mentioned above, a TOF mass analyser is very compatible with the pulsed ionization of the MALDI ion source. In the mass analyser, the ions are first accelerated by an electric field between electrodes where they gain a specific velocity. The TOF mass analyser then separates these ions based on their velocity as they drift through a flight tube, which is a part of the instrument under high vacuum, where no electric or magnetic field is present.

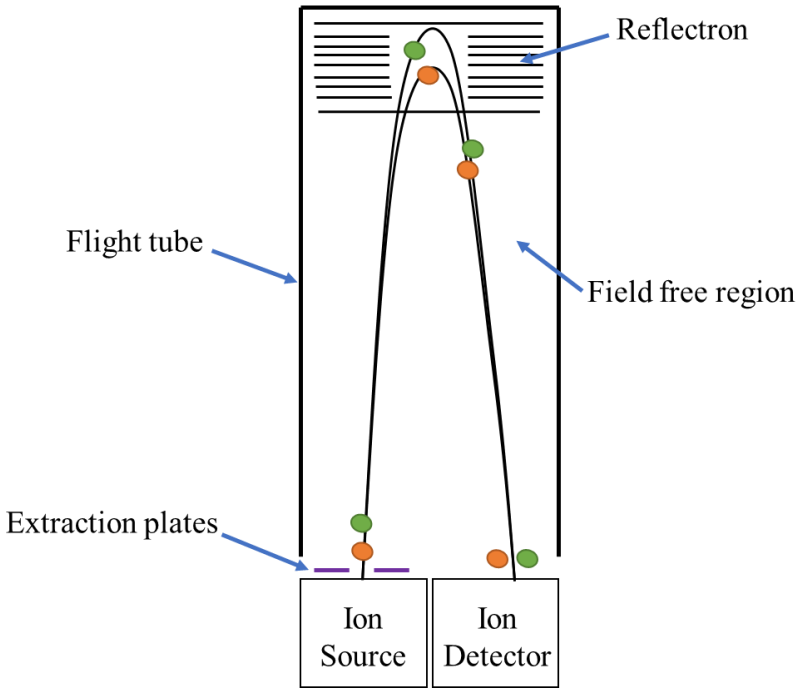

Figure 12: Schematic presentation of reflectron TOF mass analyser

All ions acquire the same amount of kinetic energy, so their velocity depends only on the value of their mass. The kinetic energy can be written as (36):

$$E_k = {}^1/_2\, mv^2 \tag{6}$$

Therefore, the ion velocity can be obtained from rearranging the previous equation:

$$v = \sqrt{2\, E_k/m} \tag{7}$$

This means that the velocity of the ion in the electric field free flight tube depends only on the mass of the ion, since the amount of the kinetic energy received is the same for all particles. This enables the ions to be separated based on their velocity before reaching the detector at the end of the flight tube. Mass to charge ratios are then determined based on the time it takes for the ion to move through the source and to the detector (36).

The ion is accelerated in the electric field by a potential V and this electric potential energy is converted to kinetic energy E_k, so the following equation is obtained for an ion with a mass m and a charge $q = z \times e$:

$$E_k = {}^1/_2\, mv^2 = z \times e \times V \tag{8}$$

A term for the ion velocity can be obtained also from the previous equation with some rearrangement:

$$v = \sqrt{2zeV/m} \tag{9}$$

After acceleration in the electric field, the ions move at a constant velocity through the flight tube to the detector. The time t needed to travel the distance L between the source and the detector is given as (36):

(10)

Using the equation for the velocity of the ion we obtain the time needed, for the ion to reach the detector:

$$t^2 = \frac{m}{z}\left(\frac{L^2}{2eV}\right) \quad (11)$$

With the above equation, we can see that the mass to charge ratio m/z can be directly calculated from the time it takes for the ion to travel through the flight tube. We can also notice that the smaller the mass of the ion, the faster it is going to move and it will reach the detector faster.

Resolution of the TOF mass analyser depends on the length of the flight tube, meaning that in a longer distance, ions can be separated better. Consequently, one way to improve the resolution is to use longer flight tubes. However, this also decreases the performance of a TOF mass analyser due to more scattering of the ions that are lost in the result. Likewise, the acceleration voltage could be lowered so that ions would have a smaller velocity, which would increase their flight time, but a lower voltage also decreases the instrument's sensitivity. That is why the only option to have both high resolution and high sensitivity is to use a longer flight tube and an acceleration voltage of at least 20 kV (36).

Consequently, a way to improve the resolution of the TOF mass analyser is with an ion mirror or an electrostatic reflector, also called a reflectron, which reflects ions and increases the flight distance. A reflectron uses an electric field, which deflects the ions backwards and sends them to travel back through the flight tube, thus increasing their flight distance and resolution. The reflectron is positioned behind the flight tube on the other side of the ion source, which means that detector has to be positioned on the side of the instrument where the ion source is. The detector can be positioned in the same axis as the ion source or it can be a little bit shifted and positioned right next to the ion source. The reflectron also corrects the initial dispersion of the kinetic energy, since ions with higher velocity will be retarded in the reflectron longer than the ions with lower velocity (35).

1.4.4. Ion detector

As the ions pass through the mass analyser they are separated and afterwards detected and transformed into a signal by a detector positioned at the end of the mass analyser. Usually the detector receives the signal from the ions and transforms it to an electrical signal, for example an electric current that can be used for further analysis. There are two types of ion detectors. One count the ions as they reach a certain point in a detector in time, so they count ions one after the other (point ion collectors). The second type of detectors consist of multi-array photographic plates which can detect more ions simultaneously(36).

The most common types of ion detectors are listed below (36):

- → Faraday cup
- → Electron multipliers
- → Electro-optical ion detectors

In the following work, a microchannel plate detector (MCP) was used in reflectron mode. It functions as an electron multiplier in such a way that it amplifies a single particle reaching the detector to a cloud of electrons via secondary emission. Emitted electrons are then converted into an electric current (35). MCPs consist of many channels positioned at an around 10° to 20° angle in respect to the normal surface. This enables the electrons to hit the walls of each specific channel in order to multiply the signal.

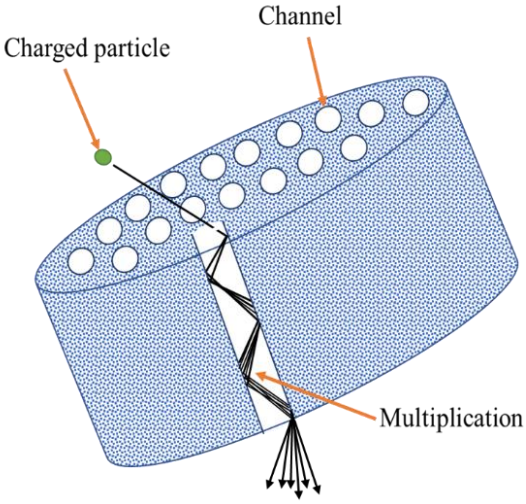

Figure 13: Schematic presentation of MCP ion detector

As an electron hits the inner wall of the channel, it becomes multiplied by generating new electrons. New electrons are thus formed all the way through the channel.

2. MATERIALS AND METHODS

2.1. Materials

2.1.1 Chemicals

Chemical (lot number)	Quality	Company
Ammonium acetate	≥ 99.99 %	Sigma Aldrich (Steinheim, Germany)
Ammonium hydroxide	ACS reagent	Sigma Aldrich (Steinheim, Germany)
2,4,6-Trihydroxyacetophenon monohydrate	≥ 99.5 %	Fluka (Buchs, Switzerland)
Sinapic acid	99.0%	Sigma Aldrich (Steinheim, Germany)
α-cyano-3-hydroxycinnamic acid	≥ 99.99 %	Sigma Aldrich (Steinheim, Germany)
Chloroform	EMSURE, for analysis	Merck (Darmstadt, Germany)
Methanol	LiChrosolv, hypergrade for LC-MS	Merck (Darmstadt, Germany)
L-α-phosphatidylcholine hydrogenated (Soy) (HSPC) (840058P)	/	Avanti Polar Lipids (Alabaster, AL, USA)
1,2-dioctadecanoyl-sn-glycero-3-phosphoethanolamine (18:0 PE, DSPE) (850715P)	/	Avanti Polar Lipids (Alabaster, AL, USA)
Cholesterol (700000P)	≥ 98.0%	Avanti Polar Lipids (Alabaster, AL, USA)
VLDL from human plasma	(≥ 95.0%)	Calbiochem (Millipore, Billerica, MA, USA)
D-Panthenol (BCBR8961V)	≥ 98.0% (NT)	Sigma Aldrich (Steinheim, Germany)
Melatonin (SLBN1002V)	≥ 98.0% (TLC)	Sigma Aldrich (Steinheim, Germany)
L-Ascorbic acid (SLBC7863V)	BioXtra, ≥ 99.0%	Sigma Aldrich (Steinheim, Germany)
Vanillin (BCBV5242)	ReagentPlus, 99%	Sigma Aldrich (Steinheim, Germany)
Hemoglobin (86H9310)	/	Sigma Aldrich (Steinheim, Germany)
Bovine Serum Albumin (SLBN7156V)	≥ 96.0%	Sigma Aldrich (Steinheim, Germany)

y-Globulins from bovine blood (SLBQ4603V)	≥ 99.0%	Sigma Aldrich (Steinheim, Germany)
Castor oil	/	/
Acetonitrile	EMSURE, for analysis	Merck (Darmstadt, Germany)
Trifluoroacetic acid (SLBD(8958V)	99%	Sigma Aldrich (Steinheim, Germany)
Isopropanol	LiChrosolv, gradient grade for LC	Merck (Darmstadt, Germany)
Sodium chloride (71376)	Ultra	Fluka (Buchs, Switzerland)

Table 6: List of all chemicals used for the following work

2.1.2 Buffers and electrolytes

40 mM ammonium acetate (NH_4OAc) with pH 8.4 was used as the main electrolyte for all of the following experiments. Prepared NH_4OAc was filtered through 0.2 µm pore size syringe filters (surfactant free cellulose acetate membrane from Sartorius, Göttingen, Germany) before use. NH_4OAc was used for preparation of liposomes and as the aqueous electrolyte for gas-phase electrophoresis.

List of solutions used for the passive loading of the cargo inside the liposomes:

Compound	Solution
L-Ascorbic acid	20 mM ascorbic acid in 20 mM NH_4OAc
Melatonin	4 mM melatonin in 40 mM NH_4OAc
Vanilin	20 mM vanillin in 40 mM NH_4OAc
D-Panthenol	20 mM panthenol in 40 mM NH_4OAc

Table 7: List of cargo molecule solutions

List of solutions used for protein mixtures:

Compound	Solution
Immunoglobulin G	0.5 µM immunoglobulin G in 40 mM NH_4OAc
Bovine serum albumin	0.5 µM bovine serum albumin in 40 mM NH_4OAc
Hemoglobin	0.5 µM hemoglobin in 40 mM NH_4OAc

Table 8: List of protein solutions

For all solutions and electrolytes, Millipore grade water (Merck Millipore, Billerica, CA, USA) was used with 18.2 MΩcm resistivity at 25°C.

2.2. General instrumentation and disposable materials

Instrument	Company	Town, Country
Centrifuge Sigma	Linder Labortechnik	Wien, AT
Analytical balance Extend	Sartorius	Göttingen, DE
Milipore Simplicity UV	Merck	Billerica, CA, USA
pH meter Fire easy	Mettler Toledo	Columbus, OH, USA
Extrusion set	Avanti Polar lipids	Alabaster, AL, USA
Zoom stereomicroscope	Nikon	Melville, NY, USA
Capillary	Polymicro Technologies	Phoenix, AZ, USA
Syringe filters, 0.2 µm pore size	Sartorius	Göttingen, Germany
10 kDA cut-off filters	VWR	Wien, AT
Silver pigment	Agar scientific	Stansted, Essex, UK
CO_2	Messes	Gumpoldskirchen, AT
Donaldson Membrane Dryer	Ludvik Industriegeräte	Wien, AT
Ultrasonic bath	Sonorex	Berlin, DE

2.2.1. Capillary tip sharpening

Homemade capillary tips were produced with a use of a rotating fine sand paper spinner and a rotational capillary holder (39). 25 cm long capillaries were cut with a use of a sharp rotating blade (diamond capillary cutter) from a 25 m capillary (25 µm inner diameter, 150 µm outer diameter, polyimide coated fused silica from Polymicro Technologies, Phoenix, AZ, USA). One end of the capillary was fixed to the rotational capillary holder while the other one was inserted through a tight sleeve and positioned close to the rough surface of the sand paper. As the sand paper was rotating at a high speed the capillary was brought in contact with the sand paper and as it turned around its own axis the tip became conically shaped. This shape helped to stabilize the Taylor cone for subsequent nES processes.

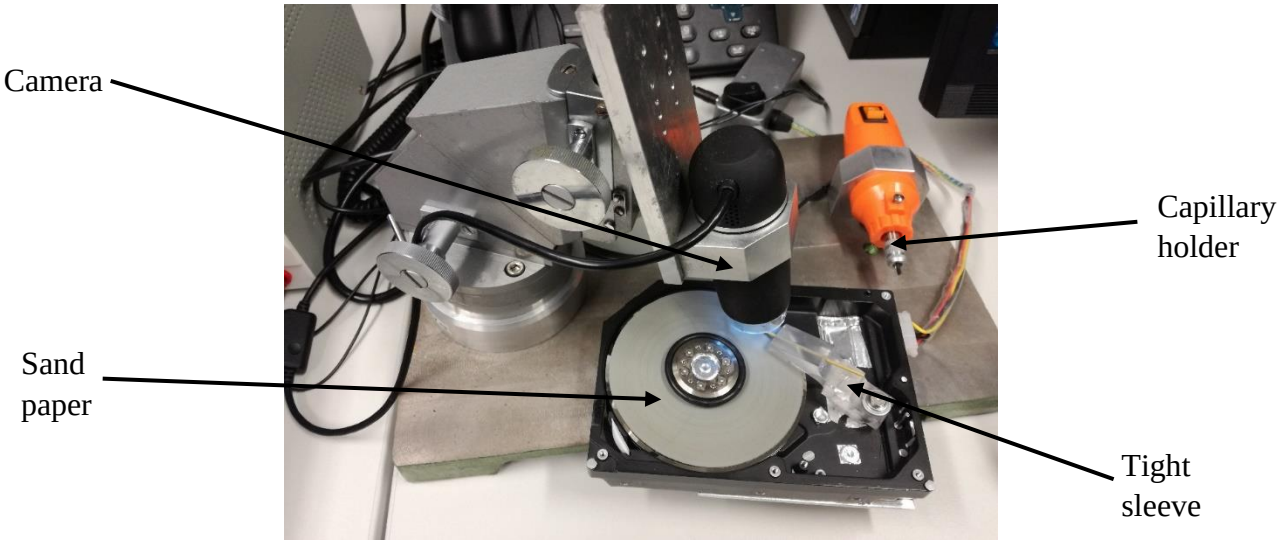

Figure 14: Setup for capillary tip sharpening

2.3. Liposome preparation

2.3.1. Lipids

Two different types of phospholipids were used and cholesterol was added as well. 1,2-dioctadecanoyl-sn-glycero-3-phosphoethanolamine (18:0 PE, DSPE) and L-α-phosphatidylcholine hydrogenated (Soy) (HSPC) were used.

Phospholipids and cholesterol were mixed in the following ratio:

HSPC	Cholesterol	DSPE	
4	3	3	[µmol]
3,135	1,160	2,244	[mg]

Table 9: Ratios of lipid composition

A final lipid concentration of 10 mM in aqueous electrolyte solutions was obtained by dispersing lipids in one ml of each respective solution as described in detail below.

2.3.2. Thin lipid film hydration method

The thin lipid layer hydration method is a mechanical dispersion method, which enables passive loading of desired compounds in the interior core of the formed liposomes. It is a very common method for preparation of solute-filled liposomes in the laboratory. Its principle is a formation of thin film of dried lipids in a round-bottom flask due to evaporation of an organic solvent by application of a N_2 flow. Afterwards an aqueous solution is added and mechanical agitation as well as gentle heating causes formation of liposomes.

First, lipids were weighted to round-bottomed flask to obtain their desired ratio. Afterwards 1 ml of the organic solvent mix, chloroform:methanol in 3:1 volume ratio, was added to homogeneously dissolve the lipids. After mixing, the organic solvent was evaporated under a gentle N_2 stream in the fume hood to obtain a thin film of lipids on the bottom of the flask. Lipids were further dried for approximately 2 hours in a desiccator employing vacuum. Afterwards the hydration of the lipids was carried out using one ml of 40 mM NH_4OAc to yield a final 10 mM lipid concentration. This dispersion was vortexed and heated to around 65°C in a water bath. This enabled the lipid phase transition due to the elevated temperature. Mechanical agitation was used to detach the dried lipids from the round-bottomed flask and allow them so self-assembly into liposomes.

Different sized liposomes are obtained via the thin lipid layer hydration method. Subsequently, extrusion of prepared liposomes was applied to obtain small unilamellar vesicles. Extrusion was done 21 times through 100 nm pore size polycarbonate membrane filters. An Avanti extruder set was used. Firstly, the extruder block was heated to allow the liposome solution to reach transition temperature. Afterwards two filter supports were pre-wetted with Millipore grade water and positioned on top of two teflon holders (internal membrane supporters) presented on Figure 15. Two 100 nm pore size polycarbonate membrane filters were pre-wetted as well and positioned over the two filter supports.

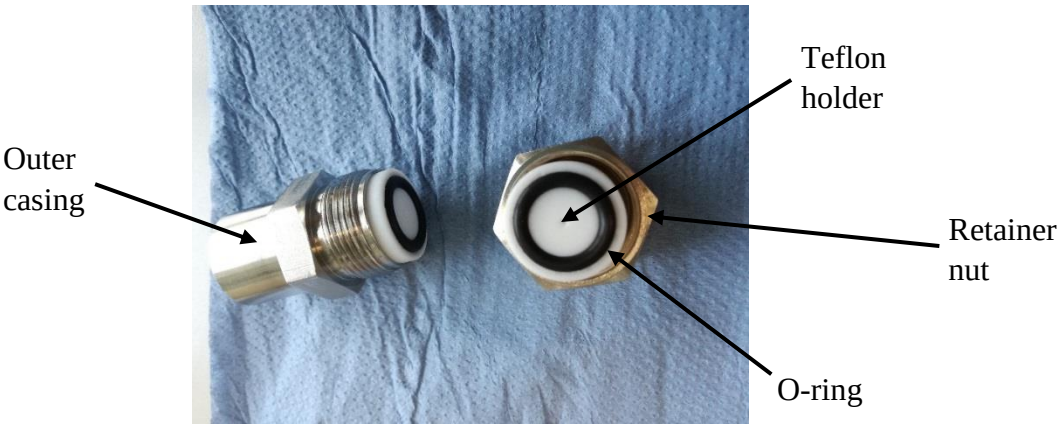

Figure 15: Teflon parts to be joined together. Filters are positioned in between the teflon parts.

Both parts of the teflon holders were joined together so that the two filters were facing each other and strongly tightened in the given metal holder consisting of an extruder outer casing and a retainer nut. The structure of the extrusion device can be seen on the Figure 16 below:

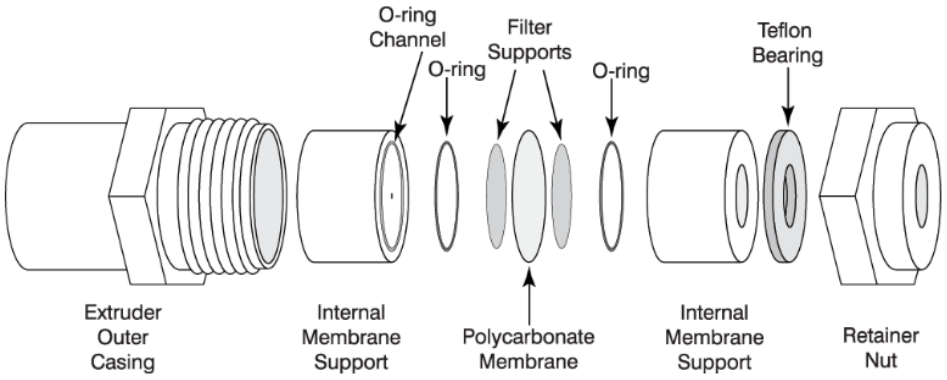

Figure 16: Layout of the extrusion device obtained from Avanti Polar Lipids (https://avantilipids.com/divisions/equipment-products)

When the whole instrument was assembled, two 1000 µl syringes were inserted through the extruder. One of the syringes was filled with water to test if the filters were positioned correctly (5 times pressurization). After that, the water was removed from the syringe and liposome solution was filled into one of the syringes and filtered 21 times through the extrusion device.

Figure 17: Setup for the extrusion process. Heating block, round-bottomed flask, syringes, polycarbonate membrane filters, filter supporters, teflon holders and outer casing to hold it all together

For the extrusion process two larger pore size polycarbonate membrane filters were used as well, 200 nm and 400 nm pore size filters respectively. With these setups, putatively larger liposomes were obtained.

Liposome stock solutions were than stored in brown glass vial at 4°C until further use.

All liposome preparations are listed below:

Date	Sample	HSPC:Chol:DSPE [µmol]	Buffer	Extrusion filter size
3.10.2018	Liposomes with ascorbic acid	4:3:3	20 mM ascorbic acid in 20 mM NH_4OAc	100 nm
3.10.2018	Liposomes with melatonin	4:3:3	4 mM melatonin in 40 mM NH_4OAc	100 nm
3.10.2018	Liposomes with vanillin	4:3:3	20 mM vanillin in 40 mM NH_4OAc	100 nm
3.10.2018	Liposomes with panthenol	4:3:3	20 mM panthenol in 40 mM NH_4OAc	100 nm
9.10.2018	Liposomes with ascorbic acid	4:3:3	20 mM ascorbic acid in 20 mM NH_4OAc	100 nm
9.10.2018	Liposomes with melatonin	4:3:3	4 mM melatonin in 40 mM NH_4OAc	100 nm
9.10.2018	Liposomes with vanillin	4:3:3	20 mM vanillin in 40 mM NH_4OAc	100 nm
9.10.2018	Liposomes with panthenol	4:3:3	20 mM panthenol in 40 mM NH_4OAc	100 nm
19.11.2018	Liposomes with panthenol	4:3:3	20 mM panthenol in 40 mM NH_4OAc	100 nm
28.11.2018	Liposomes with melatonin	4:3:3	7.8 mM melatonin in 40 mM NH_4OAc	100 nm
18.12.2018	Empty liposomes*	4:3:3	40 mM NH_4OAc	100 nm
24.1.2018	Empty liposomes*	4:3:3	40 mM NH_4OAc	200 nm
24.1.2018	Empty liposomes*	4:3:3	40 mM NH_4OAc	400 nm

*Table 10: List of all liposome preparations; * empty liposomes only contained the corresponding electrolyte solution*

2.3.3. Cargo material and encapsulation

Different cargo material was encapsulated into the hydrophilic core of the liposomes. All of the cargo molecules were loaded passively, meaning that they were encapsulated during the formation of the liposomes.

The compounds ascorbic acid, melatonin, panthenol and vanillin were chosen as cargo materials, respectively.

Solutions were prepared with the desired cargo material as described in chapter 2.1.2. For the loading of the cargo, the thin lipid hydration method for liposome preparation was used. Again, lipids were mixed in chloroform:methanol 3:1 volume ratio and dried using N_2 flow to obtain a dried lipid film on the bottom of the round flask. Dried lipids were further dried for approximately 2 hours in a desiccator. For the lipid re-hydration, the cargo filled solutions in NH_4OAc were used, to allow the encapsulation of the cargo material. Therefore, e.g. one ml of the ascorbic acid buffer was used, when we wished to encapsulate ascorbic acid molecules in the interior of the prepared liposomes. The same was done for all other buffers with desired cargo material.

Following the hydration, the liposomes were extruded as described before to obtain liposomes with the diameter near the pore size of the extrusion filters. Liposomes with cargo material were stored in their respectful solutions with the cargo material in brown glass vials at 4°C until further use.

2.4. Buffer exchange via spin filtration

Before analysis and characterization of the liposomes and VLDLs, stock solutions had to be filtered in order to remove non-volatile buffer components from solutions. This process also filtered out the low size particles and remaining cargo molecules from the exterior of the liposomes and salts from VLDL solutions, meaning that all of the non-encapsulated cargo and small size salt molecules were flushed away.

For filtration, a centrifuge filter was used with a 10 kDa molecular weight cut-off membrane (MWCO, polyethersulfone membrane, VWR, Vienna, Austria). All samples were washed 3 times at 9300×g for approximately 7 minutes on the filter membranes.

For subsequent liposomes analysis via gas-phase electrophoresis, a 1:10 (v:v) dilution was used. Hence, the same dilution was used during buffer exchange. Ten µl of each stock solution was applied to a 10 kDa cut-off filter with 490 µl of filtered NH_4OAc. After every round of centrifugation, approximately 10 µl of supernatant should remain above the filter and fresh 490 µl of filtered NH_4OAc was added. This process was repeated two times. At the end 100 µl of the liposome solution (i.e. a 1:10 volumetric dilution) was obtained on top of the filter membrane.

For VLDLs, a 1:30 dilution was used. Hence, only 5 µl of the stock solution was applied to the 10 kDa cut-off filter with 495 µl of filtered NH_4OAc. After every round of centrifugation approximately 5 µl of supernatant should remain above the filter and fresh 495 µl of filtered NH_4OAc was added. This process was repeated two times. At the end, 150 µl of the VLDL solution (i.e. a 1:30 volumetric dilution) was obtained.

For a set of experiments, VLDLs were mixed with immunoglobulin G (IgG), bovine serum albumin (BSA) and hemoglobin (HEM), prepared as described before. A mixture of all the protein

stocks (as detailed above) was prepared in a 1:1:1 volumetric ratio for IgG:BSA:HEM. Five µl of VLDL stock solution was applied to the 10 kDa cut-off filters with 495 µl of filtered NH_4OAc. After the first two rounds of centrifugation approximately 5 µl of supernatant should remain on top of the filter and fresh 495 µl of filtered NH_4OAc was added. After the third and last round of centrifuging was completed the protein mix solution was added to yield 150 µl of a 1:30 (v:v) VLDL solution.

For another set of experiments, VLDLs should be analysed in the presence of liposomes. Hence, empty liposomes were mixed with the VLDL stock. 10 µl of the empty liposome stock solution and 3.33 µl of the VLDL stock solution were applied to the 10 kDa cut-off filters with 486.7 µl of filtered NH_4OAc. After every round of centrifugation was completed approximately 13.3 µl of supernatant should remain on top of the filter and fresh 486.7 µl of filtered NH_4OAc was added. This process was repeated two times. At the end, 100 µl of 1:10 (v:v) liposomes with 1:30 (v:v) VLDL solution was obtained.

The list of sample preparations are summarized in the table below:

Sample	Dillution	Buffer	Centrifuge parameters	Centrifuge time	Final volume
Empty liposomes	1:10	40 mM NH_4OAc	3 × 9300 g	3 × 6 min	100 µl
Liposomes with ascorbic acid	1:10	40 mM NH_4OAc	3 × 9300 g	3 × 6 min	100 µl
Liposomes with melatonin	1:10	40 mM NH_4OAc	3 × 9300 g	3 × 6 min	100 µl
Liposomes with vanillin	1:10	40 mM NH_4OAc	3 × 9300 g	3 × 6 min	100 µl
Liposomes with panthenol	1:10	40 mM NH_4OAc	3 × 9300 g	3 × 6 min	100 µl
VLDLs	1:30	40 mM NH_4OAc	3 × 9300 g	3 × 9 min	150 µl
VLDLs	1:30	Protein mix in 40 mM NH_4OAc	3 × 9300 g	3 × 10 min	150 µl
VLDLs	1:20	40 mM NH_4OAc	3 × 9300 g	3 × 8 min	100 µl
VLDLs with empty liposomes	1:30 VLDLs 1:10 liposomes	40 mM NH_4OAc	3 × 9300 g	3 × 10 min	100 µl

Table 11: List of sample dilutions and filtrations

2.5. MALDI-MS measurements of liposomes and VLDLs

The aim of the work was to connect two different analytical techniques, nES GEMMA and MALDI MS. To demonstrate that this hyphenation is a suitable option for analysis of compounds from complex mixtures, samples were subjected to the following work protocol:

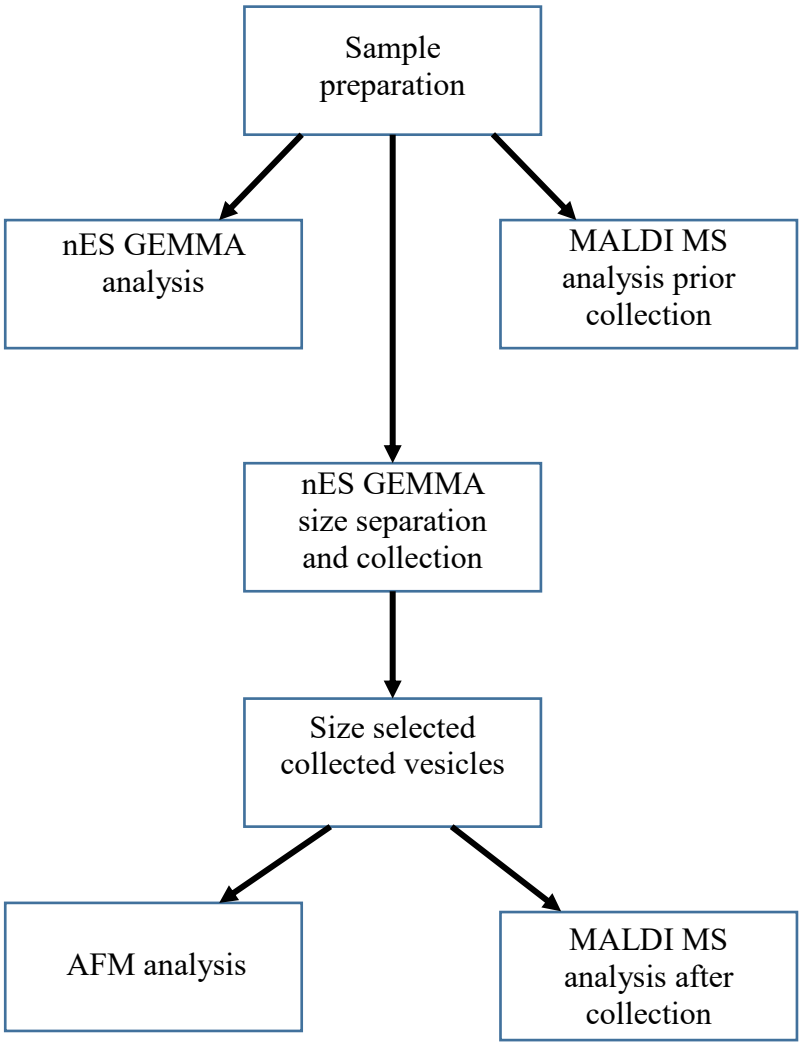

Figure 18: Experimental workflow

Analyte samples consisting of a mix of liposomes and VLDLs in 10:3 volumetric ratio were prepared and firstly a nES GEMMA analysis was carried out to determine the particle counts and visualize the size distribution of the analytes in the sample. Prepared liposomes have a distinguishable and repeatable size distribution spectrum. When mixed with VLDLs, a different spectrum was obtained for the nES GEMMA analysis. With the help of the spectra acquired before the size separation, the particle size for collection was determined.

Prior to collection, samples were analysed with the use of MALDI MS, to obtain the results without gas-phase electrophoresis fractionation. Diluted liposomes and VLDLs after buffer exchange were mixed 1:1 (v:v) with 20 mM THAP matrix solution and applied to the target plate. The mixed sample of liposomes and VLDLs was likewise combined with 10 mM THAP matrix and applied

to the target plate. With MALDI MS, lipid molecules were detected. Furthermore, cholesterol and different ion molecules were detectable as well. Data obtained prior to collection served as a comparison to prove, how gas-phase electrophoresis fractionation can successfully separate molecules out of complex mixtures.

Size separation of desired molecules from the sample solution was achieved via collection of monodisperse aerosol from the nDMA on the gold-coated silicon wafers. Collection was carried out for 150 min at 85 nm particle size for liposomes or 300 min at 38 nm particle size for VLDLs. Gold-coated silicon wafers with collected analytes were attached to the target plate and THAP matrix was applied to the centre of the wafer. MALDI MS spectra were always obtained prior and after the nES GEMMA size selection and collection. Measurements were carried out in reflectron positive ion mode with rastering. Data was analysed using a MALDI MS Launchpad software from Shimadzu.

Work protocols are described in detail in the following chapters.

2.6. Gas-phase electrophoresis

2.6.1. Instrumentation

Nano-electrospray (nES) gas-phase molecular mobility analysis (GEMMA) is a name for a setup of different instruments used for separation of single-charged particles in the gas-phase based only on their size. All instruments used were from TSI Inc (Shoreview, MN, USA). For generation of single-charged dried particles, a nES aerosol generator (model 3480) including a ^{210}Po source was used. For particle classification an electrostatic classifier based on a nano differential mobility analyser (model 3080) was used. For particle detection, a n-butanol based ultrafine condensation particle counter (model 3776C) was applied.

The instrument setup is presented on figure 19.

Figure 19: Setup for the gas-phase electrophoresis. Aerosol generator, electrostatic classifier with nDMA, ultrafine condensation particle counter and nanometre aerosol sampler

2.6.1.1. Aerosol generator

With the nES aerosol generator (model 3480) a polydisperse aerosol is generated. A liquid sample is pushed through the capillary due to a pressure difference between the sample vial and the capillary tip. An electric field is then exerted on the capillary tip and a liquid cone is formed. The formed droplets are multiple-charged. Subsequently, the liquid solvent dries due to CO_2 and air flow. Multiple charges of droplets are then reduced by an ionizer source, before they pass to the particle classifier.

General properties of the aerosol generator were obtained from the TSI manual and are presented in the table below:

Properties	Value
Particle generation rate	>107 particles/cm3
Particle size range	~ 150 nm
Differential pressure	0 to 5 psi (3.7 psi nominal)
Air flowrate	0.2 to 2.5 L/min (1 L/min nominal)
CO_2 flowrate	0.05 to 0.5 L/min (0.1 L/min nominal)

Table 12: Properties of aerosol generator

2.6.1.2. Electrostatic classifier

For separation of single-charged particles, an electrostatic classifier (model 3080) with a nano differential mobility analyser (nDMA) as presented in Figure 20 was used.

Figure 20: Nano Differential Mobility analyser

The polydisperse aerosol obtained after the nES process with subsequent charge equilibration is introduced to the nDMA. The nDMA output is a monodisperse aerosol of known particle size in dependence of the applied field strength of the nDMA. Furthermore, when used in scanning mode the monodisperse aerosol which exits the electrostatic classifier can be detected via the condensation particle counter and particle number concentration can be obtained. Thus, the particle number-based size distribution of the aerosol can be measured.

General properties of the electrostatic classifier were obtained from the TSI manual and are presented in the table below:

Properties	Value
Aerosol flow rate	0 to 3 L/min
Sheath flow rate	0 to 15 L/min

Aerosol pressure range	70 to 120 kPa
Maximum input concentration	108 particles/cm^3 at 10 nm
Voltage	10 to 10000 VDC

Table 13: General properties of the ultrafine condensation particle counter

2.6.1.3. Ultrafine condensation particle counter

For detection of monodisperse aerosol particles at the exit of electrostatic classifier, a n-butanol based ultrafine condensation particle counter (CPC, model 3776C) was used.

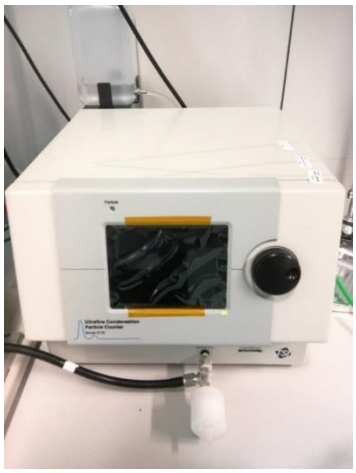

Figure 21: Ultrafine condensation particle counter

The particles in CPC are first enlarged by condensing vapour to form larger droplets, which can be detected more easily. This principle allows number-based particle detection in accordance with recommendations of the European Commission for nanoparticle characterization (2011/696/EU from October 18th, 2011). An uCPC setup is able to detect particles as small as 2.5 nanometres. The higher the saturation ratio, the smaller particle sizes can be counted.

A CPC can count up to 300,000 particles/cm^3 with an aerosol flow rate of 50 cm^3/min as stated in the TSI manual.

2.6.1.4. Nanometre aerosol sampler

Collection of size-separated particles was performed with an Electrostatic nanometre aerosol sampler (ENAS, model 3089) from TSI Inc.

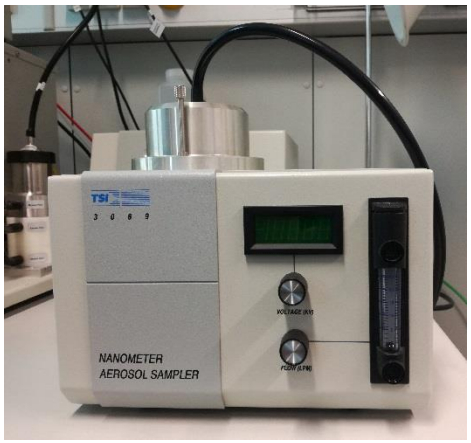

Figure 22: Electrostatic nanometre aerosol sampler

The outlet of the electrostatic classifier was mounted to the nanometre aerosol sampler instead of the ultrafine condensation particle counter and the charged particles drifting in the gas flow were collected on a one cm^2 gold coated silicon wafers for further analysis.

The aerosol sampler uses an electrode to attract the particles and control the spot size for the deposition of the sample particles on the gold coated silicon wafers. The gold wafer was carefully mounted to the sampler electrode using double sided adhesive tape.

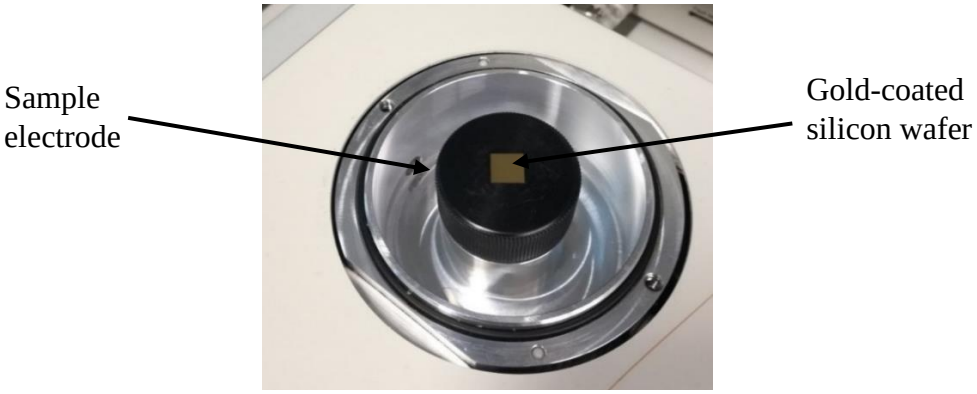

Figure 23: Positioning of the gold coated silicon wafer inside the nanometre aerosol sampler

The lid of the sampler was afterwards closed shut and the collection was started.

2.6.2. Size distribution determination

When the size distribution of the particles in our sample solution was of question, the voltage of the electrostatic classifier or nDMA was varied over a range of different values. With this, particles of specific electrophoretic mobility, consequently of specific particle size were able to exit the outlet slit of the nDMA and were detected with the condensation particle counter. Different voltage applied to the cylindrical electrodes of the nDMA generated different electric fields and thus different sized particles were retained more than others. Therefore, this variation of the applied electric field enables to scan different sized particles in the time scale of second to minutes, yielding a corresponding spectrum.

Samples were applied to the aerosol generator using small cylindrical vials. The bottom half of the pressure chamber can be removed and the sample can be positioned so that the platinum electrode wire and the inlet of the capillary are submerged in the solution. The liquid was then pushed through the capillary by increasing the pressure in the pressure chamber. An applied voltage also aids in the movement of the liquid through the capillary and in the formation of a stable Taylor cone.

Before the analysis was started the capillary was always exchanged to reduce the possibility of cross contamination. In order to do so, the capillary was flushed with isopropanol:water in 1:1 volumetric ratio to remove any contaminants before inserting it to the aerosol generator. The capillary was positioned in such a way, that it was centred when viewed through the viewing window.

Firstly, the solution of 40 mM NH_4OAc was always run through the system to rinse the capillary and to ensure there is no contamination present. Afterwards the sample solution was positioned to the aerosol generator and flushed through the system for at least 3 minutes in order to obtain a stable electrospray process.

The electrostatic classifier can be operated in two different modes as mentioned above. In ‘panel mode’ the nDMA voltage and consequently the particle size is constant, thus particle size-selection can be achieved. In ‘analog mode’, the nDMA voltage is varied over a wide range of nDMA voltages and consequently particle sizes in order to obtain the size distribution of particles present in an investigated sample solution.

The spray capillary was rinsed with the electrolyte solution between sample solutions in order to remove analyte particles attached to the inner surface of the capillary and hence to reduce analyte carry-over. Measurements for different samples were carried out at specific instrumental parameters, which are listed in chapter 2.5.4. Every sample was measured four times, for 180 seconds each, corresponding to 150 seconds of voltage adjustment and a 30-second window for the instrument to return to idle state of low voltage again.

Data was recorded with a macro IMS manager 2.0.1 software from TSI Inc (Shoreview, MN, USA). So called ‘raw counts’ were obtained, which gives us a direct value of number of particles detected for each specific particle diameter.

Obtained data was further analysed using Microsoft Excel. The median of the four measurements was calculated to yield one spectrum. Graphs were plotted in Origin Pro 9.1.0, Origin Lab Corporation (Northampton, MA, USA).

2.6.3. Size separation and collection

Nanoparticle collection was carried out at a specific particle size thus employing a constant voltage of the differential mobility analyser (see Chapter 2.6.4. for detailed info on instrument parameters). This means that only particles with the set electrophoretic mobility diameter were able to exit the outlet slit of the nDMA and were consequently collected with the nanometre aerosol sampler on the gold coated silicon wafer. This enables the separation of desired particles from complex mixtures based on particle size.

The collection process was started with the acquisition of the particle size distribution. Setting up of the instrument and the sample application were the same as described in the previous chapter. Subsequently, when size separation of nanoparticles should be achieved with the nDMA, the desired particle size was set with the use of the command unit of the electrostatic classifier or with the help of a software called Termite (CompuPhase, Bussum, NE).

The instrument hardware set-up had to be changed as well. The outlet of the electrostatic classifier had to be connected to nanometre aerosol sampler in order to collect particles on the gold coated silicon wafers. The collection chamber with electrodes in the nanometre aerosol sampler was cleaned with isopropanol before every collection.

Collection of size selected analyte particles was carried out for up to 5 hours (300 minutes). After the collection process, the size distribution with varying nDMA voltage was acquired again to ensure that the capillary did not get clogged during the collection. Comparing nES GEMMA spectra prior and after particle collection enabled us to assume stability of the system also during the particle collection period.

Instrumental parameters used for analysis of different sample solutions are presented in the next chapter.

2.6.4. Instrument settings for size distribution and collection

2.6.4.1. Parameters for liposomes with encapsulated cargo

Aerosol Generator	
Voltage	~ 2 kV
Current	-350 nA to -400 nA
Pressure difference	4 pounds per square inch differential (28 kPa)
Air flow	1,0 L/min
CO_2 flow	0,1 L/min
Capillary diameter	25 µm

Table 14: Parameters used for operation of aerosol generator for liposomes with encapsulated cargo material

Electrostatic classifier	
Size distribution	4.83 nm – 183.4 nm
Collection	85 nm
DMA voltage	10 V – 10 000 V
Sheath flow	2,5 L/min

Table 15: Parameters used for operation of electrostatic classifier for liposomes with encapsulated cargo material

Ultrafine Condensation Particle Counter	
Scan time up	150 s
Scan time down	30 s
Scheduling	1 x 4

Table 16: Parameters used for operation of ultrafine condensation particle counter for liposomes with encapsulated cargo material

Nanometre Aerosol Sampler	
Voltage	-3.0 to -3.2 kV
Flow	1 L/min
Collection time	150 min and up to 300 min

Table 17: Parameters used for operation of nanometre aerosol sampler for collection of liposomes with encapsulated cargo material

2.6.4.2. Parameters for very low-density lipoproteins

Aerosol Generator	
Voltage	~ 2 kV
Current	-350 nA to -400 nA
Pressure difference	4 pounds per square inch differential (28 kPa)
Air flow	1,0 L/min
CO_2 flow	0,1 L/min
Capillary diameter	25 µm

Table 18: Parameters used for operation of aerosol generator for VLDLs

Electrostatic classifier	
Size distribution	4.83 nm – 183.4 nm
Collection	28 nm, 33 nm, 38 nm, 43 nm
DMA voltage	10 V – 10 000 V
Sheath flow	2,5 L/min

Table 19: Parameters used for operation of electrostatic classifier for VLDLs

Ultrafine Condensation Particle Counter	
Scan time up	150 s
Scan time down	30 s
Scheduling	1 x 4

Table 20: Parameters used for operation of ultrafine condensation particle counter for VLDLs

Nanometre Aerosol Sampler	
Voltage	-3.0 to -3.2 kV
Flow	1 L/min
Collection time	300 min

Table 21: Parameters used for operation of nanometre aerosol sampler for collection of VLDLs

2.6.4.3. Parameters for very low-density lipoproteins with added proteins

Aerosol Generator	
Voltage	~ 2 kV
Current	-350 nA to -400 nA
Pressure difference	4 pounds per square inch differential (28 kPa)
Air flow	1,0 L/min
CO_2 flow	0,1 L/min
Capillary diameter	25 µm

Table 22: Parameters used for operation of aerosol generator for VLDLs with added protein mixture

Electrostatic classifier	
Size distribution	4.83 nm – 183.4 nm, 3.08 nm – 108.4 nm, 2.67 nm – 91.4 nm, 4.83 nm – 80.6 nm, **4.83 nm – 73.0 nm**
Collection	38 nm
DMA voltage	~ 10 V – 10 000V
Sheath flow	2,5 L/min, 6 L/min, 8 L/min, 10 L/min, **12 L /min**

Table 23: Parameters used for operation of electrostatic classifier for VLDLs with added protein mixture. Values in bold were used for the final experiments

Ultrafine Condensation Particle Counter	
Scan time up	150 s
Scan time down	30 s
Scheduling	1 x 4

Table 24: Parameters used for operation of ultrafine condensation particle counter for VLDLs with added protein mixture

Nanometre Aerosol Sampler	
Voltage	-3.0 to -3.2 kV
Flow	1 L/min
Collection time	300 min

Table 25: Parameters used for operation of nanometre aerosol sampler for VLDLs with added protein mixture

2.6.4.4. Parameters for very low-density lipoproteins with empty liposomes

Aerosol Generator	
Voltage	~ 2 kV
Current	-350 nA to -400 nA
Pressure difference	4 pounds per square inch differential (28 kPa)
Air flow	1,0 L/min
CO_2 flow	0,1 L/min
Capillary diameter	25 µm

Table 26: Parameters used for operation of aerosol generator for VLDLs with empty liposomes

Electrostatic classifier	
Size distribution	4.83 nm – 183.4 nm
Collection	85 nm
DMA voltage	10 V – 10 000 V
Sheath flow	2,5 L/min

Table 27: Parameters used for operation of electrostatic classifier for VLDLs with added empty liposomes

Ultrafine Condensation Particle Counter	
Scan time up	150 s
Scan time down	30 s
Scheduling	1 x 4

Table 28: Parameters used for operation of ultrafine condensation particle counter for VLDLs with empty liposomes

Nanometre Aerosol Sampler	
Voltage	-3.0 to -3.2 kV
Flow	1 L/min
Collection time	300 min

Table 29: Parameters used for operation of nanometre aerosol sampler for collection of VLDLs with empty liposomes

2.7. Atomic Force Microscopy

2.7.1. Instrumentation

AFM of the collected samples was carried out on Nanoscope 8 Multimode AFM (Bruker, Santa Barbara, USA).

Figure 24: Multimode AFM used for the experiments

An AFM microscope is designed to image small samples in ambient conditions with a raster scan of the sample surface. Imaging was carried out in tapping mode.

A Nanoscope 8 Multimode instrument has different interchangeable scanning areas. For our experiments a 10 x 10 μm^2 scanning area was used.

Firstly, the collected analytes on a gold-coated silicon wafer were applied to the sample holder. Furthermore, a silicon cantilever was chosen. The tip with the cantilever was mounted to a tip holder and viewed under an optical microscope to make sure it was positioned correctly.

The wafer glued to the sample holder was then positioned on top of the scanner and the tip holder was placed in the head of the AFM. The whole instrument was then raised on a flexible mounting to minimize unwanted vibrations.

2.7.2. Instrument settings and image generation

AFM images of the collected sample were obtained in tapping mode with monolithic silicon cantilevers. The length of the cantilevers was 125 µm with a nominal spring constant of 42 N/m. The resonance frequency of the cantilever was 320 kHz. The tip was shaped like a polygon-based pyramid with a height of 10 - 15 µm. More images were acquired on different spots of the gold-coated silicon wafer on which the sample was collected.

2.8. MALDI mass spectrometry

2.8.1. Instrumentation

For mass spectrometry analysis, an AXIMA TOF^2 mass spectrometer from Kratos Analytical, a Shimadzu group company (Manchester, United Kingdom) was used.

Figure 25: AXIMA TOF^2 mass spectrometer

This mass spectrometer uses a MALDI ionization technique and a TOF^2 mass analyser. In the following work a reflectron TOF^2 was used. For detection, a microchannel plate detector was used.

Two different nickel-coated aluminium MALDI MS targets were used for (i) deposition of samples prior and (ii) after the size selection and collection with the nES GEMMA. For analysis of samples prior to collection, a DE2115TA target plate was used. For analysis of the collected samples, the gold coated silicon wafers were glued to target plate number TO-482P00.

Target plate for samples prior nES GEMMA size selection

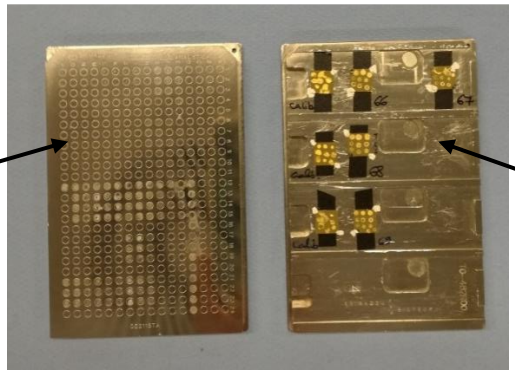

Target plate for samples after nES GEMMA size selection

Figure 26: Target plates used for MALDI MS. Target plate DE2115TA is positioned on the left side and target plate TO-482P00 is positioned on the right side

The following schematic diagram was obtained from the AXIMA performance getting started guide. It represents the components of the AXIMA TOF^2:

Figure legend:

1. Laser beam directed onto the sample
2. Desorption and ionization of the sample
3. Extraction plates
4. Ion lenses
5. Deflector plates
6. Ion gate
7. CID (collision induced dissociation) cell
8. Deflector plates
9. Linear mode
10. Reflectron for reflectron mode
11. Reflectron detector

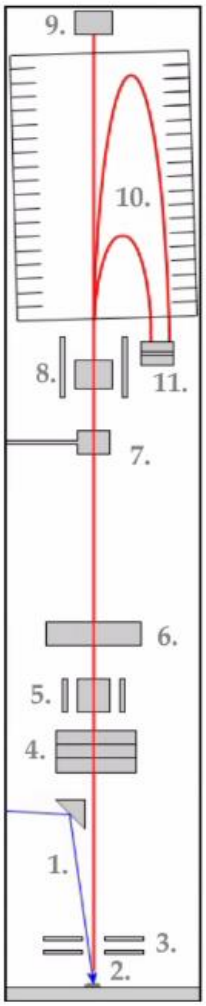

2.8.2. Instrument settings

General instrumental parameters of the AXIMA TOF^2 are given in the table below:

Parameter	Value
Instrument design	Reflectron TOF^2
Type of reflectron	Curved field
Acceleration voltage	20 kV
Collision gas	Helium
Vacuum	10^{-6}
Reflectron energy acceptance	95 %

Reflectron effective drift length	2 m
Target plates	DE2115TA, TO-482P00
Laser wavelength	N_2, 337 nm
Maximum repetition rate	20 Hz
Camera	CCD camera system
Detector – reflectron mode	Microchannel plate

Table 30: General parameters for AXIMA TOF²

For calibration, castor oil was used. The matrix solution for castor oil was prepared with 20 mM THAP with additional NaCl.

The instrument settings used for the following experiments are presented in the tables below:

Acquisition	
Laser power	>120 a.u.
Profiles per sample	Same as number of raster points
Shots accumulated per profile	5
Ion gate (Da)	off
Pulsed extraction optimized at (Da)	800

Exp. Tech.	
Tuning mode	Reflectron
Mass range	m/z 1.0 – 1000
Max. Laser Rep. Rate	20 Hz

Raster	
Type	Regular rectangular
Spacing	1200x1200, 40 µm
Calculated raster	676

2.8.3. Selected MALDI matrices

Three different molecules were chosen to be tested as MALDI matrix. All of the compounds have a very good absorption of the light at the wavelength (337 nm) of the used laser.

Matrix	Abbreviation	Chemical structure
2,4,6,-Trihydroxyacetophenone monohydrate	THAP	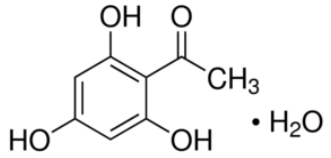
α-Cyano-4-hydroxycinnamic acid	CHCA	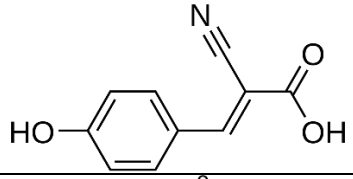
3,5-Dimethoxy-4-hydroxycinnamic acid (sinapic)	SA	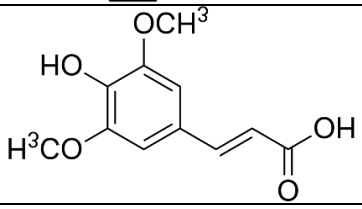

Table 31: Selected MALDI matrices. THAP chemical structure: (https://www.sigmaaldrich.com/content/dam/sigma-aldrich/structure0/172/mfcd00149091.eps/_jcr_content/renditions/mfcd00149091-large.png). CHCA chemical structure: (https://www.sigmaaldrich.com/content/dam/sigma-aldrich/structure2/026/mfcd00004204.eps/_jcr_content/renditions/mfcd00004204-large.png). SA chemical structure: (https://www.sigmaaldrich.com/content/dam/sigma-aldrich/structure7/099/mfcd00004401.eps/_jcr_content/renditions/mfcd00004401-large.png)

For preparation of matrix solutions methanol or acetonitrile/H_2O (1:1 volumetric ratio) with 0.1% TFA were used. Matrix solutions for the MALDI MS analysis are written below:

Matrix compound	Matrix solution	Concentration
2,4,6-Trihydroxyacetophenone monohydrate (THAP)	MeOH	5 mM 10 mM 15 mM, 20 mM
α-Cyano-4-hydroxycinnamic acid (SA)	H_2O:ACN = 1:1 (v:v) + 0.1% TFA	5 mM 10 mM 15 mM
3,5-Dimethoxy-4-hydroxycinnamic acid (sinapic) (CHCA)	H_2O:ACN = 1:1 (v:v) + 0.1% TFA	5 mM 10 mM 15 mM

Table 32: Prepared concentrations for selected MALDI MS matrices

2.8.4. Applied sample deposition /preparation technique

Nickel-coated aluminium MALDI MS targets were always wiped with ethanol and water prior to sample deposition.

2.8.4.1. Sample deposition/preparation prior to collection

Before collection, molecules of interest were present in an aqueous solution. Preparation of the samples for the MALDI MS analysis was as follows:

Matrix solution and sample solution were mixed in 1:1 volume ratio. This solution mix was then deposited on the target plate with a volume of 0.9 µl. Three spots were prepared for each specific sample.

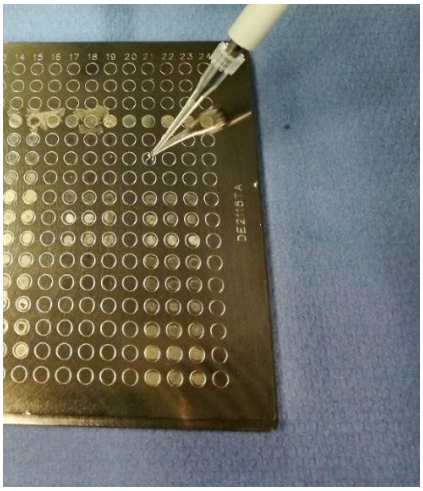

Figure 27: Deposition of matrix/sample mix to the target plate

Other options for sample deposition were also investigated. Firstly, 0.5 µl of the sample solution were deposited on the target plate. After drying, 0.5 µl of matrix solution was layered on top. In addition, another option was tested (similar to the latter one), which included addition of 1 µl of 1:1 (v:v) MeOH:H_2O over the first two layers in order to re-crystalize the matrix in presence of analyte molecules.

In the following work, the first preparation method was used, where sample solution and matrix solution are mixed in 1:1 volume ratio prior to the deposition on the target plate. With this method, best crystallization and consequently best MALDI MS results were obtained.

2.8.4.2. Sample deposition/preparation after collection

The sample after nES GEMMA based collection was no longer in a liquid state since analytes were already present on a solid sample support. Thus, only the matrix solution was applied directly to the wafer. This step should dissolve the sample collected on the wafer and generate crystals of the matrix together with analyte molecules.

The gold-coated silicon wafer was firstly attached to the target plate with use of a double sided carbon tape. Two corners of the wafer were dotted with silver pigment containing thermoplastic resin to achieve better conduction. Nine matrix solution spots were carefully deposited on one single wafer to obtain results for different matrix solutions applied to the same nES GEMMA based sample collection.

3. REFERENCES

1. Patel KN, Patel JK, Patel MP, Rajput GC, Patel HA. Introduction to hyphenated techniques and their applications in pharmacy. Pharmaceutical methods. 2010;1(1):2-13.
2. Yadav D SK, Pandey D, Dutta RK. Liposomes for Drug Delivery. J Biotechnol Biomater. 2017;7.
3. Abbot ES. The Causal Relations between Structure and Function in Biology. The American Journal of Psychology. 1916;27.
4. Li J, Wang X, Zhang T, Wang C, Huang Z, Luo X, et al. A review on phospholipids and their main applications in drug delivery systems. Asian Journal of Pharmaceutical Sciences. 2015;10(2):81-98.
5. Bogdanov WDaM. Functional roles of lipids in membranes. Biochemistry of Lipids, Lipoproteins and Membranes. 2002.
6. van Meer G, Voelker DR, Feigenson GW. Membrane lipids: where they are and how they behave. Nature reviews Molecular cell biology. 2008;9(2):112-24.
7. Lasic DD. Novel applications of liposomes. Tibtech. 1998;16.
8. Akbarzadeh A, Rezaei-Sadabady R, Davaran S, Joo SW, Zarghami N, Hanifehpour Y, et al. Liposome: classification, preparation, and applications. Nanoscale research letters. 2013;8(1):102.
9. Fan Y, Zhang Q. Development of liposomal formulations: From concept to clinical investigations. Asian Journal of Pharmaceutical Sciences. 2013;8(2):81-7.
10. Bangham AD, Standish MM, Watkins JC. Diffusion of univalent ions across the lamellae of swollen phospholipids. Journal of molecular biology. 1965;13(1):238-52.
11. Gregoriadis G. The carrier potential of liposomes in biology and medicine (first of two parts). The New England journal of medicine. 1976;295(13):704-10.
12. Ganapathi R, Krishan A, Wodinsky I, Zubrod CG, Lesko LJ. Effect of cholesterol content on antitumor activity and toxicity of liposome-encapsulated 1-beta-D-arabinofuranosylcytosine in vivo. Cancer research. 1980;40(3):630-3.
13. Allen TM, Cullis PR. Liposomal drug delivery systems: from concept to clinical applications. Advanced drug delivery reviews. 2013;65(1):36-48.
14. Zylberberg C, Matosevic S. Pharmaceutical liposomal drug delivery: a review of new delivery systems and a look at the regulatory landscape. Drug delivery. 2016;23(9):3319-29.
15. Torchilin VP. Recent advances with liposomes as pharmaceutical carriers. Nature reviews Drug discovery. 2005;4(2):145-60.
16. Feingold KR, Grunfeld C. Introduction to Lipids and Lipoproteins. In: Feingold KR, Anawalt B, Boyce A, Chrousos G, Dungan K, Grossman A, et al., editors. Endotext. South Dartmouth (MA): MDText.com, Inc.; 2000.
17. Gotto AM, Jr. Interrelationship of triglycerides with lipoproteins and high-density lipoproteins. The American journal of cardiology. 1990;66(6):20a-3a.
18. Thomas L. What are lipoproteins 2018 [updated 23.8.2018; cited 2019 12.1]. Available from: https://www.news-medical.net/life-sciences/What-are-Lipoproteins.aspx.
19. Gibbons GF, Wiggins D, Brown AM, Hebbachi AM. Synthesis and function of hepatic very-low-density lipoprotein. Biochemical Society transactions. 2004;32(Pt 1):59-64.
20. Caulfield MP, Li S, Lee G, Blanche PJ, Salameh WA, Benner WH, et al. Direct determination of lipoprotein particle sizes and concentrations by ion mobility analysis. Clinical chemistry. 2008;54(8):1307-16.
21. György Hegyi JK, Mihály Kovács, András Málnási-Csizmadia, László Nyitray, Gábor Pál, László, Radnai AR, and István Venekei. Introduction to Practical Biochemistry. Eötvös Loránd University2013.

22. Collins DC, Lee ML. Electrospray ionization gas-phase electrophoresis under ambient conditions and it's potential or high-speed separations. Fresenius' journal of analytical chemistry. 2001;369(3-4):225-33.
23. Wilm M. Principles of electrospray ionization. Molecular & cellular proteomics : MCP. 2011;10(7):M111.009407.
24. Kaufman SL, Skogen JW, Dorman FD, Zarrin F, Lewis KC. Macromolecule analysis based on electrophoretic mobility in air: globular proteins. Analytical chemistry. 1996;68(11):1895-904.
25. MacMillan AC, Morrison JB, Harmon CW, Nizkorodov SA. Enhancement of Surfactants in Nanoparticles Produced by an Electrospray Aerosol Generator. Aerosol Science and Technology. 2012;46(11):1239-45.
26. Weiss VU, Urey C, Gondikas A, Golesne M, Friedbacher G, von der Kammer F, et al. Nano electrospray gas-phase electrophoretic mobility molecular analysis (nES GEMMA) of liposomes: applicability of the technique for nano vesicle batch control. The Analyst. 2016;141(21):6042-50.
27. Stolzenburg MR, Scheckman JHT, Attoui M, Han H-S, McMurry PH. Characterization of the TSI model 3086 differential mobility analyzer for classifying aerosols down to 1 nm. Aerosol Science and Technology. 2018;52(7):748-56.
28. Weiss VU, Wieland K, Schwaighofer A, Lendl B, Allmaier G. Native nano electrospray differential mobility analyzer (nS GEMMA) enables size-selection of liposomal nanocarriers combined with subsequent spectroscopic analysis. Analytical chemistry. 2018;in press.
29. Various. Aerosol Measurement: Principles, Techniques, and Applications, 3rd Edition. Pramod Kulkarni PAB, Klaus Willeke, editor: Wiley; 2011.
30. Moller C, Allen M, Elings V, Engel A, Muller DJ. Tapping-mode atomic force microscopy produces faithful high-resolution images of protein surfaces. Biophysical journal. 1999;77(2):1150-8.
31. Bonazza K, Rottensteiner H, Seyfried BK, Schrenk G, Allmaier G, Turecek PL, et al. Visualization of a protein-protein interaction at a single-molecule level by atomic force microscopy. Analytical and bioanalytical chemistry. 2014;406(5):1411-21.
32. P. K. Hansma VBE, 0. Marti, C. E. Bracker. Scanning Tunneling Microscopy and Atomic Force Microscopy: Application to Biology and Technology. 1988;242 (4867).
33. Various. Handbook of instrumental Techniques for analytical chemistry. Settle FA, editor. New Jersey: Prentice-Hall; 1997.
34. Yingchoncharoen P, Kalinowski DS, Richardson DR. Lipid-Based Drug Delivery Systems in Cancer Therapy: What Is Available and What Is Yet to Come. Pharmacol Rev. 2016;68(3):701-87.
35. Singhal N, Kumar M, Kanaujia PK, Virdi JS. MALDI-TOF mass spectrometry: an emerging technology for microbial identification and diagnosis. Frontiers in microbiology. 2015;6:791.
36. Edmond de Hoffmann VS. Mass Spectrometry: Principles and Applications, 3rd Edition. Great Britain: Wiley; 2007.
37. Karas M, Hillenkamp F. Laser desorption ionization of proteins with molecular masses exceeding 10,000 daltons. Analytical chemistry. 1988;60(20):2299-301.
38. Various. MALDI MS, A Practical Guide to Instrumentation, Methods, andApplications. Franz Hillenkamp JP-K, editor. Germany: Wiley-VCH Verlag GmbH & Co. KGaA; 2014.
39. Tycova A, Prikryl J, Foret F. Reproducible preparation of nanospray tips for capillary electrophoresis coupled to mass spectrometry using 3D printed grinding device. Electrophoresis. 2016;37(7-8):924-30.

4. RESULTS AND DISCUSSION

4.1. Corresponding manuscript

Results of the work were presented in a paper titled '*Nano electrospray differential mobility analysis based size-selection of liposomes and very-low density lipoprotein particles for offline hyphenation to MALDI mass spectrometry'* published in the Journal of Chromatography A in 2019.

Work was conducted under the supervision of Asst.Prof.Dr. Victor U. Weiss and Univ.Prof.Dr. Günter Allmaier. MS and AFM measurements were carried out with the help of Dr. Ernst Pittenauer and Ao.Prof.Dr. Gernot Friedbacher, respectively.

Sample preparations and experimental measurements of liposomes and VLDLs were conducted by myself under the guidance of Asst.Prof.Dr. Victor U. Weiss. Further author contributions are listed in the manuscript.

Journal of Chromatography A

Nano electrospray differential mobility analysis based size-selection of liposomes and very-low density lipoprotein particles for offline hyphenation to MALDI mass spectrometry

Victor U. Weiss[1], Katja Balantic[1], Ernst Pittenauer[1], Carla Tripisciano[2], Gernot Friedbacher[1], Viktoria Weber[2], Martina Marchetti-Deschmann[1], Günter Allmaier[1]

[1] *Institute of Chemical Technologies and Analytics, TU Wien, Vienna, Austria*

[2] *Center for Biomedical Technology and CD-Laboratory for Innovative Therapy Approaches in Sepsis, Danube University Krems, Krems, Austria*

Corresponding author: Victor U. Weiss, Institute of Chemical Technologies and Analytics, Vienna University of Technology (TU Wien), Getreidemarkt 9/164, A-1060 Vienna, Austria

e-mail: victor.weiss@tuwien.ac.at

Tel: +43 1 58801 151611

Fax: +43 1 58801 16199

TOC graphic:

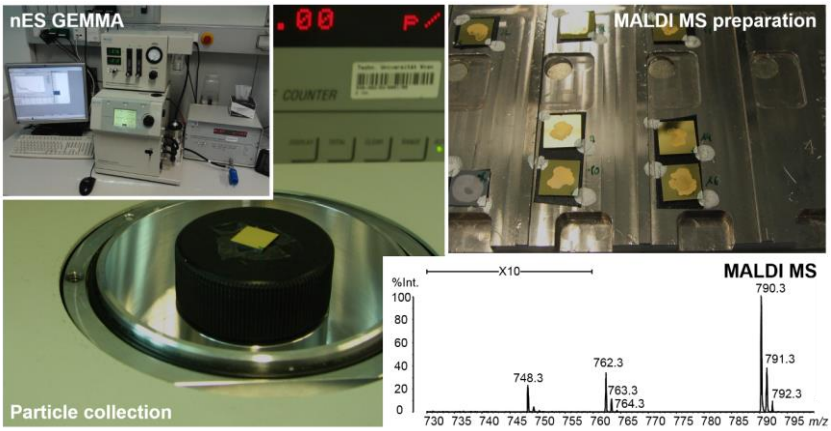

Keywords: nES GEMMA, DMA, liposome, VLDL particle, MALDI MS

Abstract

Gas-phase electrophoresis of single-charged analytes (nanoparticles) enables their separation according to the surface-dry particle size (Electrophoretic Mobility Diameter, EMD), which corresponds to the diameter of spherical shaped particles. Employing a nano Electrospray Differential Mobility Analyser (nES DMA), also known as nES Gas-phase Electrophoretic Mobility Molecular Analyser (nES GEMMA), allows sizing/size-separation and determination of particle-number concentrations. Separations are based on a constant high laminar sheath flow and a tunable, orthogonal electric field enabling scanning of EMDs in the nanometre size range. Additionally, keeping the voltage constant, only nanoparticles of a given EMD pass the instrument and can be collected on corresponding supporting materials for subsequent nanoparticle analyses applying e.g. microscopic, immunologic or spectroscopic techniques. In our proof-of-concept study we now focus for the first time on mass spectrometric (MS) characterization of DMA size-selected material. We carried out size-selection of liposomes, vesicles consisting of a lipid bilayer and an aqueous lumen employed as carriers in e.g. pharmaceutic, cosmetic or nutritional applications. Particles of 85 nm EMD were collected on gold-coated silicon wafers. Subsequently, matrix was applied and Matrix-Assisted Laser Desorption / Ionization (MALDI) MS carried out. However, we not only focused on plain liposomes but also demonstrated the applicability of our approach for very low density lipoprotein particles (VLDL), a transporter of lipid metabolism. Our novel *offline* hyphenation of gas-phase electrophoresis (nES DMA also known as nES GEMMA) and MALDI-MS opens the avenue to size-select nanoparticles of complex nature prior to detailed MS analysis.

Introduction

Gas-phase electrophoresis on a nano Electrospray Gas-phase Electrophoretic Mobility Molecular Analyser (nES GEMMA) was first described in 1996 by Kaufman and colleagues [1]: Surface-dry, single-charged particles are obtained after a nano electrospray process with subsequent drying of droplets and charge equilibration in a bipolar atmosphere induced by e.g. a 210Po α-particle source, a 241Am source emitting mainly α-particles, a soft X-Ray charger [2] or a corona discharge [3]. Next, polydisperse surface-dry analytes are separated in a constant high laminar sheath flow of particle-free air and an orthogonal, tunable electric field inside a Differential Mobility Analyser (DMA). By variation of the field strength, a monodisperse aerosol is generated at the exit slit of the DMA: Separation is only based on the particle electrophoretic mobility diameter (EMD), which, in case of spherical particles, corresponds to the actual size/diameter of analytes. Following size-separation, nanoparticles are detected in a ultrafine Condensation Particle Counter (CPC) enabling particle-number concentration based detection in accordance with recommendations of the European Commission for nanoparticle characterization (2011/696/EU from October 18th, 2011). Depending on the employed DMA, particles of several single-digit to up to several hundred nm EMD can be separated. It is of note that besides the name nES GEMMA, the same setup is also known as nES DMA, MacroIMS, ES SMPS or LiquiScan ES [4-6].

Besides the applicability of this system in the research of proteins and protein aggregates [7-11], noncovalent biocomplexes [12, 13], organic and inorganic nanoparticles [14-16] as well as viruses and virus-like particles [9, 17-24], the use of nES GEMMA for the characterization of liposomes in terms of vesicle size, particle number and the occurrence of smaller sized sample components has been demonstrated [25-29]. Liposomes are vesicles consisting of a lipid bilayer encapsulating an aqueous lumen. Corresponding nanoparticles are for instance used for shielded, targeted transport of (sometimes toxic) cargo material. Cargo might either be encapsulated inside the vesicle lumen, in the bilayer or be vesicle-associated depending on various cargo characteristics, e.g. molecule hydrophobicity. Sustained release at target sites, e.g. in pharmaceutical, cosmetic,

nutritional or similar applications is desired. It was now our intention to offline hyphenate for the first time nES GEMMA with mass spectrometric analysis (MS) of the mentioned nanovesicles after size selection.

Exchanging the particle-number concentration measuring CPC unit of the nES GEMMA instrument to an electrostatic nanometre aerosol sampler (ENAS) enables to collect size-selected particles (by keeping the separation voltage inside the DMA constant) on supporting materials suited for orthogonal analysis methods [10, 30]. Such, size-selected particles have previously been made accessible to e.g. atomic force microscopy (AFM) [18, 27], electron microscopy (EM) [10, 30, 31], immuno dot blot [12, 18], spectroscopic [32, 33] or even cell-culture based [34] analyses following particle collection after nES GEMMA-based sizing. Application of MS after particle size separation and collection has to date to our knowledge never been shown. It will for the first time aid the identification of collected material, as only MS and MS/MS analyses allow the necessary unambiguous identification of collected analyte species.

It was our intention to demonstrate this approach via liposomes consisting of the three lipids phosphatidylcholine (PC), phosphoethanolamine (PE) and cholesterol in a 4:3:3 starting molar ratio. Vesicles of similar lipid composition are employed in pharmaceutical applications [35]. In our proof-of-concept study we aimed for plain liposomes (only encapsulating a corresponding electrolyte) as well as very low density lipoprotein particles (VLDL) as bionanoparticles of interest whereas the latter nanoobjects are of importance in lipoprotein metabolism and hence for cardiovascular diseases [36]. It is of note that nES GEMMA based analysis of VLDL as well as other lipoprotein particles purified from blood or serum of human volunteers has already been described [10, 37].

MS data prior and after size-selection were compared. We believe that our novel approach paves the way for MS analyses of analytes (e.g. macromolecules like proteins or polysaccharides and their complexes) even out of nanoparticles and mixtures. Taking such a sample directly to MALDI MS might result in loss of information due to size-dependence as well as ion suppression. The combination of gas-phase electrophoresis (size-selection) and MALDI MS therefore will not

only yield information on surface-dry particle size, size distribution and particle number concentration but also will lead to a MS based unambiguous nanoparticle characterization and further on to information on size-dependent composition variations.

Materials and Methods

Chemicals: Ammonium acetate (NH4OAc, ≥ 99.99 %) and ammonium hydroxide (ACS reagent) were purchased from Sigma Aldrich (Steinheim, Germany). 2,4,6-Trihydroxyacetophenon monohydrate (THAP, ≥ 99.5 %) was obtained from Fluka (Buchs, Switzerland). Chloroform (Spectronorm quality) was obtained from VWR BDH Chemicals (Roncello, Italy), Methanol (LiChrosolv) from Merck (Darmstadt, Germany). Nitrogen gas was from Messer (Gumpoldskirchen, Austria). The lipids L-α-phosphatidylcholine, hydrogenated (Soy) (HSPC), 1,2-dioctadecanoyl-sn-glycero-3-phosphoethanolamine (18:0 PE, DSPE) and cholesterol (Chol) were from Avanti Polar Lipids (Alabaster, AL, USA obtained via Instruchemie, Delfzyl, The Netherlands). VLDL particles (≥ 95.0%, 1.28 mg/mL protein concentration) from human plasma was obtained from Calbiochem (Millipore, Billerica, MA, USA).

Buffers and electrolytes: NH4OAc (40 mM, pH 8.4) filtered through a 0.2 µm pore size syringe filter (surfactant free cellulose acetate membrane from Sartorius, Göttingen, Germany) was used for vesicle preparation and as aqueous electrolyte for nES-GEMMA. For all electrolyte preparations, water was applied obtained from a Simplicity apparatus (Millipore) with 18.2 MΩcm resistivity at 25°C.

Liposome preparation: Liposomes from HSPC:Chol:DSPE (4:3:3 molar ratio) were prepared from dried thin lipid films via hydration [38]. Therefore, corresponding amounts of lipids were dissolved in methanol:chloroform (1:3 mixture [v:v]). Subsequently, a thin, regular film was formed under a constant stream of nitrogen gas. The film was further dried in a desiccator for approx. 2 hours. Afterwards, hydration of the lipid film was performed with 1 mL NH4OAc. This yielded dispersions of 10 mM total lipid concentration. The lipid film was detached from the flask surfaces via vortexing and heating in a water bath (approx. 65°C). Subsequently, small unilamellar vesicles were prepared via extrusion of dispersions (21 times through two pre-wetted 100 nm pore size,

polycarbonate membranes (Avanti Polar Lipids) applied in the same membrane orientation). Liposome stock solutions were stored in brown glass vials at 4°C until further use (but at least overnight prior to analysis).

Instrumentation and samples: Gas-phase electrophoresis was carried out on a TSI Inc instrument (Shoreview, MN, USA): A nES aerosol generator (Model 3480) equipped with a 210Po α-particle source, a nDMA (Model 3080) and a n-butanol-based ultrafine CPC (either model 3025A or a similar model, 3776C) were applied. The samples were introduced to the nES via a 25 µm inner diameter, fused silica capillary with a homemade tip [39] generating a stable Taylor cone. In order to exclude cross-contaminations, a fresh capillary was employed for each day of measurement. 4.0 pounds per square inch differential (psid, approx. 28 kPa) and 0.1 liters per minute (Lpm) CO2 and 1.0 Lpm compressed, particle-free air were employed for transport of analytes through the capillary through the neutralization chamber and to the nDMA unit. The air was additionally dried (Donaldson Variodry Membrane Dryer Superplus, Leuven, Belgium) to facilitate drying of nES derived droplets. Additional nES GEMMA settings (also for nanoparticle collection on approx. 1 cm² gold-coated silicon wafers via an ENAS (model 3089, TSI Inc)) were as previously described [27]. Analytes were collected for approx. 150 min at 85 nm EMD from 1 mM total lipid vesicle stocks (liposomes) or 300 min at 38 nm EMD from 42 µg/mL lipoprotein stocks after buffer exchange (VLDLs) or 300 min at 85 nm EMD for a mixed sample. Prior to gas-phase electrophoresis, low EMD material (salt content) was removed from VLDL particles via spin filtration employing 3 kDa molecular weight cutoff filters (MWCO, polyethersulfone membrane, VWR, Vienna, Austria) leading to a 1:30 [v:v] dilution of the initial stock (i.e. a final 42 µg/mL lipoprotein concentration) similar to the protocol previously described [16]. In addition, as VLDL nanoparticles contained a high amount of smaller sized sample components, bionanoparticles were passed successively over two membrane filters in contrast to the protocol presented in literature. Liposome stocks were simply diluted 1:10 [v:v] in ammonium acetate. For a mixed sample, liposomes and VLDL bionanoparticles were diluted to

equal concentrations within one sample.

Matrix-Assisted Laser Desorption / Ionization (MALDI) MS was carried out on an Axima TOF² (Shimadzu Kratos Analytical, Manchester, UK) in reflector positive ion mode and employing THAP (2,4,6-trihydroxyacetophenon, 20 mg/mL in methanol) as MALDI matrix. Diluted liposomes as well as VLDL particles after buffer exchange were mixed 1: 1 [v: v] with MALDI matrix solution prior application to a nickel-coated aluminium MALDI MS target. The mixed sample was likewise combined with THAP (10 mg/mL in methanol) prior application to the MALDI MS target. Gold-coated silicon wafers were attached to a MALDI MS target support via double-sided carbon tape. Silver pigment containing thermoplastic resin (Acheson silver DAG 1415M obtained via Christine Groepl, Tulln, Austria) applied to two corners of the wafer increased the conductivity between the target support and the wafer. In case of collected (by means of the ENAS) size-separated fractions, 1 µL of MALDI matrix solution was applied to the centre of the wafer and dried at room temperature. In case of the mixed sample the MALDI matrix volume was reduced to 0.7 µL.

Results and Discussion

It was the aim of our study to demonstrate for the first time that offline hyphenation of nES GEMMA based size-separation and MALDI MS is feasible with MS enabling the unambiguous identification of sample components. In addition, we believe that via this novel instrumental combination it will be possible to extract MS data also from complex composed bionanoparticles or nanoparticle mixtures after a gas-phase electrophoretic size separation step yielding information on surface-dry particle size and particle-number concentration.

Instrumentation for *offline* nES GEMMA / MALDI MS hyphenation: Employing an ENAS unit, we were able to collect liposomal nanoparticles on a gold-coated silicon wafer (Figure 1). During vesicle/nanoparticle collection, the wafer was held in place on top of the electrode of the ENAS via pieces of double sided tape (Figure 1A and B). After collection of vesicles we checked via AFM, whether indeed intact liposomes were detectable on the wafer surface (Figure 1C). In that context, it is of note that the flake-like structure on the silicon wafer originates from its gold coating. Subsequently, the wafer with the collected intact nanoparticles was attached to a MALDI MS target carrier plate via a double-sided carbon tape (Figure 1D). In addition, a silver pigment containing resin was applied to the corners of the silicon wafers to obtain an optimal conducting connection between the gold-coated silicon wafer and the MALDI MS carrier plate. Application of the MALDI MS matrix dissolved in methanol (Figure 1E) leads to the formation of very homogeneous crystals necessary for MALDI MS data acquisition (Figure 1F), as observed via a light microscope.

MALDI MS analysis of liposomes: In a first series of experiments, we employed liposomes encapsulating ammonium acetate, i.e. the employed electrolyte solution for subsequent experiments. Mixing such a preparation with the employed MALDI MS matrix in methanol without prior nES GEMMA based size-separation and application of the mix to a stainless steel covered MALDI MS target enabled us to obtain MS signals of all lipids employed in vesicle preparation (Figure 2). m/z

values 790.3 (monoisotopic mass 789.625 g/mol) and 762.3 (monoisotopic mass 761.593 g/mol) corresponded to the two components of HSPC, PCs with (i) two 18:0 and (ii) one 18:0 and one 16:0 fatty acid chain, respectively. Likewise, signals for DSPE at m/z 748.3 (monoisotopic mass 747.578 g/mol) and for cholesterol at m/z 369.2 (monoisotopic mass 386.664 g/mol) were detected in good accordance with data obtained for individual lipid solutions (prior to liposome formation steps) applied on a MALDI MS target and measured via MALDI MS in MS and high energy collision induced dissociation (CID) MS/MS mode (data not shown). Additional ions originated from the protonated and sodiated matrix molecules (THAP) as well as its potassium adducts.

Subsequently, vesicles were analysed via gas-phase electrophoresis on a nES GEMMA instrument with a ultrafine CPC yielding a size-distribution of sample constituents with number-based particle detection. In addition, nanoparticles were collected at 85 nm EMD on gold-coated silicon wafers and the nanoparticle integrity was assessed via AFM as previously described. In contrast to application of liposomes from solution, vesicle collection from the gas-phase yielded spherical nanostructures with a homogeneous size distribution indicating liposome stability upon transition from the liquid into the gas-phase at atmospheric pressure and upon collection on a solid surface (compare to Figure 1C). MALDI MS matrix was applied to size-selected particles on gold-coated silicon wafers and MALDI MS was subsequently carried out. As demonstrated in our proof-of-concept study, all lipid species originally employed for vesicle preparation (Figure 2) were also detected in size-selected liposomes (Figure 3, upper and middle panel). Following size-separated collection, vesicles were again analysed via gas-phase electrophoresis on a nES GEMMA instrument to compare the size distribution of analytes after the collection process with the signal obtained prior to collection (Figure 3, lower panel). As can be learned from these spectra, size-selected nanoparticle collection was based on a stable nES GEMMA signal over the whole collection time.

Therefore, not just off-line visualization of size-selected nanoparticles via microscopy techniques is feasible but also MALDI MS on collected particles can be carried out with the described setup. This off-line hyphenation of gas-phase electrophoresis with MALDI MS offers the

possibility to separate nanoparticle samples according to their surface-dry particle diameter prior to MS analysis. This approach will enable subsequent constituent's identification derived for example from unknown liposome samples or even enclosed components besides gaining information on vesicle size distribution and number-concentration from gas-phase electrophoresis experiments.

Targeting VLDL particles with the nES GEMMA / MALDI MS hyphenation: In a next step, we tested whether our developed nES GEMMA / MALDI MS hyphenation is also capable to detect other lipid containing bionanoparticles. In order to do so, we evaluated human very low density lipoprotein particles. These nanoparticles are described as being of a surface-dry nanoparticle size below 100 nm diameter [37]. Indeed, as demonstrated in Figure 4 (upper two panels), carrying out directly MALDI MS of VLDL nanoparticles after buffer exchange to ammonium acetate allowed us to detect quite a number of lipid species. Besides a peak at m/z of 369.5, which we attribute to cholesterol, several potential PC species in the m/z range of approx. 758.3 to 810.3 were detected as molecular ions (carrying out MS/MS experiments with high energy CID fragmentation enabled us to detect characteristic PC headgroup fragments at m/z 183.8 for the precursor ions at m/z 758.3 and 786.3, respectively, data not shown.) Subsequently, VLDL particles were size-separated and a fraction was collected at 38 nm EMD. Due to the fact that VLDL particles exhibited a lower EMD values (at the peak apex) than our selected liposomes targeted before, we increased the time of bionanoparticle collection from 150 to 300 min to collected sufficient sample amount on the gold-coated silicon wafer. In addition, the concentration of bionanoparticles in samples was likewise increased (compare nES GEMMA spectra of Figures 3 and 4, bottom, respectively). Via these two approaches, we intended to correct for the lower number of individual lipid molecules collected on the gold-coated silicon wafer in comparison to larger liposomes.

Indeed, when applying size-collected VLDL nanoparticles subsequently to MALDI MS, we were able to detect signals for lipid compounds as previously detected for VLDL prior to nES GEMMA based particle collection (Figure 4, middle two panels). However, as seen from the zoom

to the m/z range of 700 - 900 besides PC species at m/z 758.4 and 786.5, also other species, e.g. at m/z 746.9 or 770.9 were detected, which were originally clearly not present upon direct MALDI MS measurement. As seen in Figure 4, lower panel, nES GEMMA spectra obtained for VLDL bionanoparticles exhibited a constant size distribution over the complete period of particle collection.

nES GEMMA / MALDI MS hyphenation for a mixed bionanoparticle sample: Finally, in order to demonstrate the applicability of our hyphenated nES GEMMA / MALDI MS approach to heterogeneous samples, we combined liposomes and VLDL bionanoparticles within one sample. As seen in Figure 5 (nES GEMMA spectrum, top), data for both species combined in a way that the signals for both lipid containing species were no longer distinguishable based on gas-phase electrophoresis. Subsequently, we subjected the mixed sample to bionanoparticle collection at 85 nm EMD (as done for pure liposome samples before). MALDI MS measurements of these collected bionanoparticles revealed the successful separation of both species based on their surface-dry particle size via nES GEMMA. m/z values which were obtained for VLDLs either in a sample only containing these bionanoparticles or in a mixed sample were no longer detectable for size-selected material. For these bionanoparticles, only m/z values related to liposome species were recorded.

Concluding Remarks

In our proof-of-concept study we focused on the novel offline hyphenation of nES GEMMA based gas-phase electrophoresis and MALDI MS. Employing liposomes, lipid bilayer based vesicles encapsulating a plain electrolyte solution, we demonstrated that size-separation of these nanoobjects and their subsequent collection on gold-coated silicon wafers is possible. Especially for complex samples we expect our novel method combination to yield very promising results. Hence, besides information obtained on the vesicles themselves (i.e. surface dry particle size as well as particle-number based concentration) also unambiguous MS based component identification is directly feasible. We believe that prolonging of times for size-collection will lead to an additional increase in signals, i.e. molecular ion intensities, recorded in MALDI MS, hence enabling also the detection of minor particle or sample components. In addition, variation of the supporting material on which vesicles are collected as well as the localization of liposomes on the supporting material (i.e. concentration of nanoparticles on a central spot, in a ring-like structure or their even distribution on the surface) and possibly the optimization of the selection as well as the deposition of the applied MALDI matrix will facilitate the generation of MALDI MS data from different lipid and macromolecule classes. Our approach will thus possibly even enable targeting of cargo molecules encapsulated within liposomes. Finally, also the distribution of lipids in vesicles or lipoproteins size-collected at different EMDs from one given size distribution, respectively, will be of future biological interest.

Acknowledgements

The authors acknowledge the gift of gold-coated silicon wafers from Herbert Hutter (TU Wien). Partial funding of the NFB, LSC16-018 is acknowledged.

Author contributions

Initial idea: GA; Liposome preparation, nES GEMMA measurements: VUW, KB; AFM measurements: GF, VUW; MS measurements: EP, KB, VUW; Instrumentation: GA; Funding: GA, MMD, VW, CT; Scientific guidance: GA, MMD; Organization: VUW; All authors contributed to the manuscript.

References

[1] S.L. Kaufman, J.W. Skogen, F.D. Dorman, F. Zarrin, K.C. Lewis, Macromolecule analysis based on electrophoretic mobility in air: globular proteins, Anal Chem, 68 (1996) 1895-1904.

[2] G. Allmaier, V.U. Weiss, N.Y. Engel, M. Marchetti-Deschmann, W.W. Szymanski, Soft X-ray Radiation Applied in the Analysis of Intact Viruses and Antibodies by Means of Nano Electrospray Differential Mobility Analysis, in, Springer Netherlands, Dordrecht, 2017, pp. 149-157.

[3] P. Kallinger, W.W. Szymanski, Experimental determination of the steady-state charging probabilities and particle size conservation in non-radioactive and radioactive bipolar aerosol chargers in the size range of 5-40 nm, J Nanopart Res, 17 (2015) 171.

[4] C. Carazzone, R. Raml, S.A. Pergantis, Nanoelectrospray ion mobility spectrometry online with inductively coupled plasma-mass spectrometry for sizing large proteins, DNA, and nanoparticles, Anal Chem, 80 (2008) 5812-5818.

[5] S. Elzey, D.H. Tsai, L.L. Yu, M.R. Winchester, M.E. Kelley, V.A. Hackley, Real-time size discrimination and elemental analysis of gold nanoparticles using ES-DMA coupled to ICP-MS, Anal Bioanal Chem, 405 (2013) 2279-2288.

[6] V.B. Shah, G.S. Orf, S. Reisch, L.B. Harrington, M. Prado, R.E. Blankenship, P. Biswas, Characterization and deposition of various light-harvesting antenna complexes by electrospray atomization, Anal Bioanal Chem, 404 (2012) 2329-2338.

[7] G. Bacher, W.W. Szymanski, S.L. Kaufman, P. Zollner, D. Blaas, G. Allmaier, Charge-reduced nano electrospray ionization combined with differential mobility analysis of peptides, proteins, glycoproteins, noncovalent protein complexes and viruses, J Mass Spectrom, 36 (2001) 1038-1052.

[8] J.F. de la Mora, S. Ude, B.A. Thomson, The potential of differential mobility analysis coupled to MS for the study of very large singly and multiply charged proteins and protein complexes in the gas phase, Biotechnol J, 1 (2006) 988-997.

[9] C.S. Kaddis, S.H. Lomeli, S. Yin, B. Berhane, M.I. Apostol, V.A. Kickhoefer, L.H. Rome, J.A. Loo, Sizing large proteins and protein complexes by electrospray ionization mass spectrometry and ion mobility, J Am Soc Mass Spectrom, 18 (2007) 1206-1216.

[10] G. Allmaier, C. Laschober, W.W. Szymanski, Nano ES GEMMA and PDMA, new tools for the analysis of nanobioparticles-protein complexes, lipoparticles, and viruses, J Am Soc Mass Spectrom, 19 (2008) 1062-1068.

[11] E.A. Kapellios, S. Karamanou, M.F. Sardis, M. Aivaliotis, A. Economou, S.A. Pergantis, Using nanoelectrospray ion mobility spectrometry (GEMMA) to determine the size and relative molecular mass of proteins and protein assemblies: a comparison with MALLS and QELS, Anal Bioanal Chem, 399 (2011) 2421-2433.

[12] N.Y. Engel, V.U. Weiss, M. Marchetti-Deschmann, G. Allmaier, nES GEMMA Analysis of Lectins and Their Interactions with Glycoproteins - Separation, Detection, and Sampling of Noncovalent Biospecific Complexes, J Am Soc Mass Spectrom, 28 (2017) 77-86.

[13] J.Z. Bereszczak, M. Havlik, V.U. Weiss, M. Marchetti-Deschmann, E. van Duijn, N.R. Watts, P.T. Wingfield, G. Allmaier, A.C. Steven, A.J. Heck, Sizing up large protein complexes by electrospray ionisation-based electrophoretic mobility and native mass spectrometry: morphology selective binding of Fabs to hepatitis B virus capsids, Anal Bioanal Chem, 406 (2014) 1437-1446.

[14] H. Hinterwirth, S.K. Wiedmer, M. Moilanen, A. Lehner, G. Allmaier, T. Waitz, W. Lindner, M. Lammerhofer, Comparative method evaluation for size and size-distribution analysis of gold nanoparticles, J Sep Sci, 36 (2013) 2952-2961.

[15] V.S. Chernyshev, R. Rachamadugu, Y.H. Tseng, D.M. Belnap, Y. Jia, K.J. Branch, A.E. Butterfield, L.F. Pease, 3rd, P.S. Bernard, M. Skliar, Size and shape characterization of hydrated and desiccated exosomes, Anal Bioanal Chem, 407 (2015) 3285-3301.

[16] V.U. Weiss, A. Lehner, L. Kerul, R. Grombe, M. Kratzmeier, M. Marchetti-Deschmann, G. Allmaier, Characterization of cross-linked gelatin nanoparticles by electrophoretic techniques in the liquid and the gas phase, Electrophoresis, 34 (2013) 3267-3276.

[17] V.U. Weiss, J.Z. Bereszczazk, M. Havlik, P. Kallinger, I. Gosler, M. Kumar, D. Blaas, M. Marchetti-Deschmann, A.J. Heck, W.W. Szymanski, G. Allmaier, Analysis of a common cold virus and its subviral particles by gas-phase electrophoretic mobility molecular analysis and native mass spectrometry, Anal Chem, 87 (2015) 8709-8717.

[18] M. Havlik, M. Marchetti-Deschmann, G. Friedbacher, W. Winkler, P. Messner, L. Perez-Burgos, C. Tauer, G. Allmaier, Comprehensive size-determination of whole virus vaccine particles using gas-phase electrophoretic mobility macromolecular analyzer, atomic force microscopy, and transmission electron microscopy, Anal Chem, 87 (2015) 8657-8664.

[19] K.D. Cole, L.F. Pease, 3rd, D.H. Tsai, T. Singh, S. Lute, K.A. Brorson, L. Wang, Particle concentration measurement of virus samples using electrospray differential mobility analysis and quantitative amino acid analysis, J Chromatogr A, 1216 (2009) 5715-5722.

[20] S. Guha, L.F. Pease, 3rd, K.A. Brorson, M.J. Tarlov, M.R. Zachariah, Evaluation of electrospray differential mobility analysis for virus particle analysis: Potential applications for biomanufacturing, J Virol Methods, 178 (2011) 201-208.

[21] C.J. Hogan, Jr., E.M. Kettleson, B. Ramaswami, D.R. Chen, P. Biswas, Charge reduced electrospray size spectrometry of mega- and gigadalton complexes: whole viruses and virus fragments, Anal Chem, 78 (2006) 844-852.

[22] T.J. J., B. Bothner, J. Traina, W.H. Benner, G. Siuzdak, Electrospray ion mobility spectrometry of intact viruses, Spectroscopy, 18 (2004) 31-36.

[23] L.F. Pease, 3rd, D.I. Lipin, D.H. Tsai, M.R. Zachariah, L.H. Lua, M.J. Tarlov, A.P. Middelberg, Quantitative characterization of virus-like particles by asymmetrical flow field flow fractionation, electrospray differential mobility analysis, and transmission electron microscopy, Biotechnol Bioeng, 102 (2009) 845-855.

[24] L.F. Pease, 3rd, D.H. Tsai, K.A. Brorson, S. Guha, M.R. Zachariah, M.J. Tarlov, Physical characterization of icosahedral virus ultra structure, stability, and integrity using electrospray differential mobility analysis, Anal Chem, 83 (2011) 1753-1759.

[25] H. Epstein, E. Afergan, T. Moise, Y. Richter, Y. Rudich, G. Golomb, Number-concentration of nanoparticles in liposomal and polymeric multiparticulate preparations: empirical and calculation methods, Biomaterials, 27 (2006) 651-659.

[26] C. Urey, V.U. Weiss, A. Gondikas, F. von der Kammer, T. Hofmann, M. Marchetti-Deschmann, G. Allmaier, G. Marko-Varga, R. Andersson, Combining gas-phase electrophoretic mobility molecular analysis (GEMMA), light scattering, field flow fractionation and cryo electron microscopy in a multidimensional approach to characterize liposomal carrier vesicles, Int J Pharm, 513 (2016) 309-318.

[27] V.U. Weiss, C. Urey, A. Gondikas, M. Golesne, G. Friedbacher, F. von der Kammer, T. Hofmann, R. Andersson, G. Marko-Varga, M. Marchetti-Deschmann, G. Allmaier, Nano electrospray gas-phase electrophoretic mobility molecular analysis (nES GEMMA) of liposomes: applicability of the technique for nano vesicle batch control, Analyst, 141 (2016) 6042-6050.

[28] T.S. Chadha, S. Chattopadhyay, C. Venkataraman, P. Biswas, Study of the charge distribution on liposome particles aerosolized by air-jet atomization, Journal of aerosol medicine and pulmonary drug delivery, 25 (2012) 355-364.

[29] S. Chattopadhyay, L.B. Modesto-Lopez, C. Venkataraman, P. Biswas, Size Distribution and Morphology of Liposome Aerosols Generated By Two Methodologies, Aerosol Sci Tech, 44 (2010) 972-982.

[30] P. Kallinger, V.U. Weiss, A. Lehner, G. Allmaier, W.W. Szymanski, Analysis and handling of bio-nanoparticles and environmental nanoparticles using electrostatic aerosol mobility, Particuology, 11 (2013) 14-19.

[31] G. Allmaier, A. Maisser, C. Laschober, P. Messner, W.W. Szymanski, Parallel differential mobility analysis for electrostatic characterization and manipulation of nanoparticles and viruses, Trends Analyt Chem, 30 (2011) 123-132.

[32] V.U. Weiss, K. Wieland, A. Schwaighofer, B. Lendl, G. Allmaier, Native nano electrospray differential mobility analyzer (nS GEMMA) enables size-selection of liposomal nanocarriers

combined with subsequent spectroscopic analysis, Anal Chem, in press (2018).

[33] K. Wieland, G. Ramer, V.U. Weiss, G. Allmaier, B. Lendl, A. Centrone, Nanoscale chemical imaging of individual chemotherapeutic cytarabine-loaded liposomal nanocarriers, Nano Research, 12 (2018) 197-203.

[34] A.L. Holder, L.C. Marr, Toxicity of Silver Nanoparticles at the Air-Liquid Interface, Biomed Res Int, (2013).

[35] P. Yingchoncharoen, D.S. Kalinowski, D.R. Richardson, Lipid-Based Drug Delivery Systems in Cancer Therapy: What Is Available and What Is Yet to Come, Pharmacol Rev, 68 (2016) 701-787.

[36] I. Ramasamy, Recent advances in physiological lipoprotein metabolism, Clin Chem Lab Med, 52 (2014) 1695-1727.

[37] M.P. Caulfield, S. Li, G. Lee, P.J. Blanche, W.A. Salameh, W.H. Benner, R.E. Reitz, R.M. Krauss, Direct determination of lipoprotein particle sizes and concentrations by ion mobility analysis, Clin Chem, 54 (2008) 1307-1316.

[38] A.D. Bangham, M.M. Standish, J.C. Watkins, Diffusion of univalent ions across the lamellae of swollen phospholipids, J Mol Biol, 13 (1965) 238-252.

[39] A. Tycova, J. Prikryl, F. Foret, Reproducible preparation of nanospray tips for capillary electrophoresis coupled to mass spectrometry using 3D printed grinding device, Electrophoresis, 37 (2016) 924-930.

Figure Legend

Figure 1 – Positioning of the gold-coated silicon wafer in the electrostatic nanoparticle aerosol sampler (ENAS) prior to particle collection (A, B). After collection, liposomes were visualized by means of AFM (C) and wafers attached to a Shimadzu MALDI MS target support (D). Subsequently, MALDI MS matrix (THAP, 20 mg/ml in methanol) was applied (E), leading to the formation of even crystals on top of the gold surface as observed via a light microscope (F).

Figure 2 – Electrolyte-filled liposomes were analysed via MALDI MS prior to nES GEMMA based size-collection. Signals for PC 18:0/18:0 and PC 16:0_18:0 (both components of HSPC), PE 18:0/18:0 (DSPE) and cholesterol were detected. Additional peaks correspond to protonated and sodiated matrix molecules as well as the potassium adduct of THAP. m/z regions enlarged in subjacent panels are marked in blue, respectively.

Figure 3 – Electrolyte-filled Liposomes were analysed via MALDI MS after nES GEMMA based size-selection and particle collection at 85 nm EMD (top, compare to Figure 2 for data prior gas-phase electrophoresis). nES GEMMA spectra prior and after size-collection are shown to demonstrate the stability of the nES during particle collection (bottom). m/z regions enlarged in subjacent panels are marked in blue, respectively.

Figure 4 – VLDL particles were analysed after buffer exchange to ammonium acetate and concomitant dilution to approx. 42 µg/mL lipoprotein concentration via MALDI MS (top two panels). Subsequently, VLDL particles were size-selected at 38 nm EMD and particle collection performed. MALDI MS after 300 min of bionanoparticle collection revealed similar lipid species as detected prior to collection (middle two panels). m/z regions enlarged in subjacent panels are marked in blue, respectively. nES GEMMA spectra prior and after size-collection are shown to

demonstrate the stability of the nES during particle collection (bottom). Mind the half-logarithmic scale of the depicted nES GEMMA spectra due to high amounts of sample-inherent smaller sized components.

Figure 5 – Combining liposomes and VLDL bionanoparticles gives a sample yielding a nES GEMMA spectrum in which both species are no longer differentiable (top). nES GEMMA based size-collection at 85 nm EMD followed by MALDI MS allows to specifically size-select liposome species from the mix. m/z values detected for VLDLs (either as only sample component or present in a mixed samples) are no longer detectable (bottom).

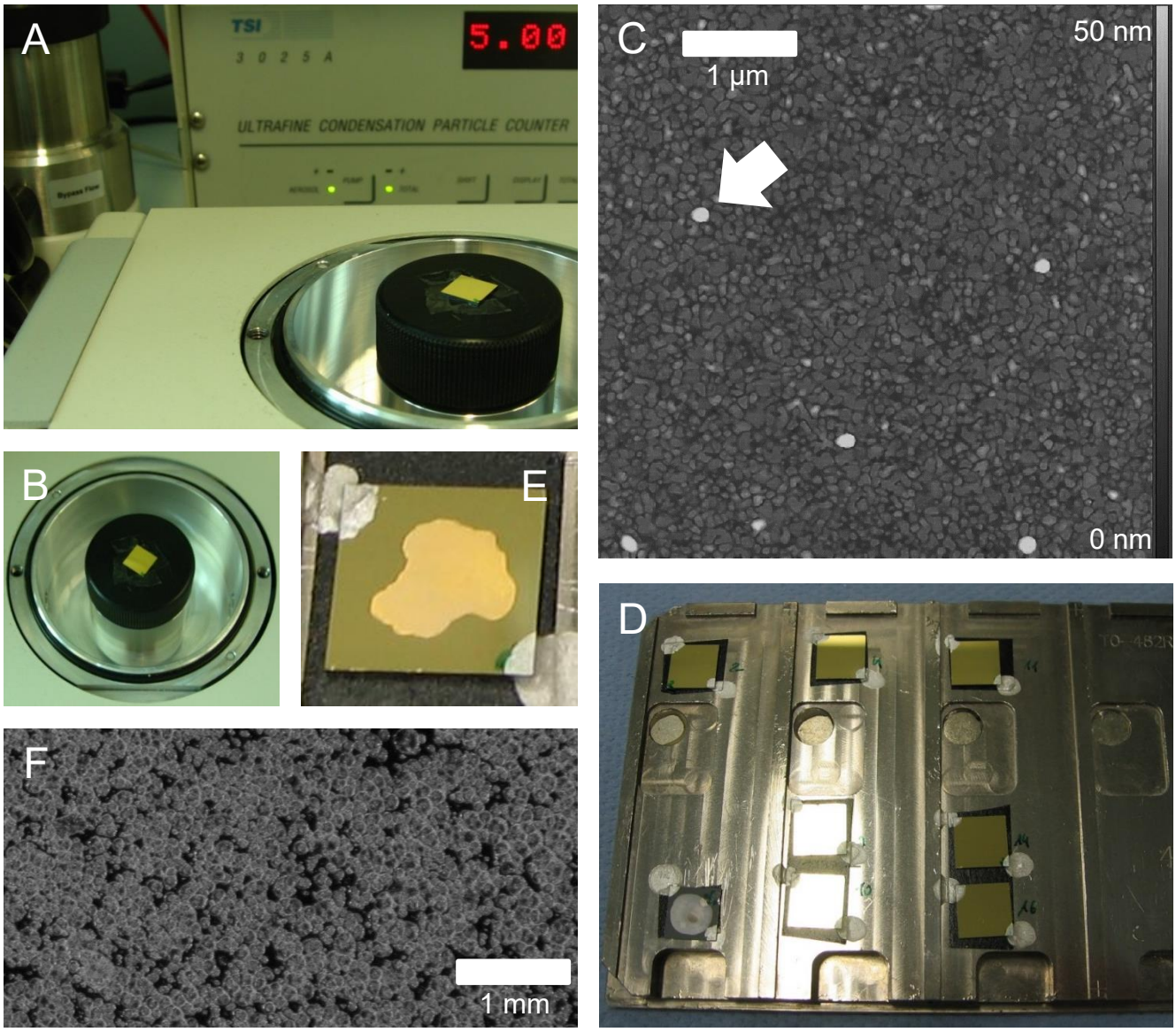
A
TSI
3025A
5.00
ULTRAFINE CONDENSATION PARTICLE COUNTER
B
E
C
1 µm
50 nm
0 nm
D
F
1 mm

Figure 1

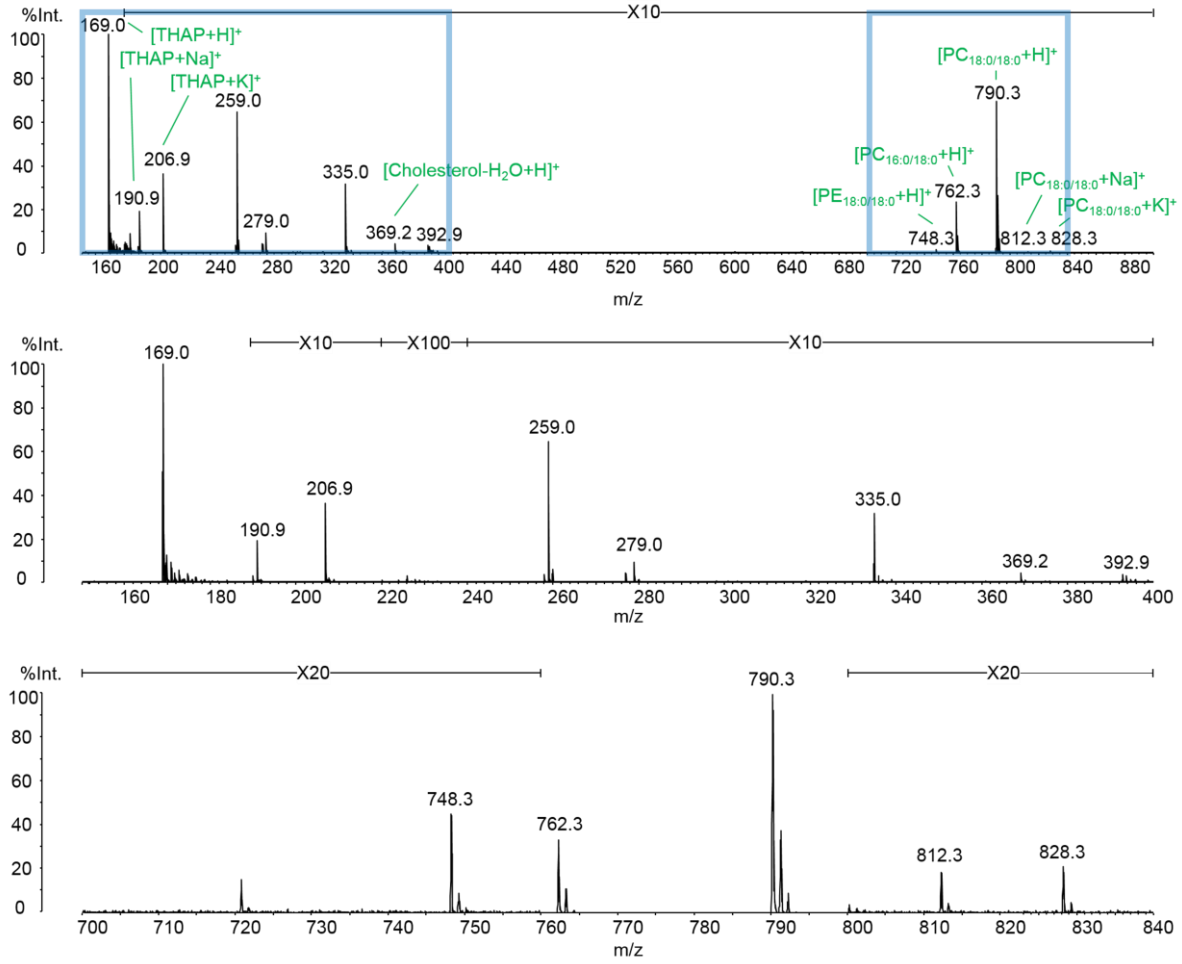
%Int.
X10
169.0
[THAP+H]+
[THAP+Na]+
[THAP+K]+
259.0
206.9
190.9
279.0
335.0
[Cholesterol-H2O+H]+
369.2 392.9
[PC18:0/18:0+H]+
790.3
[PC16:0/18:0+H]+
[PE18:0/18:0+H]+
762.3
748.3
[PC18:0/18:0+Na]+
[PC18:0/18:0+K]+
812.3 828.3
m/z
%Int.
X10
X100
X10
169.0
259.0
206.9
190.9
279.0
335.0
369.2
392.9
m/z
%Int.
X20
X20
790.3
748.3
762.3
812.3
828.3
m/z

Figure 2

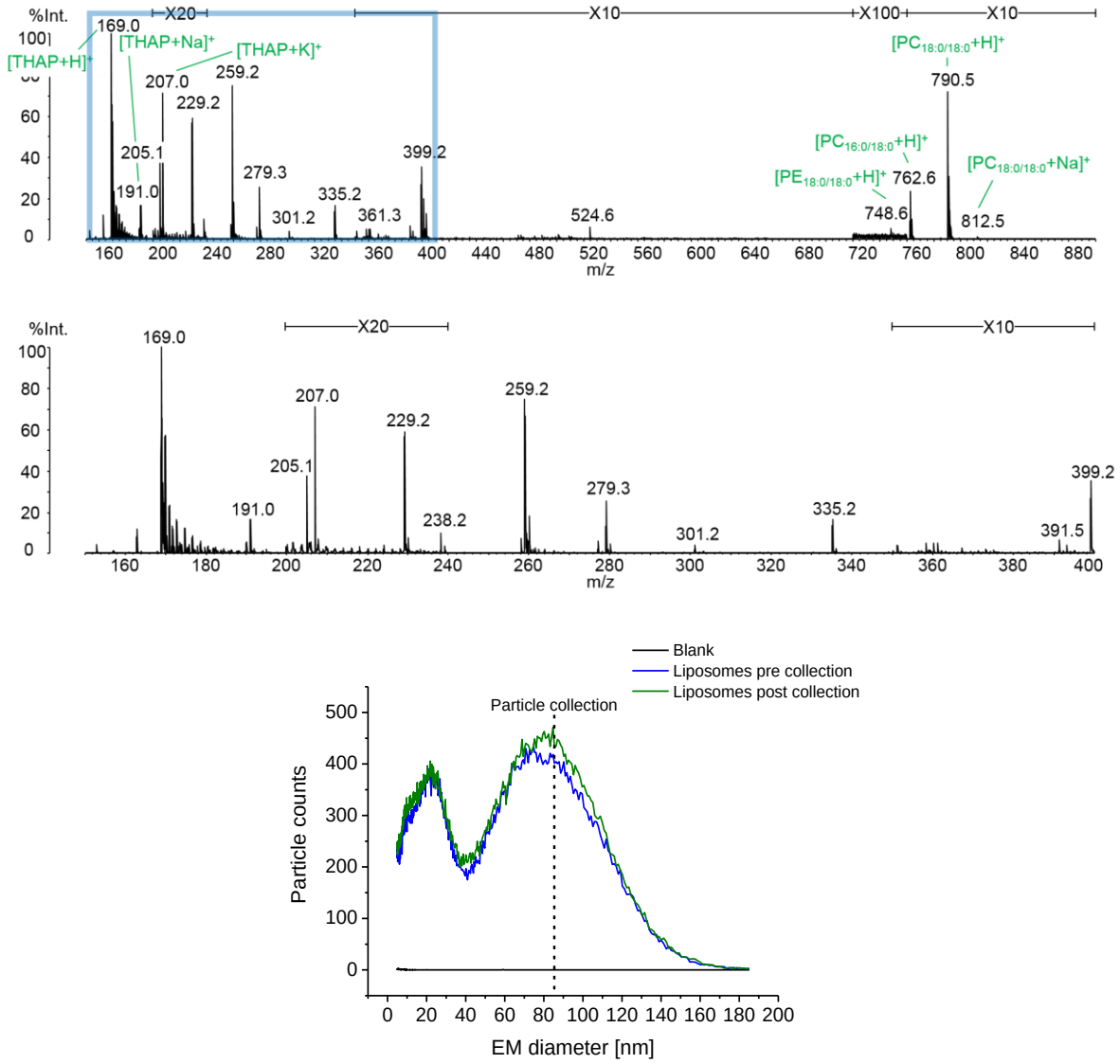
%Int.
X20
X10
X100
X10
[THAP+H]+
[THAP+Na]+
[THAP+K]+
[PC18:0/18:0+H]+
[PC16:0/18:0+H]+
[PE18:0/18:0+H]+
[PC18:0/18:0+Na]+
m/z
%Int.
X20
X10
m/z
Blank
Liposomes pre collection
Liposomes post collection
Particle collection
Particle counts
EM diameter [nm]

Figure 3

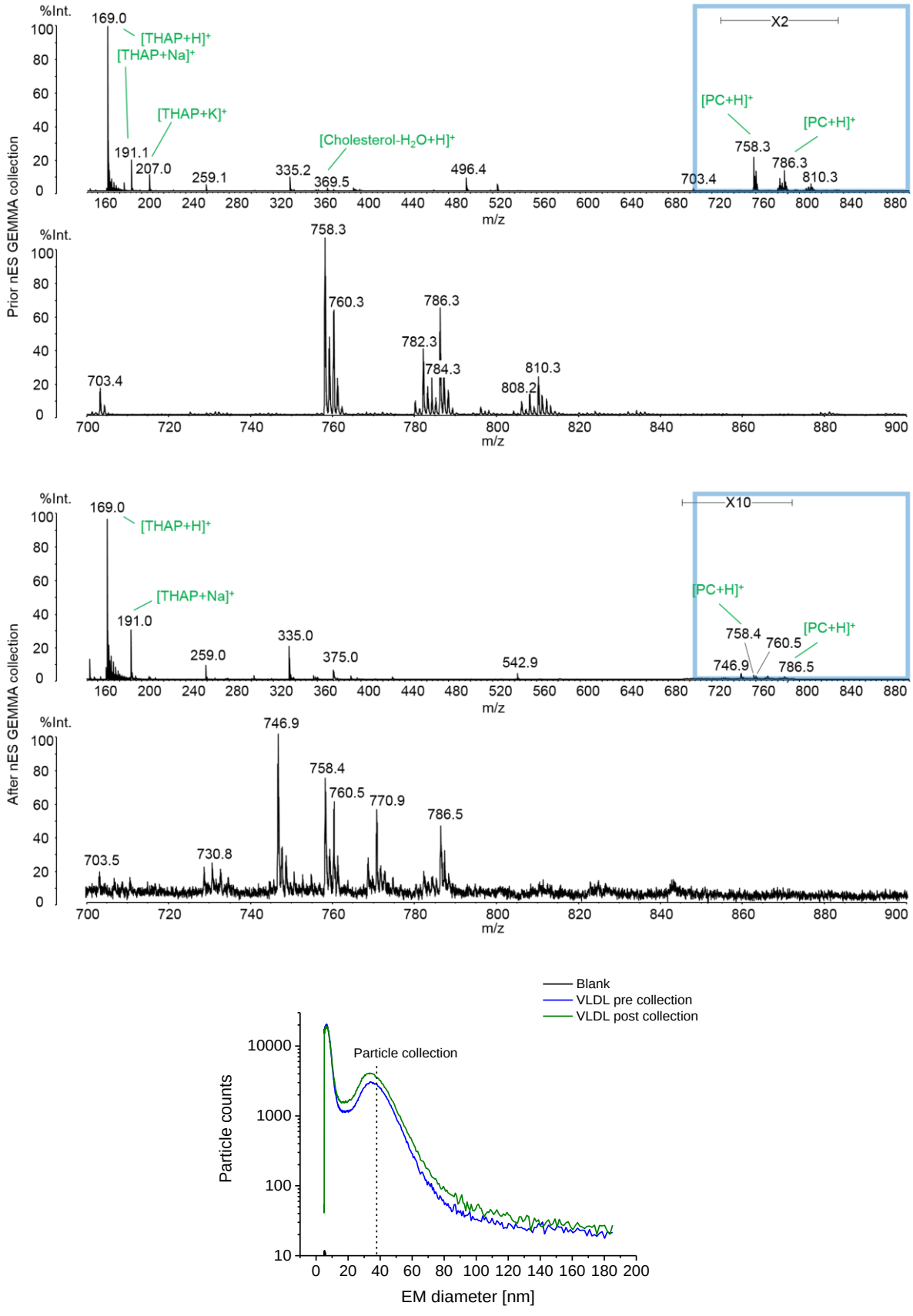
%Int.
169.0
[THAP+H]+
[THAP+Na]+
[THAP+K]+
191.1
207.0
259.1
335.2
[Cholesterol-H2O+H]+
369.5
496.4
X2
[PC+H]+
758.3
[PC+H]+
786.3
703.4
810.3
m/z
Prior nES GEMMA collection
758.3
760.3
786.3
782.3
784.3
703.4
808.2
810.3
X10
[PC+H]+
758.4
760.5
[PC+H]+
746.9
786.5
542.9
After nES GEMMA collection
746.9
758.4
760.5
770.9
786.5
703.5
730.8
Blank
VLDL pre collection
VLDL post collection
Particle collection
Particle counts
EM diameter [nm]

Figure 4

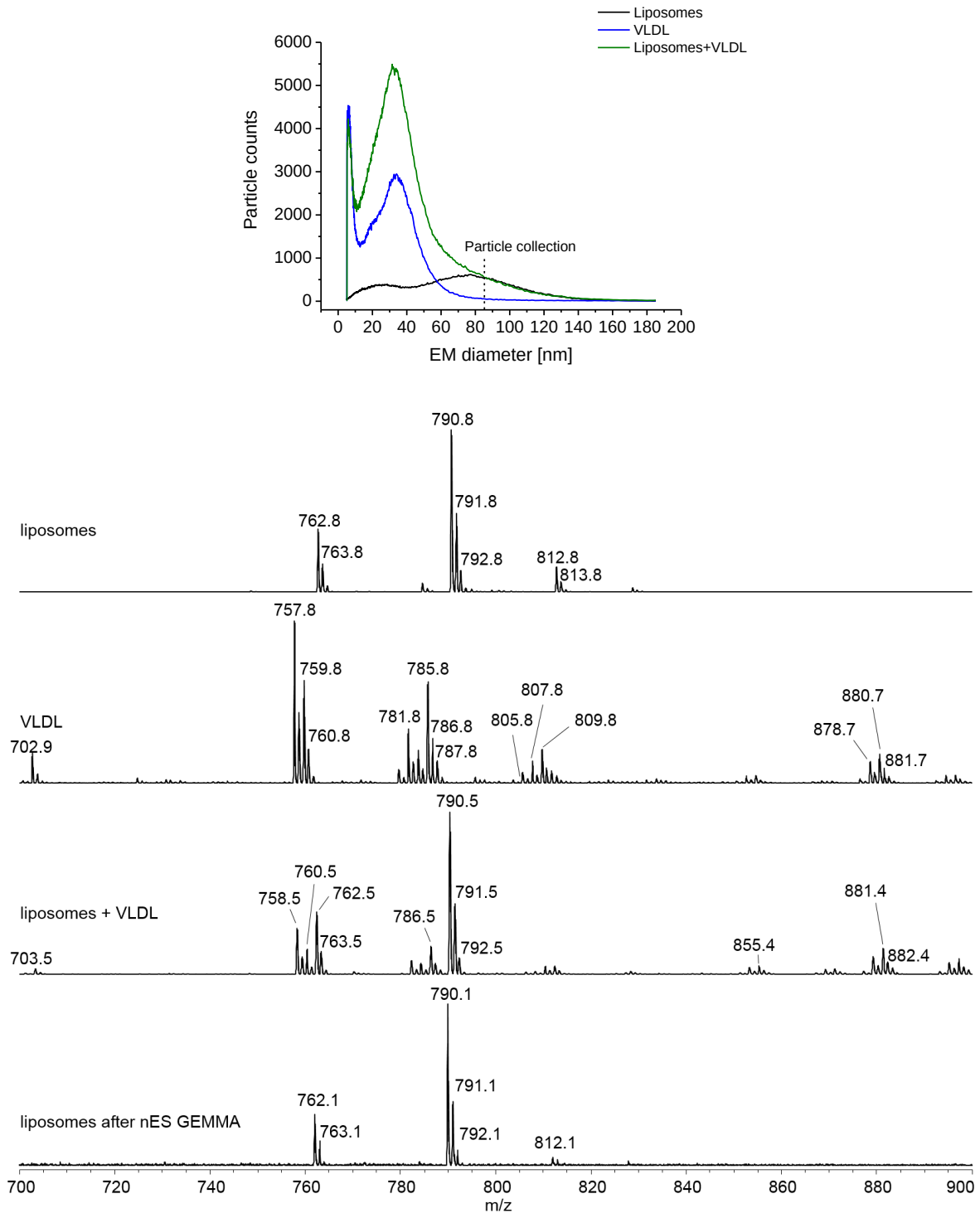
Liposomes
VLDL
Liposomes+VLDL
Particle counts
EM diameter [nm]
Particle collection
liposomes
VLDL
liposomes + VLDL
liposomes after nES GEMMA
m/z

Figure 5

5. CONCLUSION

The aim of the following work was to develop a novel offline hyphenation between a separation method nES GEMMA and a different analytical method MALDI MS. Furthermore, an application of the described hyphenation was demonstrated and described.

The novel combination of the two analytical methods could be especially useful for separation and characterization of complex mixtures. With this hyphenation not only information regarding the particle size and particle-number based concentration would be obtained, but also MS component characterization and identification.

Furthermore, prolonging the time of nES GEMMA collection could lead to the possibility of MALDI MS detection of cargo encapsulated into liposomal vesicles. This hyphenation could be used for detailed characterization of liposomes as drug carriers in the pharmaceutical industry. What is more, separation and subsequent detection of the liposomal vesicles could also be beneficial in cosmetic, food and farming industry.

6. LIST OF ABBREVIATIONS

Abbreviation	Meaning
nES	Nano electrospray
GEMMA	Gas-phase molecular mobility analysis
VLDL	Very low-density lipoproteins
nDMA	Nano differential mobility analyser
EMD	Electrophoretic mobility diameter
CPC	Condensation particle counter
AFM	Atomic force microscopy
MS	Mass spectrometry
MALDI	Matrix assisted laser desorption/ionization
UV	Ultraviolet
IR	Infrared
Nd:YAG	Neodymium-doped yttrium aluminum garnet
TOF	Time of flight
MCP	Microchannel plate
MLV	Multilamellar vesicle
LUV	Large unilamellar vesicles
SUV	Small unilamellar vesicle
IDL	Intermediate density lipoproteins
LDL	Low density lipoprotein
HDL	High density lipoprotein
THAP	Trihydroxyacetophenone
CHCA	A-cyano-4-hydroxycinnamic acid
SA	3,5-dimethoxy-4-hydroxycinnamic acid
MeOH	Methanol
IgG	Immunoglobulin G
BSA	Bovine serum albumin
HEM	Hemoglobin
NH_4OAc	Ammonium acetate
ACN	Acetonitrile
TFA	Triflioroacetic acid
HSPC	L-α-phosphatidylcholine hydrogenated (Soy)
DSPE	1,2-dioctadecanoyl-sn-glycero-3-phosphoethanolamine
Po	Polonium
CO_2	Carbon dioxide
ENAS	Electrostatic nanometre aerosol sampler
PC	Phosphatidylcholine
PE	Phosphoethanolamine
CID	Collision induced dissociation
m/z	Mass to charge ratio
NaCl	Sodium Chloride

7. LIST OF FIGURES

8. LIST OF TABLES

9. APPENDIX

9.1. MALDI mass spectrometry results of liposomes with encapsulated material

Liposomes with encapsulated cargo molecules were prepared with the thin lipid layer hydration technique as described in section 2. Prior nES GEMMA, non-encapsulated material was removed via spin filtration resulting in a 1:10 volumetric dilution of the liposome stock solution. Different cargo molecules were tested: ascorbic acid, melatonin, vanillin and panthenol. For liposomes encapsulating melatonin and panthenol a volumetric dilution factor of 1:2 was analyzed as well. Furthermore, for liposomes encapsulating panthenol, different extrusion filter pore sizes were tested. In addition to a standard 100 nm pore size filter, 200 nm and a 400 nm pore size filters were used. It was expected to generate larger liposomes, which should be able to encapsulate higher quantities of cargo molecules.

Firstly, the particle size distribution of each sample was determined via nES GEMMA. Subsequently, liposomes were collected on gold-coated silicon wafers at 85 nm EM particle diameter for approximately 5 hours (300min), each. nES GEMMA spectra prior and after size-collection (Figure 28) demonstrated the stability of the nES process during particle collection.

For MALDI MS measurements, 50 µl of each sample prior gas-phase electrophoretic fractionation was mixed with 50 µl of 20 mM THAP matrix solution and 0.9 µl of this mixture was applied to the MALDI MS target plate. Calibration was carried out with castor oil mixed with 5 mM NaCl in 20 mM THAP matrix.

After size separation and collection of liposomes with encapsulated cargo material with nES GEMMA, the gold coated silicon wafers were attached to the MS target plate and one spot of 20 mM THAP matrix was applied to the center of the wafer.

The aim was to acquire MS data for the encapsulated cargo material next to signals derived for lipid species after offline hyphenation of nES GEMMA with MALDI MS. Results are presented in the following chapters.

As presented, MALDI MS spectra relate several peaks. Usually the matrix peak can be seen, as well as the matrix adduct with sodium ions. In addition, sometimes (possibly) trace amounts of encapsulated cargo materials can be detected. Cargo materials are more abundant in mass spectra acquired for the sample prior to nES GEMMA collection. Results are presented in the following, with one spectrum covering the mass range from 150 – 900 m/z. Additionally, two regions marked in blue are enlarged, which correspond to the m/z region where cargo molecules should be present and to the lipid region (700-900 m/z). Cargo molecules are usually present in the form $[M+H]^+$ or $[M+Na]^+$.

MALDI MS spectra of liposomes with encapsulated cargo before and after nES GEMMA collection did not show high enough amounts of chosen cargo molecules. Therefore, visualization of liposome-encapsulated materials with MALDI MS after nES GEMMA size separation could in the end not be proven.

9.1.1. Liposomes with ascorbic acid

9.1.1.1. nES GEMMA measurements for liposomes with ascorbic acid

nES GEMMA measurements are described in Chapter 9.1.

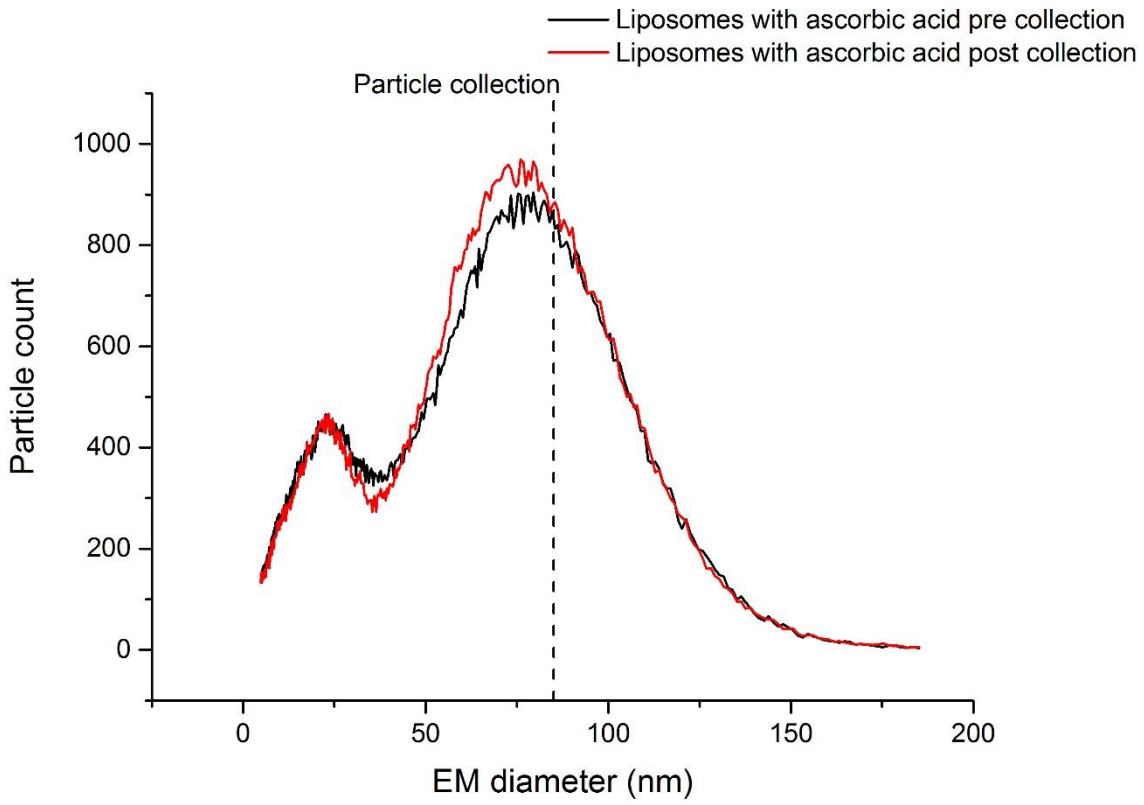

Figure 28: Size distribution of the liposomes with encapsulated ascorbic acid before and after collection with nES GEMMA and the corresponding EM collection diameter

9.1.1.2. Prior nES GEMMA collection MS spectrum (ascorbic acid, $C_6H_8O_6$, MW = 176,12 g/mol)

Sample analysis described in Chapter 9.1.

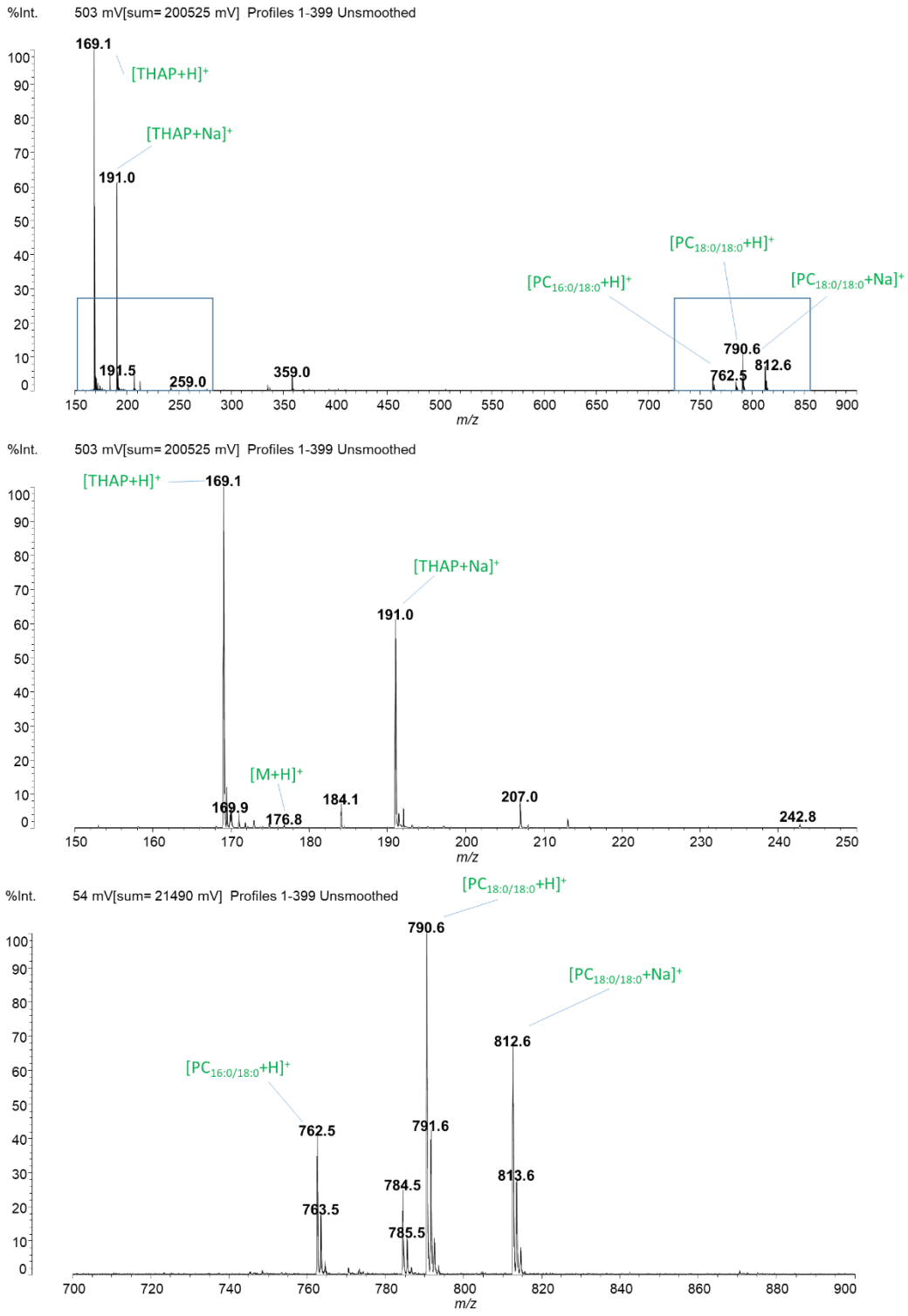

Figure 29: MS spectrum for liposomes with ascorbic acid before nES GEMMA collection. The upper panel shows the total mass range measured, the other two panel represent enlarged m/z regions (marked in blue in the upper panel). The first zoom focusses on the ascorbic acid peak, the second zoom on the lipid peaks

9.1.1.3. After nES GEMMA collection MS spectrum (ascorbic acid, $C_6H_8O_6$, MW = 176,12 g/mol)

Sample analysis described in Chapter 9.1.

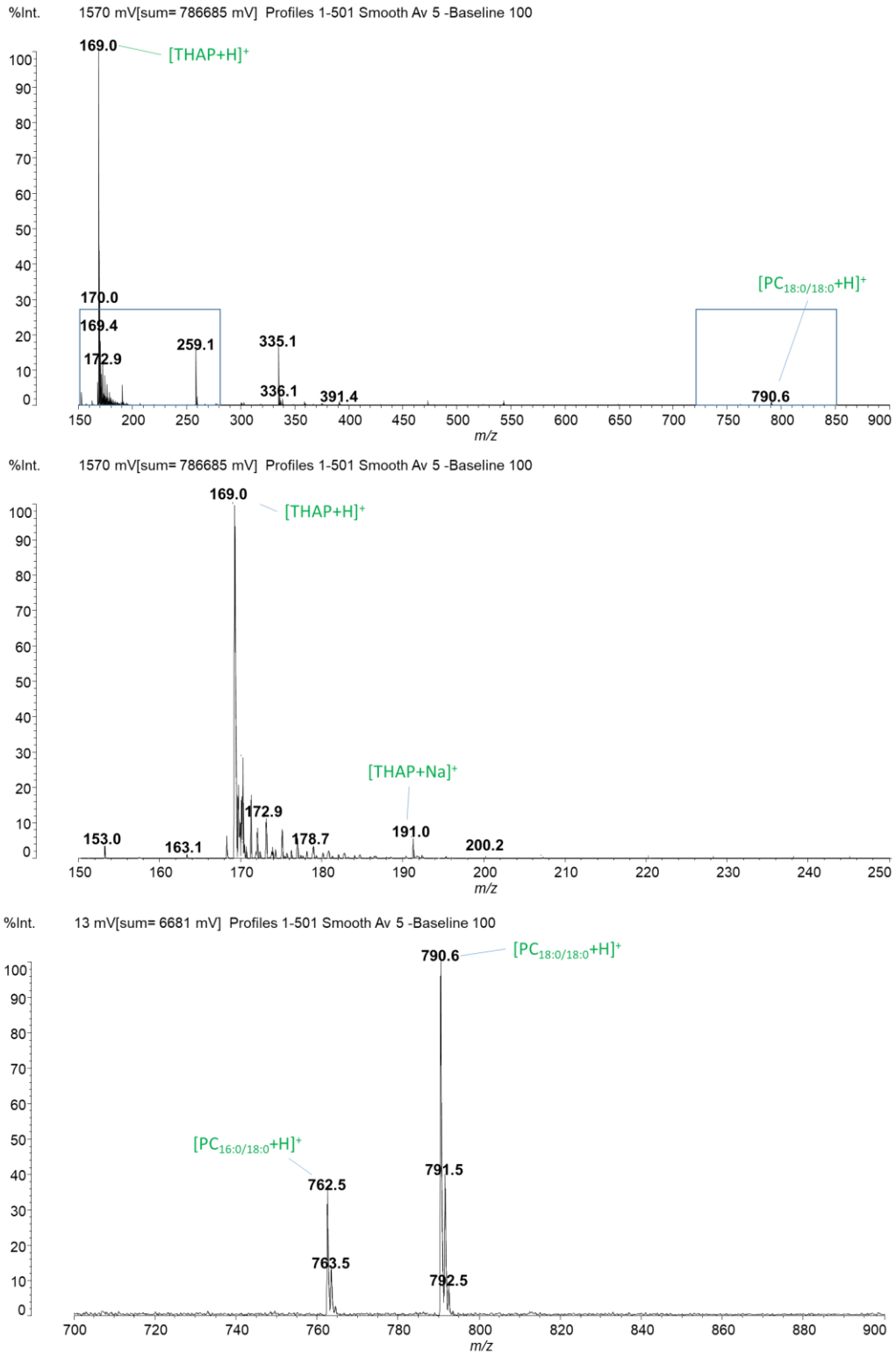

Figure 30: MS spectrum for liposomes with ascorbic acid after nES GEMMA collection. The upper panel shows the total mass range measured, the other two panel represent enlarged m/z regions (marked in blue in the upper panel). The first zoom focusses on the ascorbic acid peak, the second zoom on the lipid peaks

9.1.2. Liposomes with vanillin

9.1.2.1. nES GEMMA measurements for liposomes with vanillin

nES GEMMA measurements are described in Chapter 9.1.

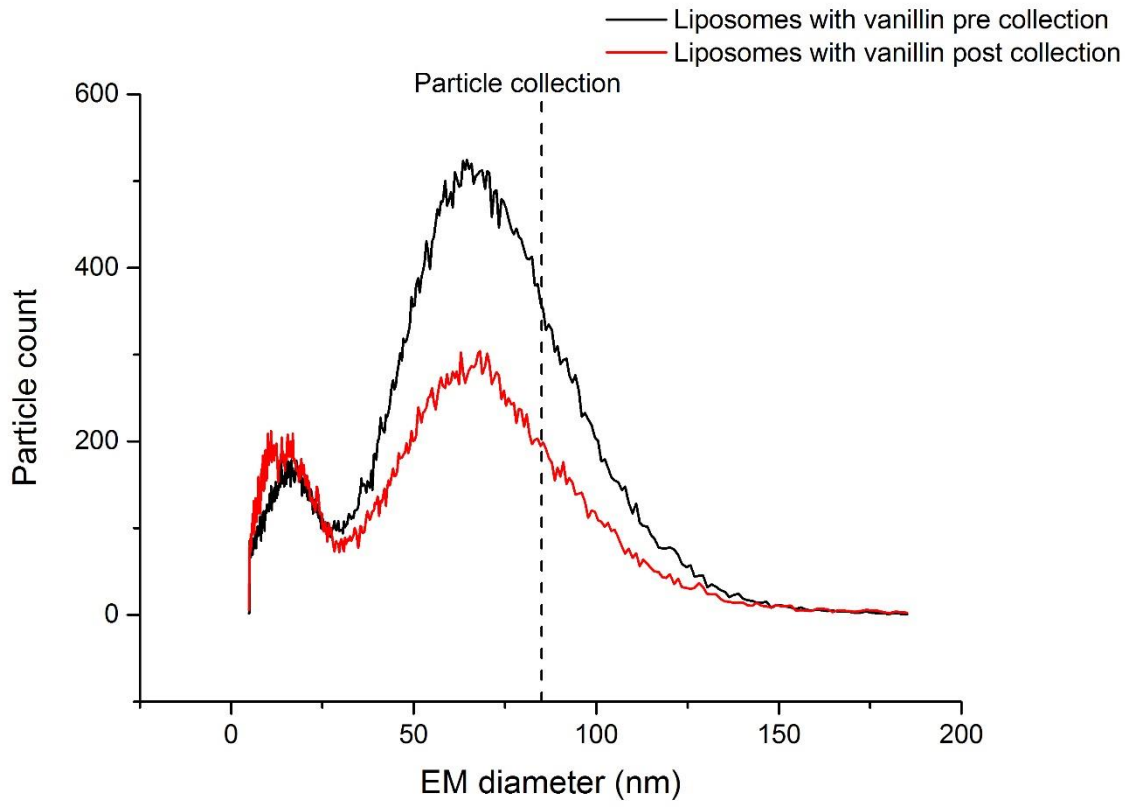

Figure 31: Size distribution of the liposomes with encapsulated vanillin before and after collection with nES GEMMA and the corresponding EM collection diameter

9.1.2.2. Prior nES GEMMA collection MS spectrum ([M] = vanillin, $C_8H_8O_3$, MW = 152,15 g/mol)

Sample analysis described in Chapter 9.1.

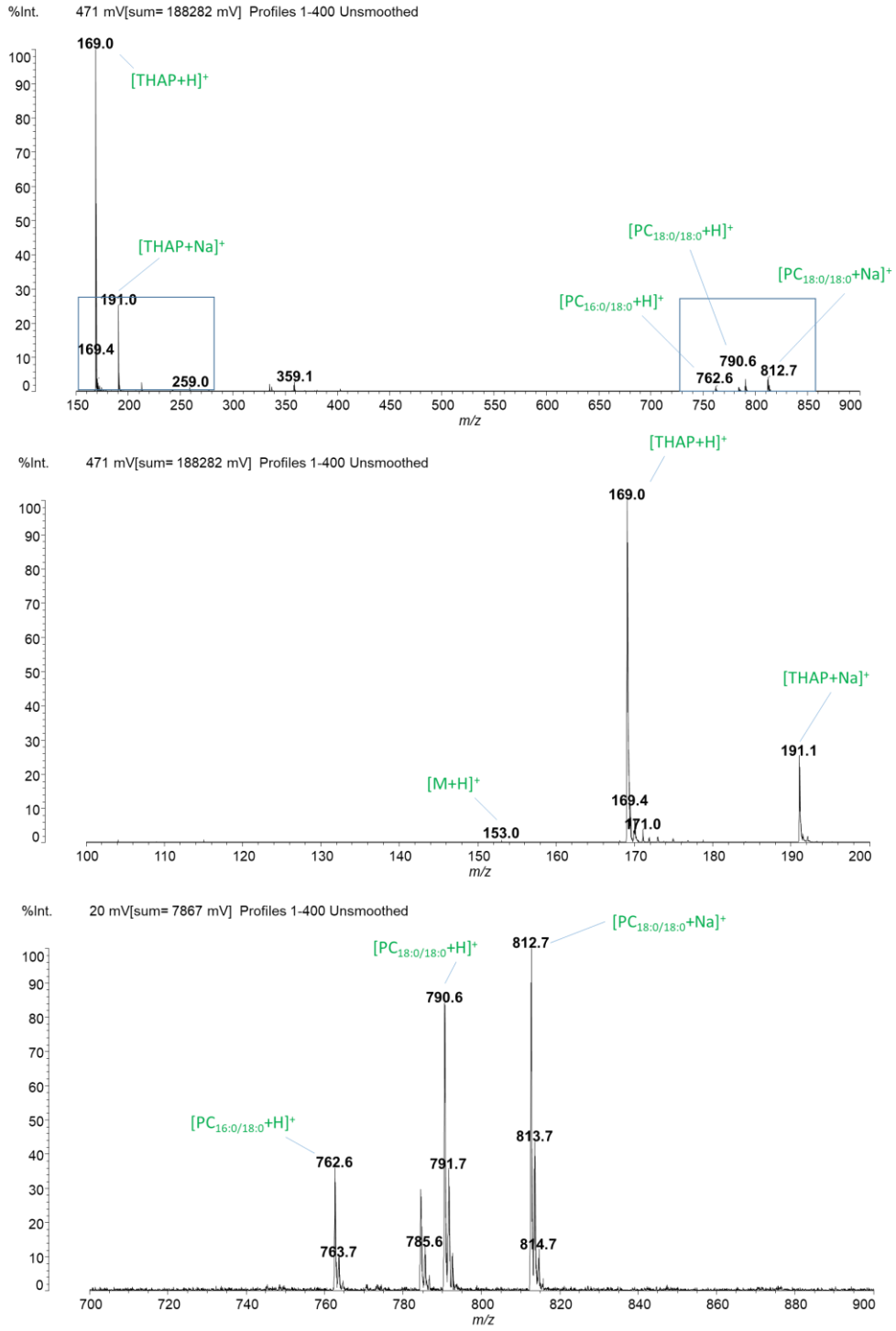

Figure 32: MS spectrum for liposomes with vanillin before nES GEMMA collection. The upper panel shows the total mass range measured, the other two panel represent enlarged m/z regions (marked in blue in the upper panel). The first zoom focusses on the ascorbic acid peak, the second zoom on the lipid peaks

9.1.2.3. After nES GEMMA collection MS spectrum ([M] = vanillin, $C_8H_8O_3$, MW = 152,15 g/mol)

Sample analysis described in Chapter 9.1.

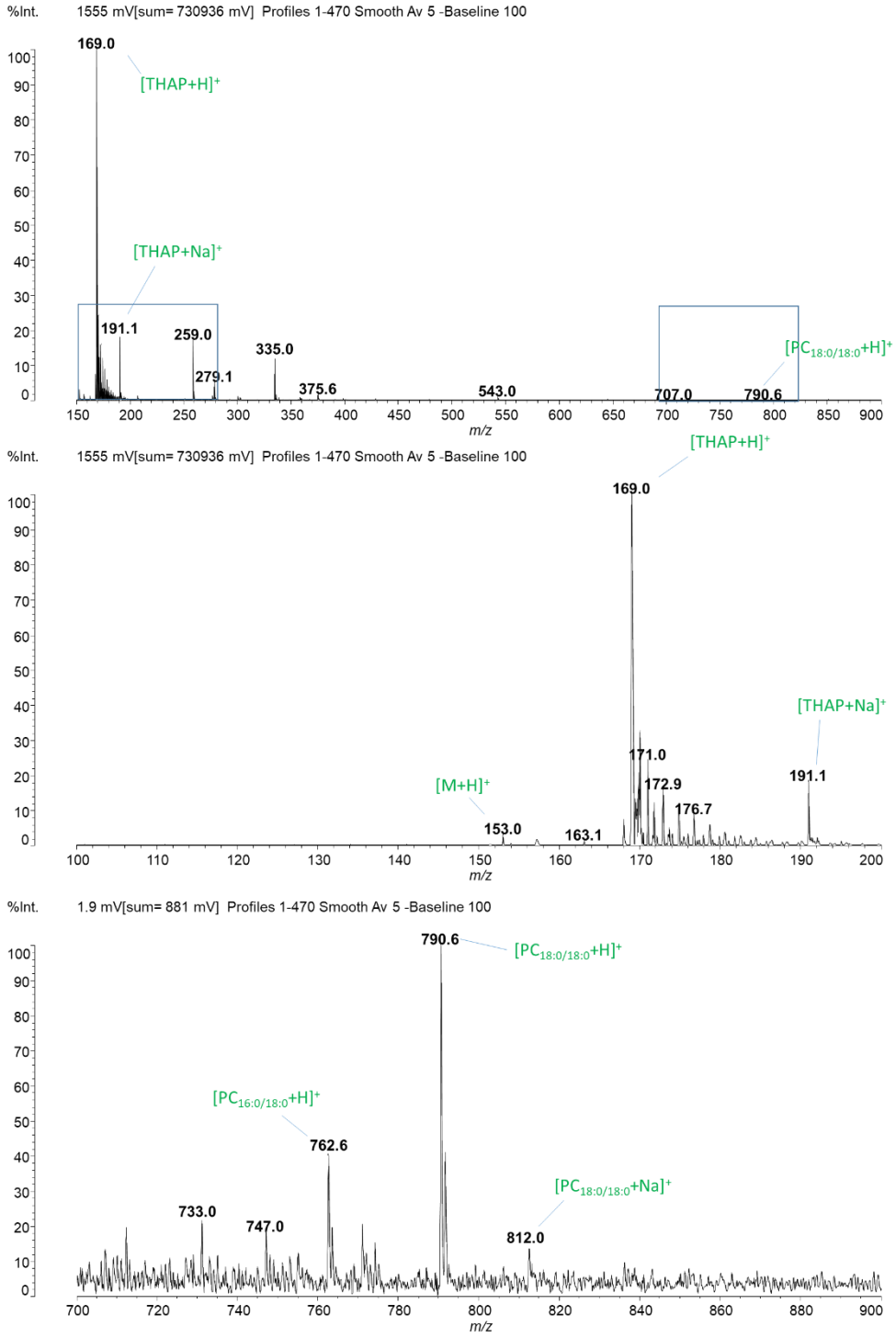

Figure 33: MS spectrum for liposomes with vanillin after nES GEMMA collection. The upper panel shows the total mass range measured, the other two panel represent enlarged m/z regions (marked in blue in the upper panel). The first zoom focusses on the ascorbic acid peak, the second zoom on the lipid peaks

9.1.3. Liposomes with melatonin

9.1.3.1. nES GEMMA measurements for liposomes with melatonin, 1:10 dilution

nES GEMMA measurements are described in Chapter 9.1.

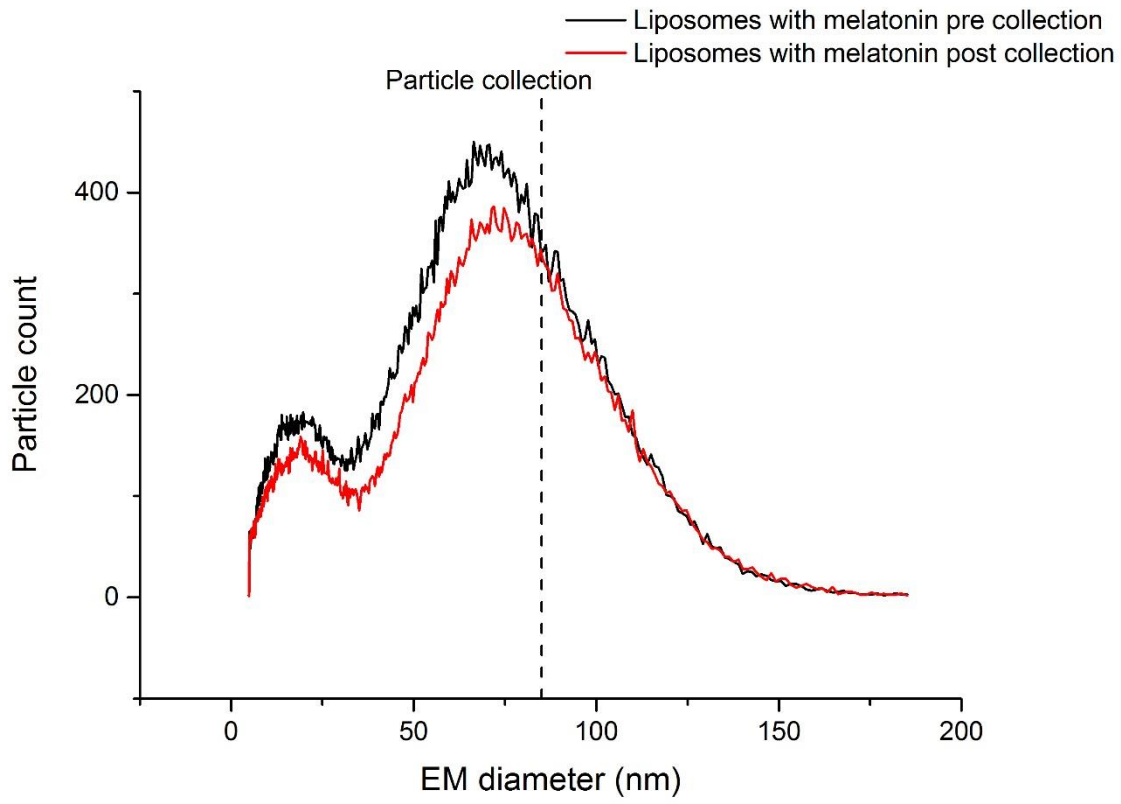

Figure 34: Size distribution of the liposomes with encapsulated melatonin, 1:10 dilution, before and after collection with nES GEMMA and the corresponding EM collection diameter

9.1.3.2. Prior nES GEMMA collection MS spectrum ([M] = melatonin, $C_{13}H_{16}N_2O_2$, 1:10, MW = 232,28 g/mol)

Sample analysis described in Chapter 9.1.

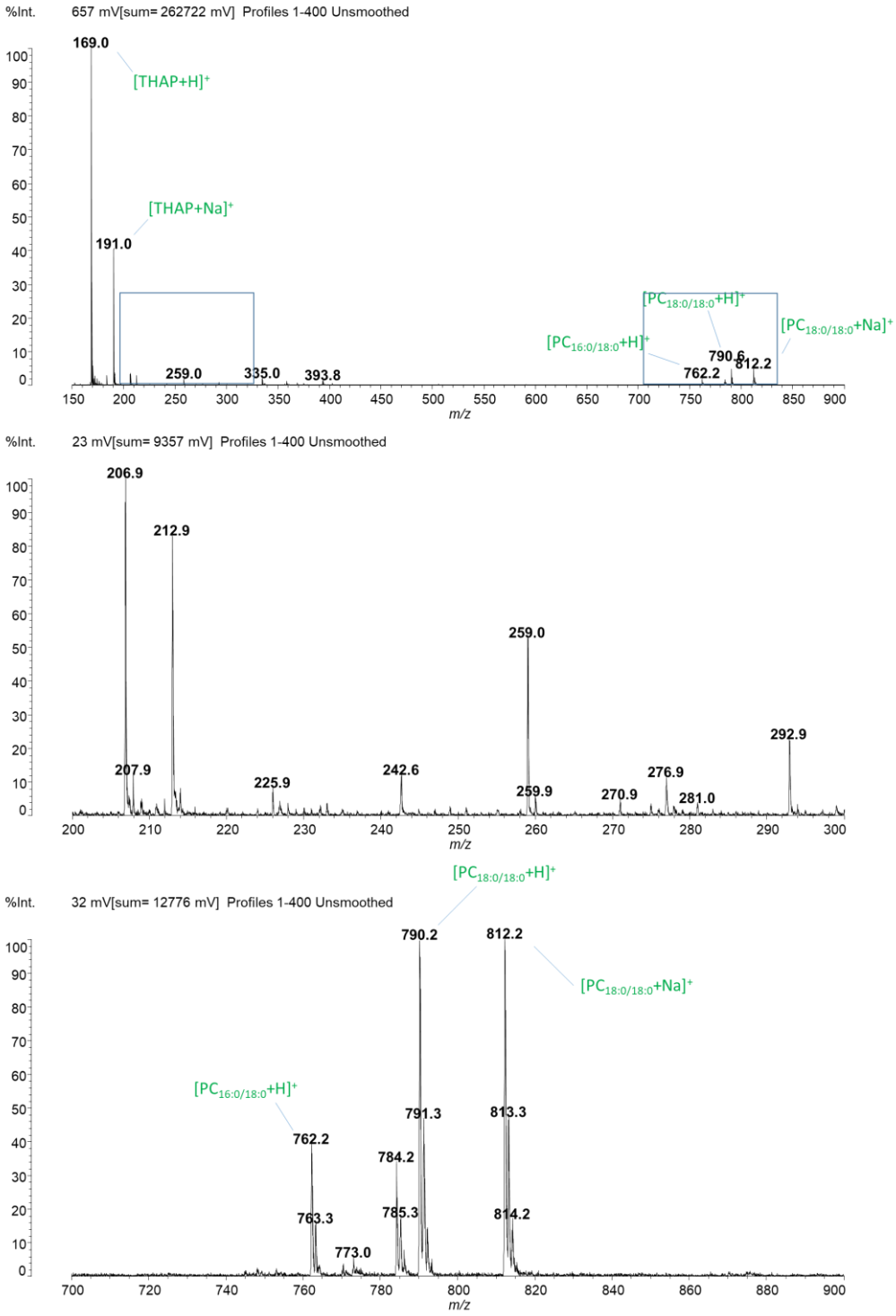

Figure 35: MS spectrum for liposomes with melatonin before nES GEMMA collectionThe upper panel shows the total mass range measured, the other two panel represent enlarged m/z regions (marked in blue in the upper panel). The first zoom focusses on the ascorbic acid peak, the second zoom on the lipid peaks

9.1.3.3. After nES GEMMA collection MS spectrum ([M] = melatonin, $C_{13}H_{16}N_2O_2$, 1:10, MW = 232,28 g/mol)

Sample analysis described in Chapter 9.1.

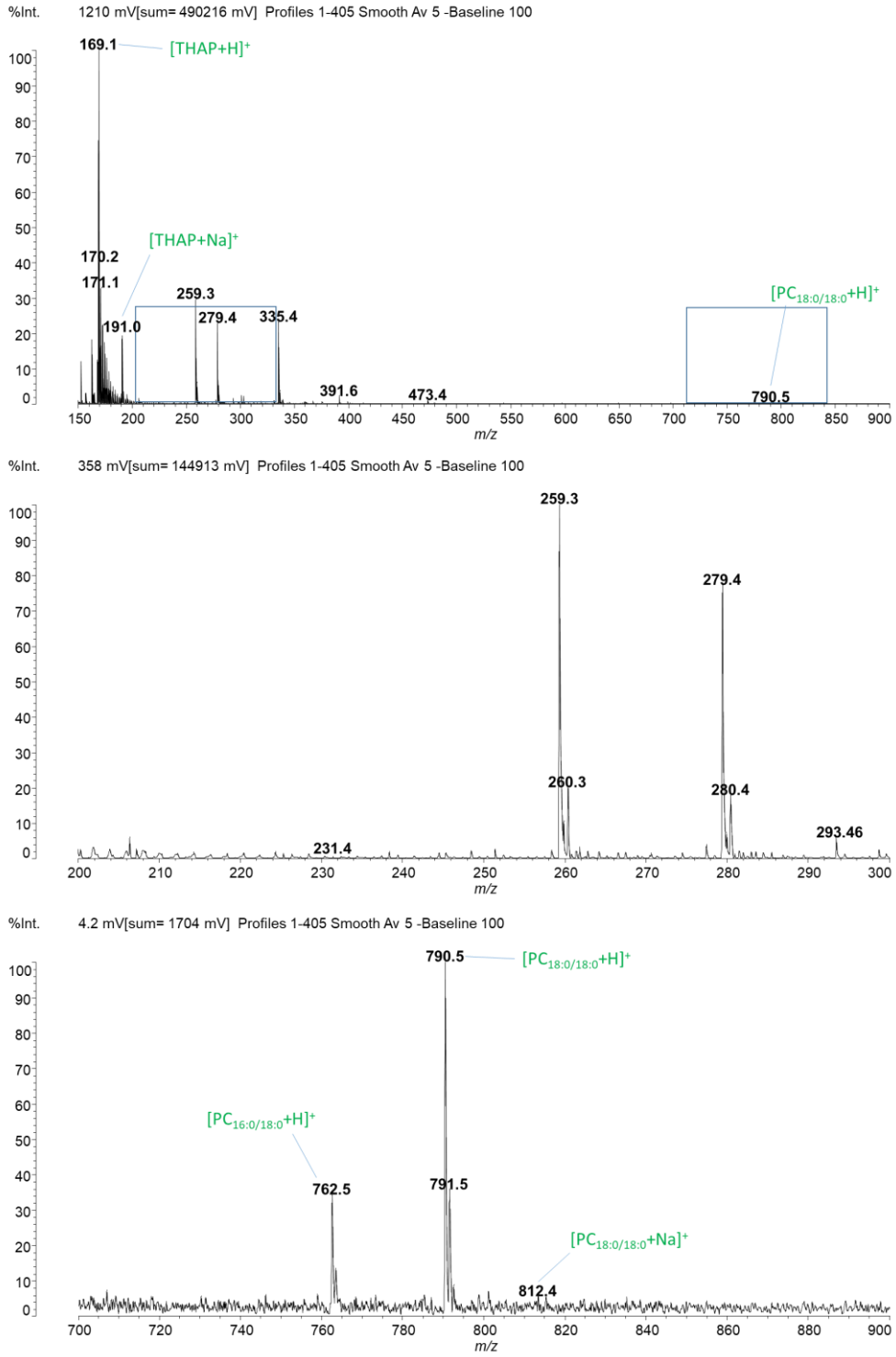

Figure 36: MS spectrum for liposomes with melatonin after nES GEMMA collection. The upper panel shows the total mass range measured, the other two panel represent enlarged m/z regions (marked in blue in the upper panel). The first zoom focusses on the ascorbic acid peak, the second zoom on the lipid peaks

9.1.3.4. nES GEMMA measurements for liposomes with melatonin, 1:2 dilution

nES GEMMA measurements are described in Chapter 9.1.

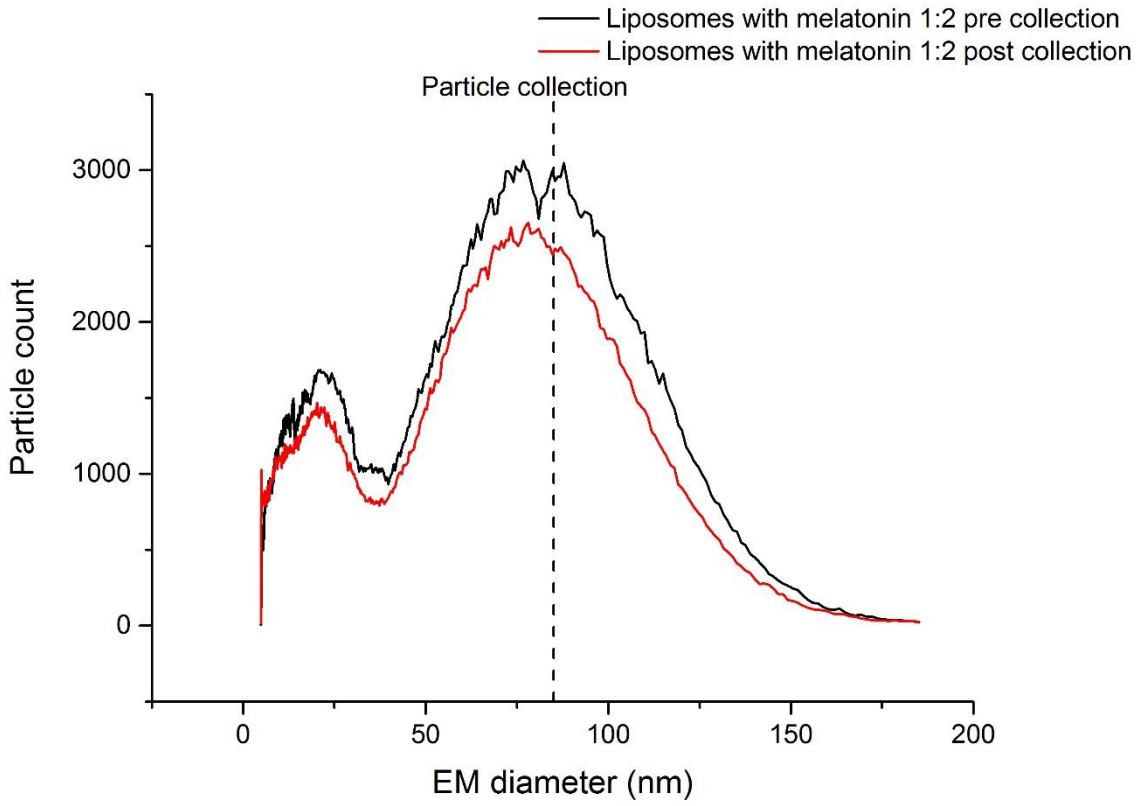

Figure 37: Size distribution of the liposomes with encapsulated melatonin, 1:2 dilution, before and after collection with nES GEMMA and the corresponding EM collection diameter

9.1.3.5. Prior nES GEMMA collection MS spectrum ([M] = melatonin, $C_{13}H_{16}N_2O_2$, 1:2, MW = 232,28 g/mol)

Sample analysis described in Chapter 9.1.

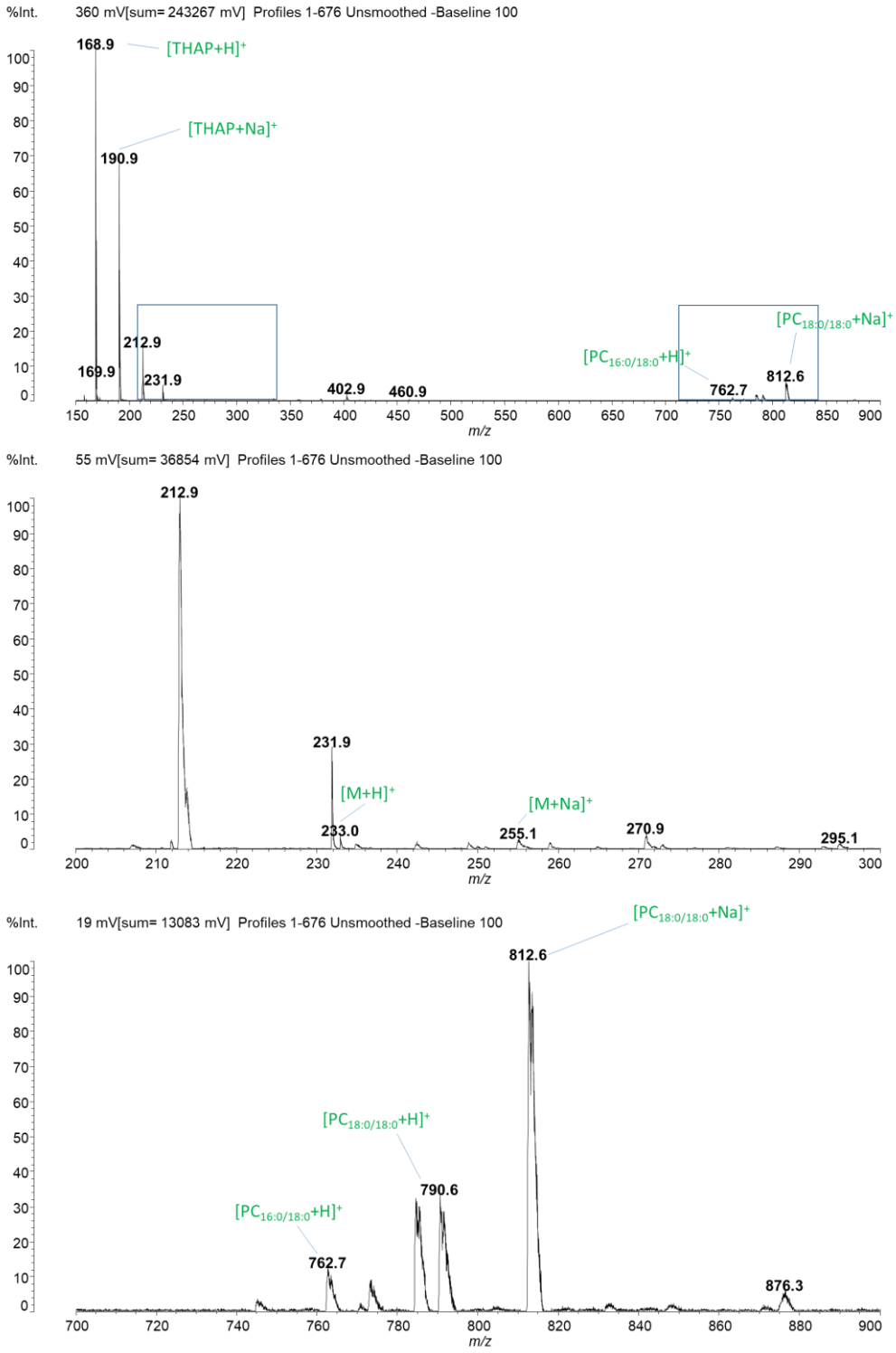

Figure 38: MS spectrum for liposomes with melatonin before nES GEMMA collection. The upper panel shows the total mass range measured, the other two panel represent enlarged m/z regions (marked in blue in the upper panel). The first zoom focusses on the ascorbic acid peak, the second zoom on the lipid peaks

9.1.3.6. After nES GEMMA collection MS spectrum ([M] = melatonin, $C_{13}H_{16}N_2O_2$, 1:2, MW = 232,28 g/mol)

Sample analysis described in Chapter 9.1.

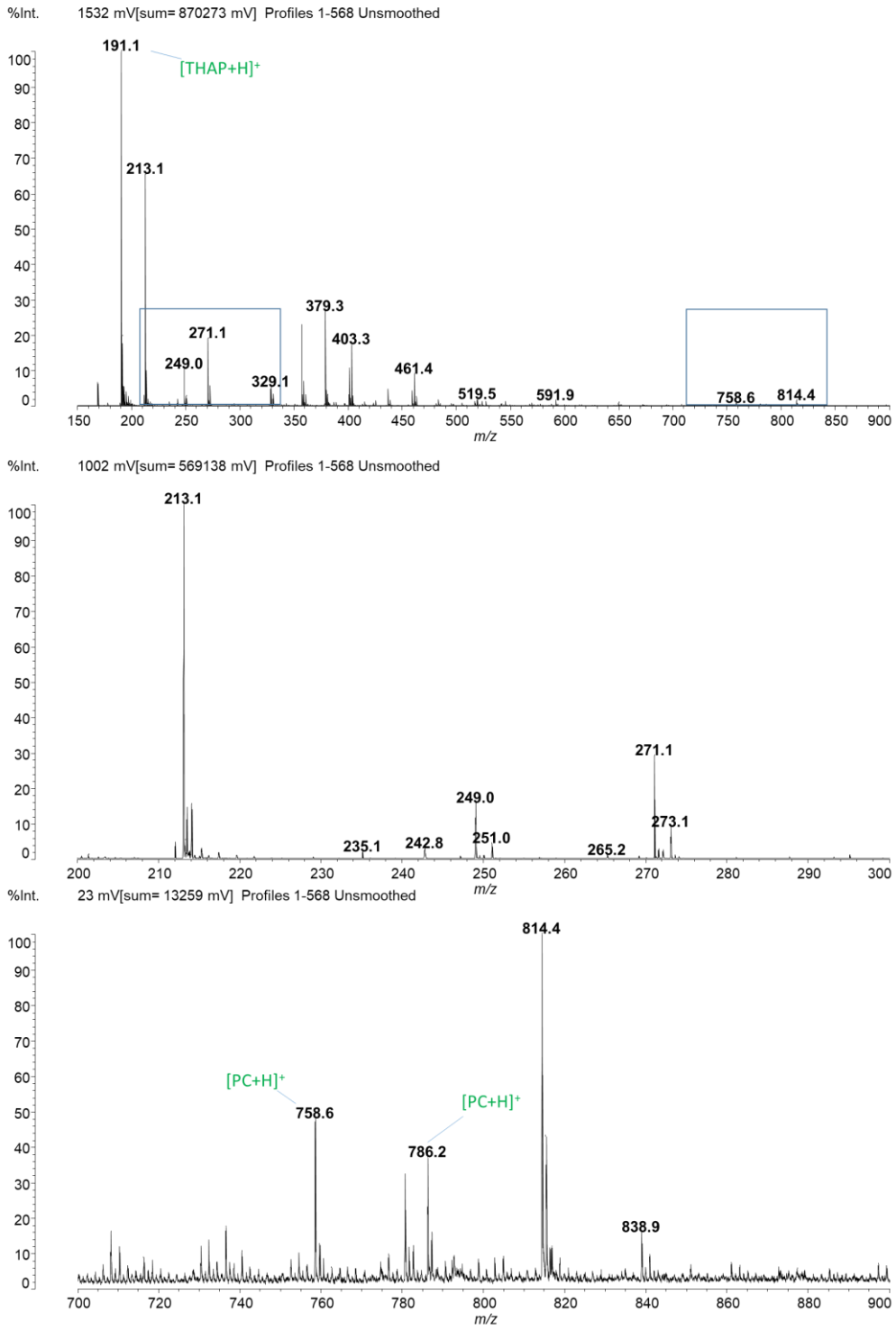

Figure 39: MS spectrum for liposomes with melatonin after nES GEMMA collection. The upper panel shows the total mass range measured, the other two panel represent enlarged m/z regions (marked in blue in the upper panel). The first zoom focusses on the ascorbic acid peak, the second zoom on the lipid peaks

9.1.4. Liposomes with panthenol

9.1.4.1. nES GEMMA measurements for liposomes with panthenol, 1:10 dilution

nES GEMMA measurements are described in Chapter 9.1.

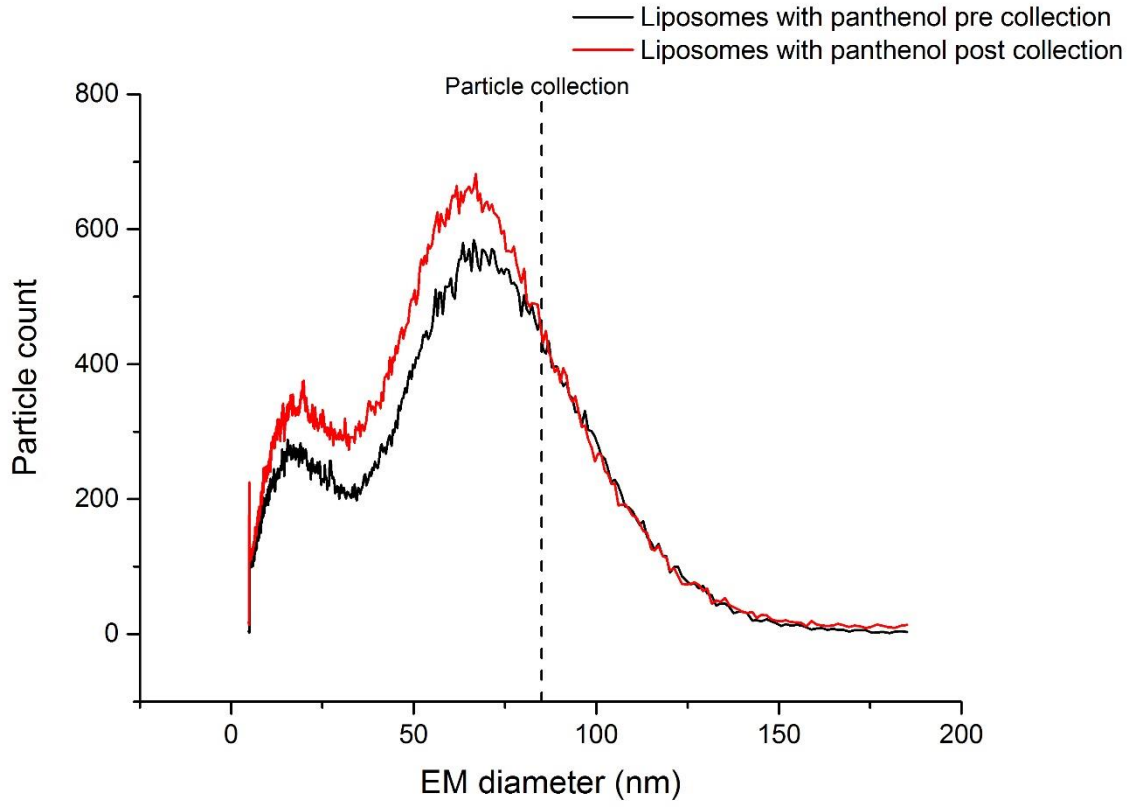

Figure 40: Size distribution of the liposomes with encapsulated panthenol, 1:10 dilution, before and after collection with nES GEMMA and the corresponding EM collection diameter

9.1.4.2. Prior nES GEMMA collection MS spectrum ([M] = panthenol, $C_9H_{19}NO_4$, 1:10, MW = 205,251 g/mol)

Sample analysis described in Chapter 9.1.

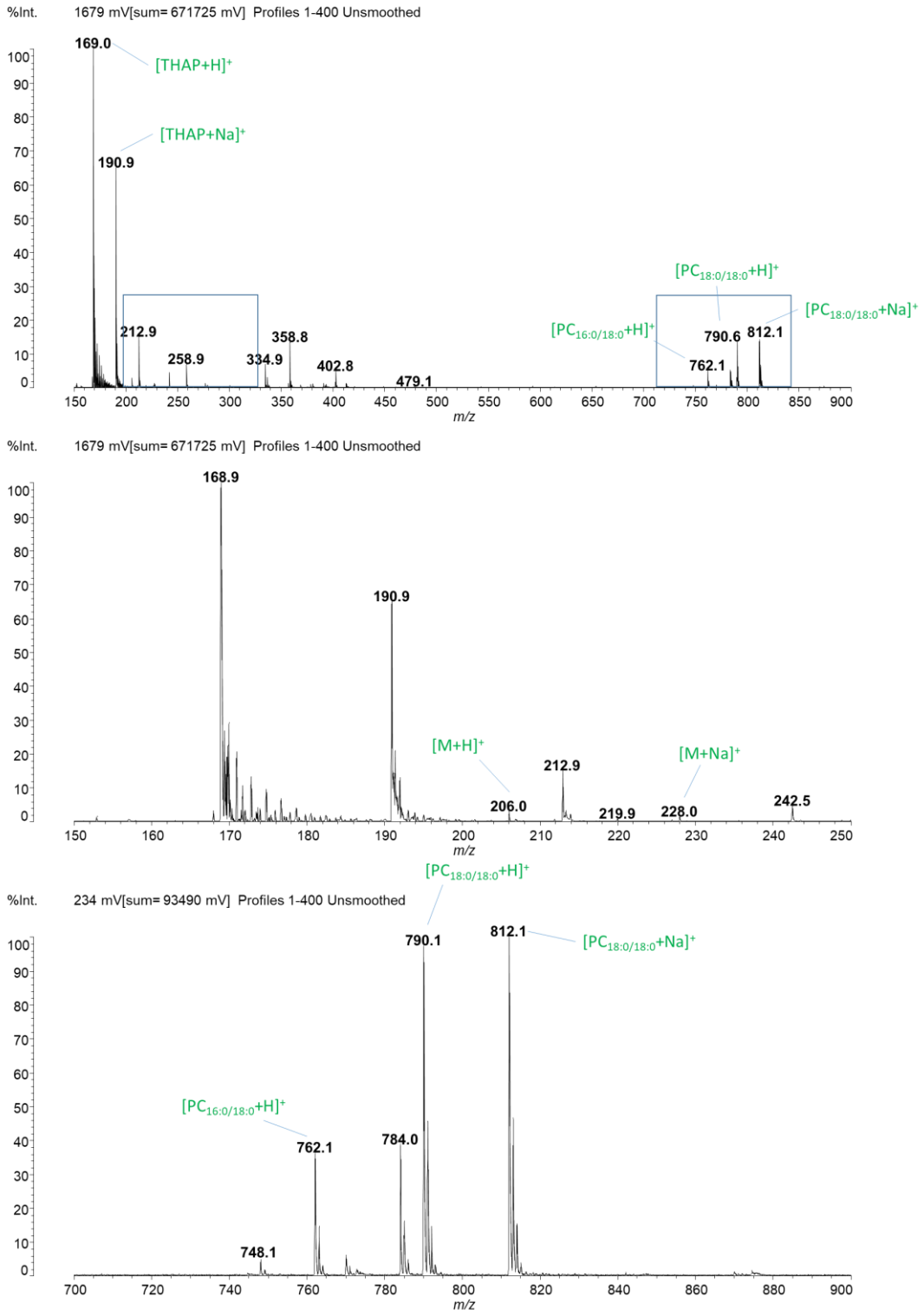

Figure 41: MS spectrum for liposomes with panthenol before nES GEMMA collection. The upper panel shows the total mass range measured, the other two panel represent enlarged m/z regions (marked in blue in the upper panel). The first zoom focusses on the ascorbic acid peak, the second zoom on the lipid peaks

9.1.4.3. After nES GEMMA collection MS spectrum ([M] = panthenol, $C_9H_{19}NO_4$, 1:10, MW = 205,251 g/mol)

Sample analysis described in Chapter 9.1.

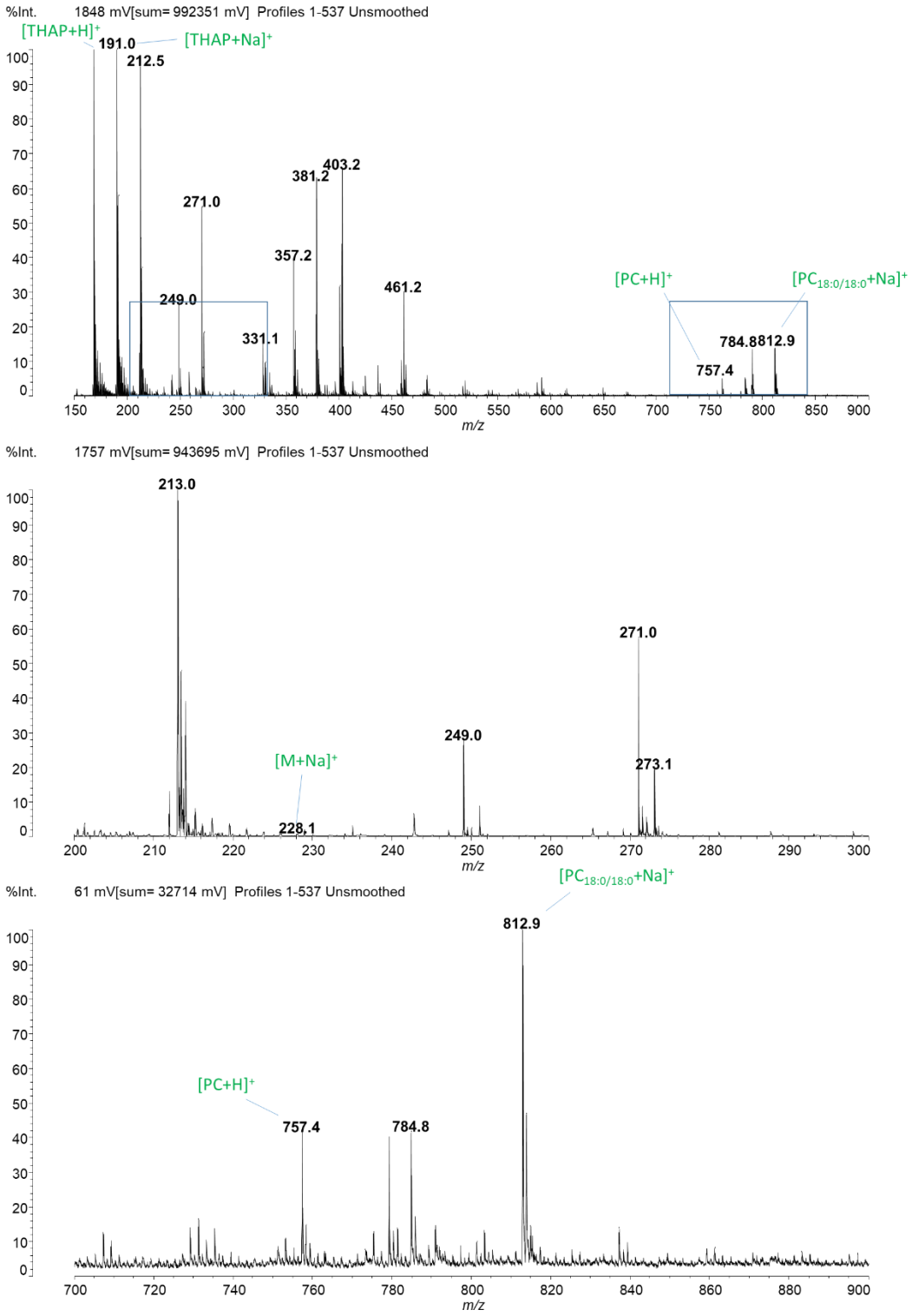

Figure 42: MS spectrum for liposomes with panthenol after nES GEMMA collection. The upper panel shows the total mass range measured, the other two panel represent enlarged m/z regions (marked in blue in the upper panel). The first zoom focusses on the ascorbic acid peak, the second zoom on the lipid peaks

9.1.4.4. nES GEMMA measurements for liposomes with panthenol, 1:2 dilution

nES GEMMA measurements are described in Chapter 9.1.

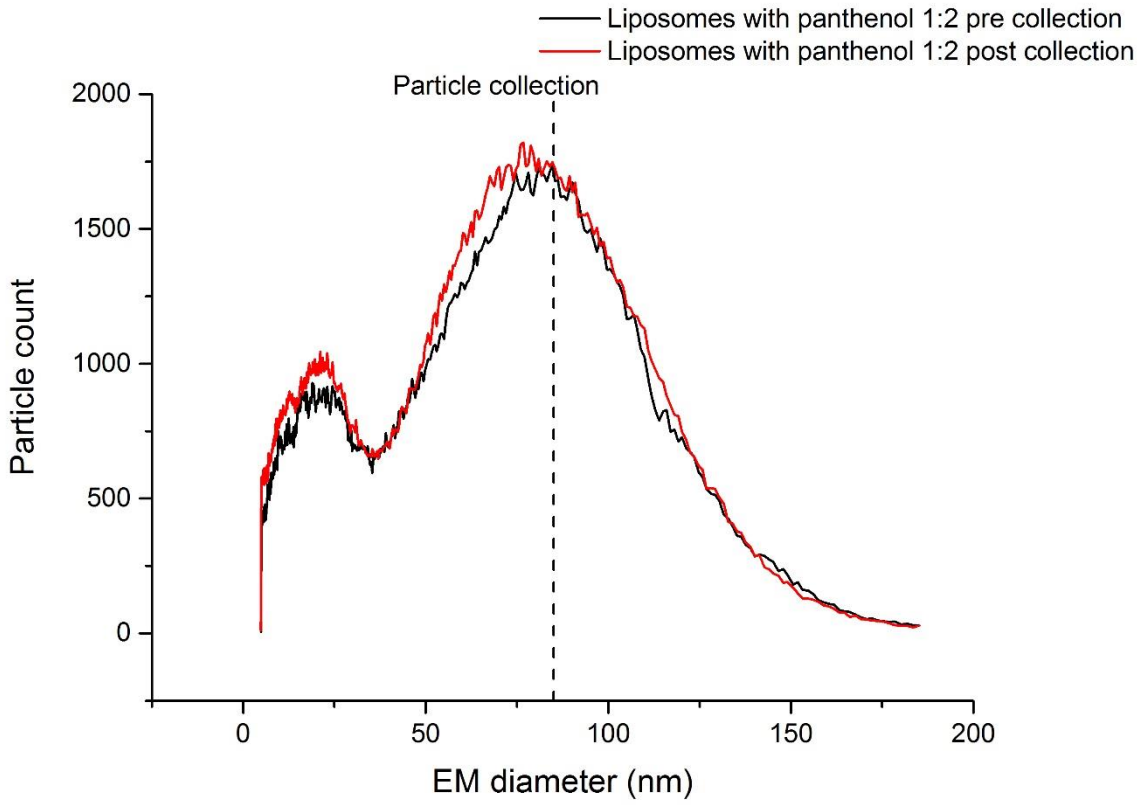

Figure 43: Size distribution of the liposomes with encapsulated panthenol, 1:2 dilution, before and after collection with nES GEMMA and the corresponding EM collection diameter

9.1.4.5. Prior nES GEMMA collection MS spectrum ([M] = panthenol, $C_9H_{19}NO_4$, 1:2, MW = 205,251 g/mol)

Sample analysis described in Chapter 9.1.

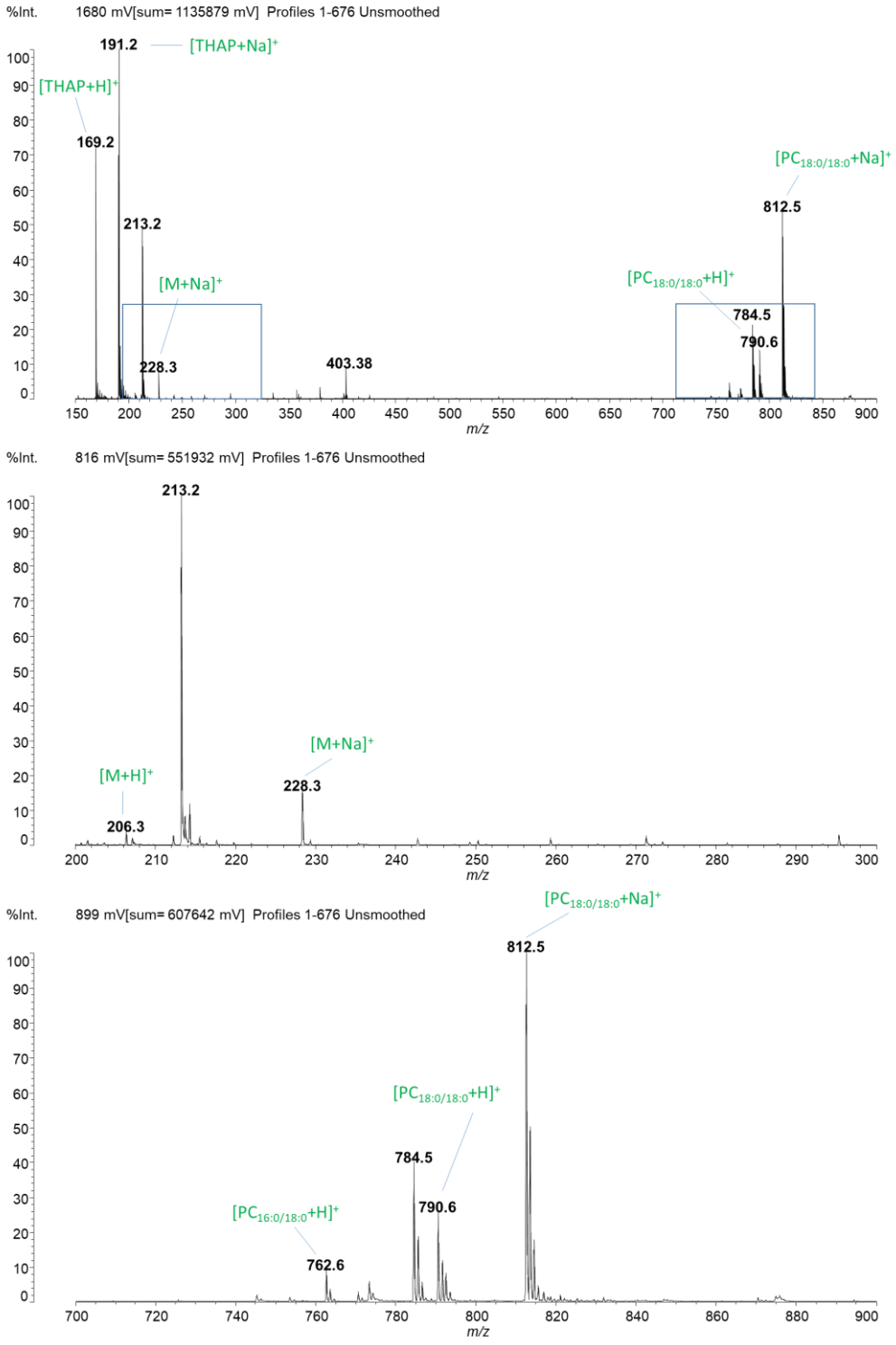

Figure 44: MS spectrum for liposomes with panthenol before nES GEMMA collection. The upper panel shows the total mass range measured, the other two panel represent enlarged m/z regions (marked in blue in the upper panel). The first zoom focusses on the ascorbic acid peak, the second zoom on the lipid peaks

9.1.4.6. After nES GEMMA collection MS spectrum ([M] = panthenol, $C_9H_{19}NO_4$, 1:2, MW = 205,251 g/mol)

Sample analysis described in Chapter 9.1.

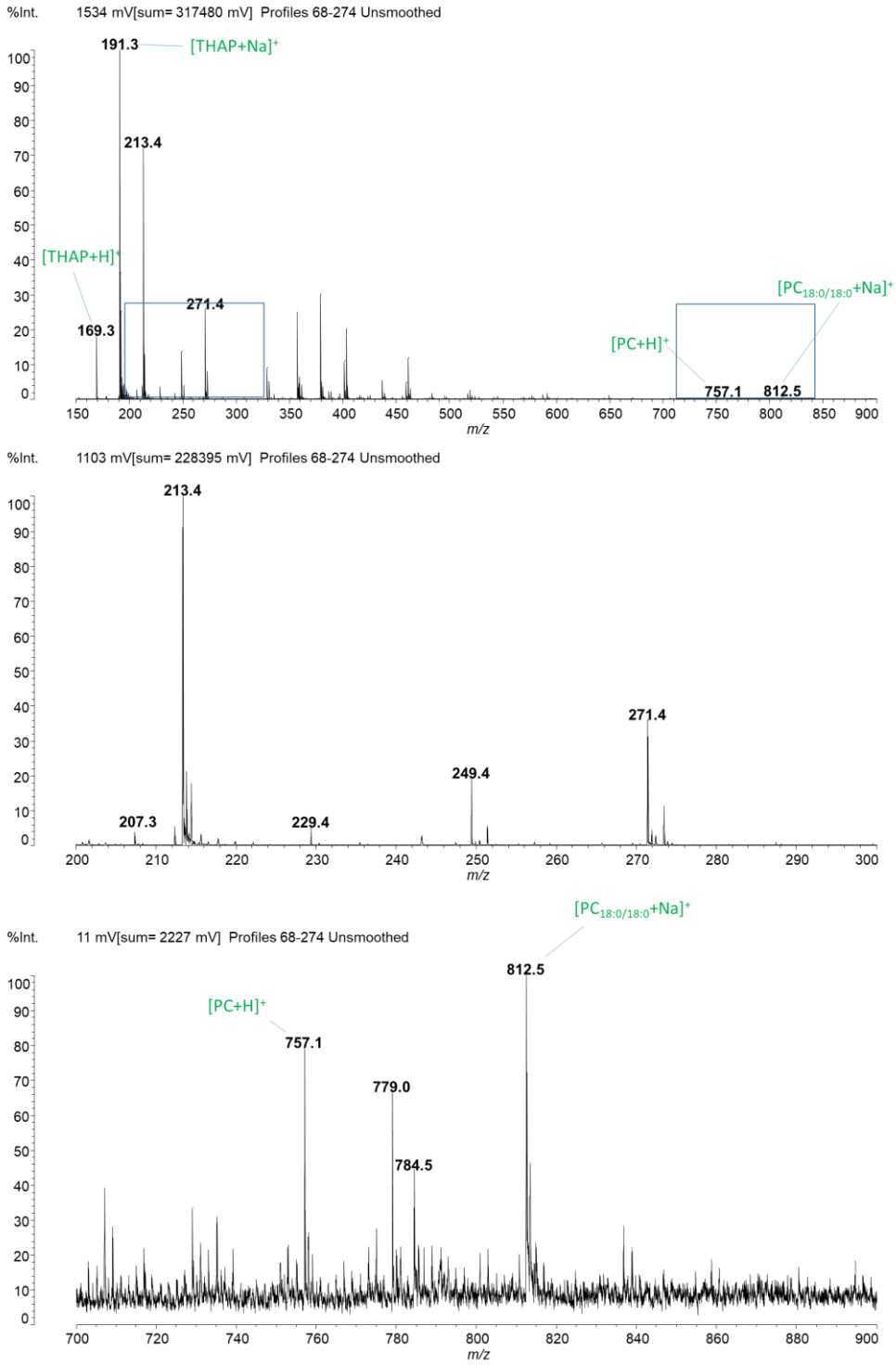

Figure 45: MS spectrum for liposomes with panthenol after nES GEMMA collection. The upper panel shows the total mass range measured, the other two panel represent enlarged m/z regions (marked in blue in the upper panel). The first zoom focusses on the ascorbic acid peak, the second zoom on the lipid peaks

9.1.4.7. nES GEMMA measurements for liposomes with panthenol, 1:4 dilution, 200 nm extrusion filter size

nES GEMMA measurements are described in Chapter 9.1.

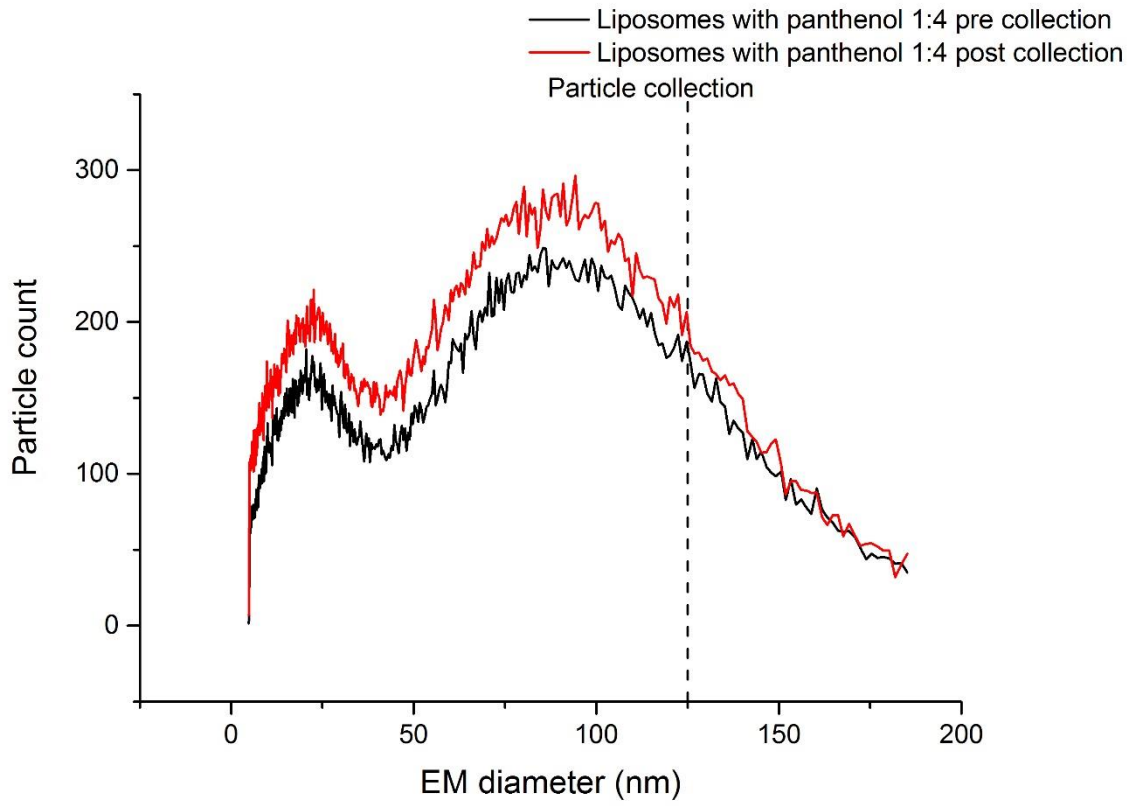

Figure 46: Size distribution of the liposomes with encapsulated panthenol, 1:4 dilution, extruded through larger pore size filters (200nm), before and after collection with nES GEMMA and the corresponding EM collection diameter

9.1.4.8. After nES GEMMA collection MS spectrum ([M] = panthenol, $C_9H_{19}NO_4$, 1:4, MW = 205,251 g/mol)

Sample analysis described in Chapter 9.1.

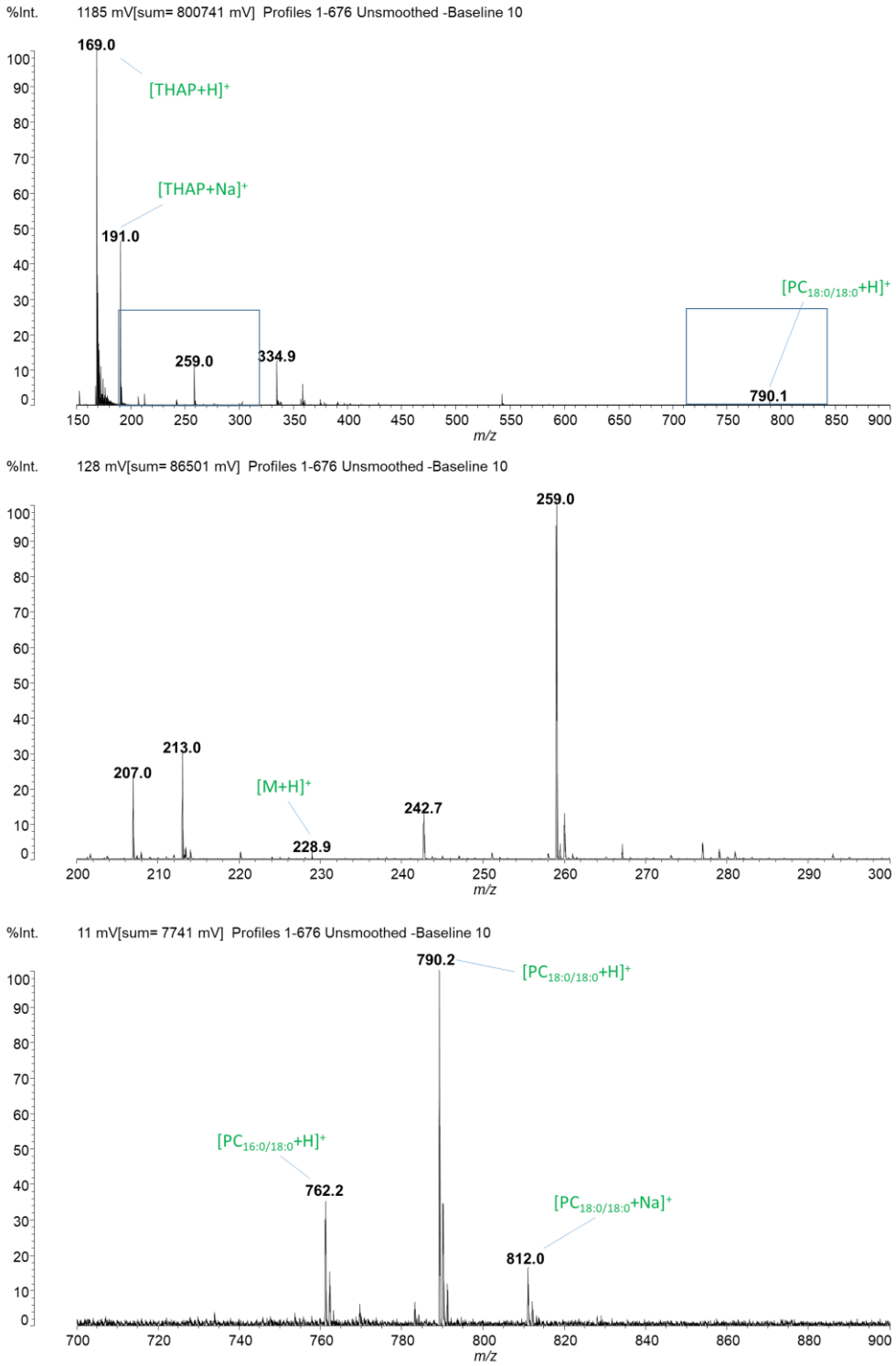

Figure 47: MS spectrum for liposomes with panthenol after nES GEMMA collection. The upper panel shows the total mass range measured, the other two panel represent enlarged m/z regions (marked in blue in the upper panel). The first zoom focusses on the ascorbic acid peak, the second zoom on the lipid peaks. Liposomes were extruded through larger pore size filters (200nm).

9.1.4.9. nES GEMMA measurements for liposomes with panthenol, 1:4 dilution, 400 nm extrusion filter size

nES GEMMA measurements are described in Chapter 9.1.

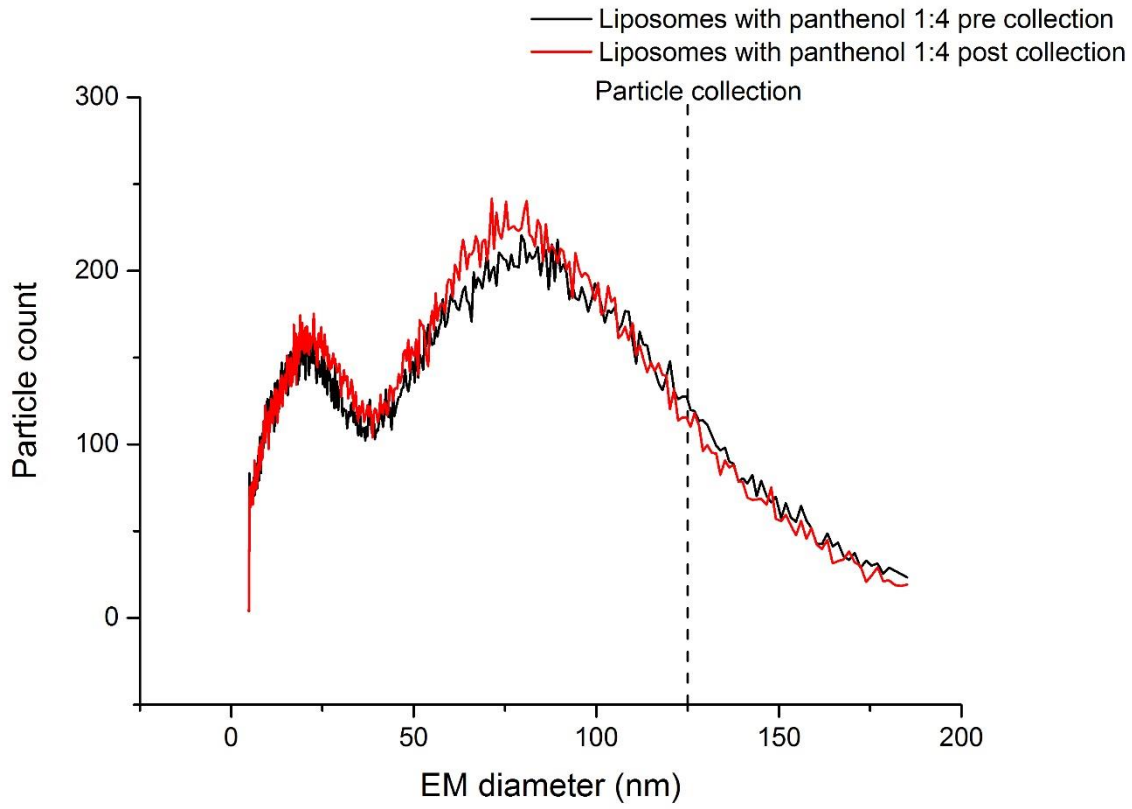

Figure 48: Size distribution of the liposomes with encapsulated panthenol, 1:4 dilution, extruded through larger pore size filters (400nm), before and after collection with nES GEMMA and the corresponding EM collection diameter

9.1.4.10. After nES GEMMA collection MS spectrum ([M] = panthenol, $C_9H_{19}NO_4$, 1:4, MW = 205,251 g/mol)

Sample analysis described in Chapter 9.1.

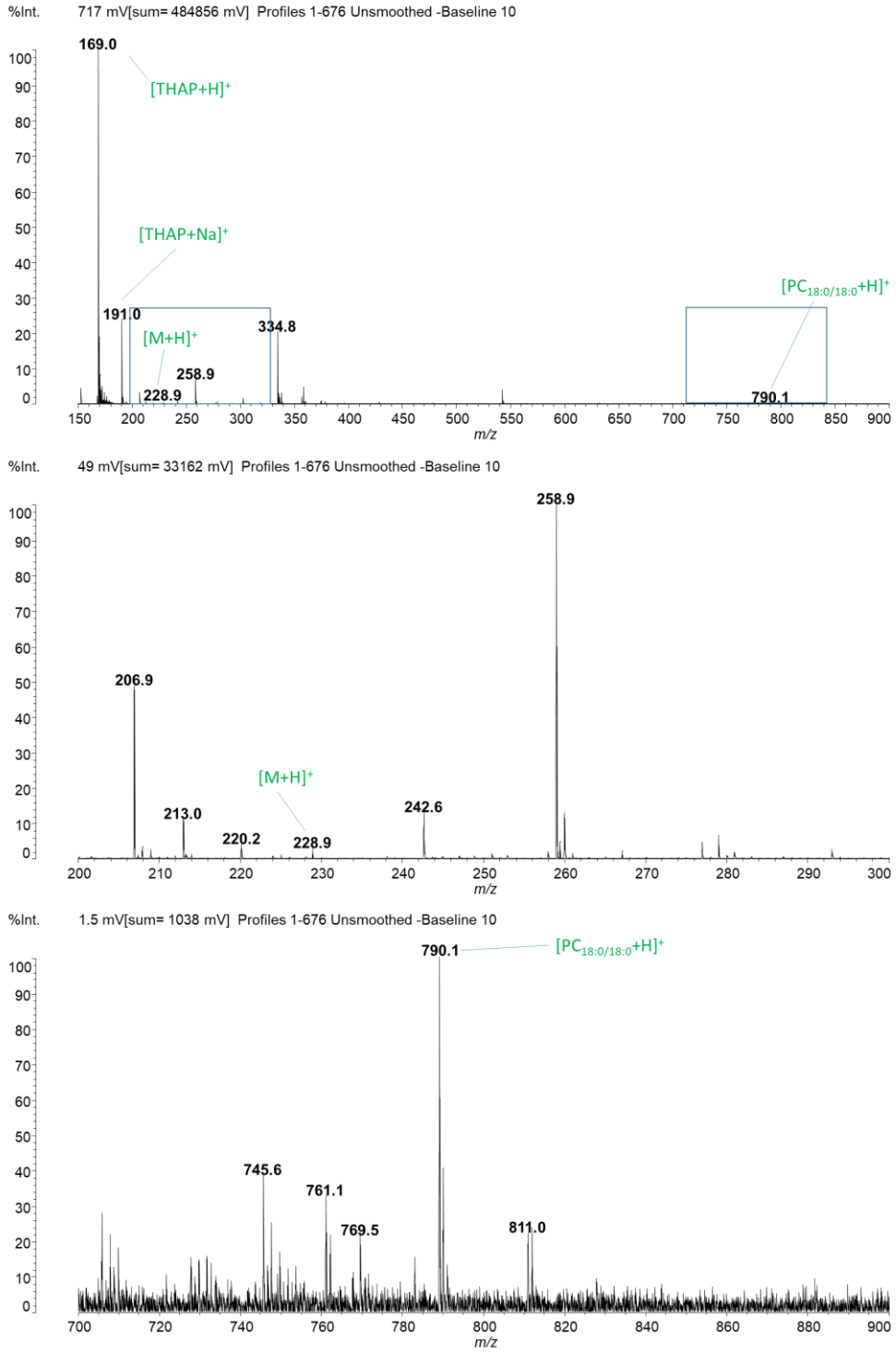

Figure 49: MS spectrum for liposomes with panthenol after nES GEMMA collection. The upper panel shows the total mass range measured, the other two panel represent enlarged m/z regions (marked in blue in the upper panel). The first zoom focusses on the ascorbic acid peak, the second zoom on the lipid peaks. Liposomes were extruded through larger pore size filters (400nm).

9.2. MALDI mass spectrometry results of VLDLs with added proteins

VLDLs were mixed with proteins and analyzed with nES GEMMA and MALDI MS. The aim was to separate the lipoprotein particles from the protein mixture.

Firstly, VLDLs were subjected to buffer exchange and volumetric dilution (1:30) via spin filtration. This process also removed small EM diameter material and salts present in the stock solution.

Firstly, the size distribution of the sample was acquired via nES GEMMA. Afterwards analytes were collected on gold-coated silicon wafers at 38 nm EM particle diameter for approximately 5 hours (300 min). nES GEMMA spectra prior and after size-collection demonstrated the stability of the nES process during particle collection.

For MALDI MS measurements, 50 µl of each sample prior gas-phase electrophoretic fractionation were mixed with 50 µl of 10 mM THAP matrix solution and 0.85 µl of the mixture was applied to the MALDI MS target plate. For VLDL samples, different MALDI matrices were tested to obtain the optimal matrix compound and matrix concentration, which yields best results. Results are presented in chapter 9.4. Finally, 10 mM THAP matrix was chosen. Calibration was carried out with castor oil mixed with 5 mM NaCl in 20 mM THAP matrix.

After size separation and collection of the VLDLs from the protein mixture with nES GEMMA, the gold-coated silicon wafer was attached to the MS target plate and one spot of 10 mM THAP matrix was applied to the centre of the wafer.

The aim was to acquire MS data for VLDLs prior and after offline hyphenation of nES GEMMA with MALDI MS. Results are presented in the following chapters.

MALDI MS spectra relate several peaks: usually the matrix peak can be seen as well as a peak for the matrix adduct with sodium and peaks for lipid species. Lipid peaks are more abundant in mass spectra acquired prior to nES GEMMA collection. All detected peaks are presented on a large mass range scale (150 – 900 m/z) with subsequently enlarged m/z regions marked in blue. Enlarged m/z regions correspond to the m/z range of 550-900, showing putatively lipid species.

MALDI MS spectra for VLDLs mixed with proteins were expected to be more complex with many additional peaks. However, this was not observed initially. Therefore, the intended proof-of-principle for efficient size separation with nES GEMMA could not be shown with this complex mixture of VLDLs and proteins.

9.2.1. nES GEMMA measurements for VLDLs and proteins

nES GEMMA measurements are described in Chapter 9.2.

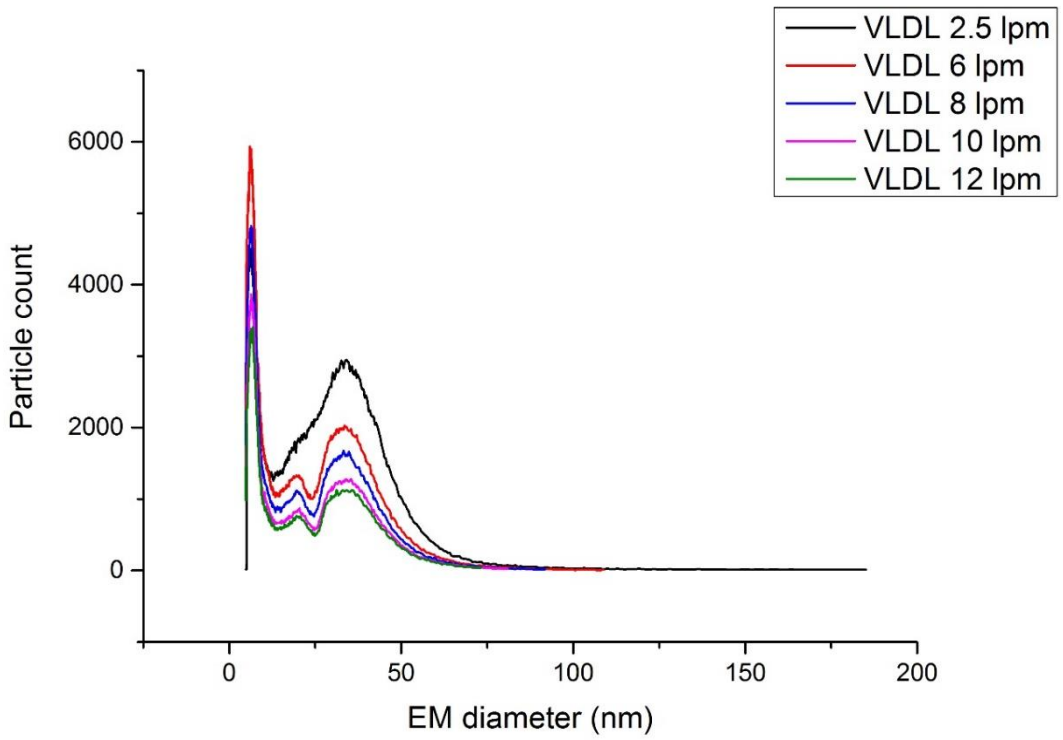

Figure 50: Size distribution of very low-density lipoprotein particles with different sheath flow settings on electrostatic classifier

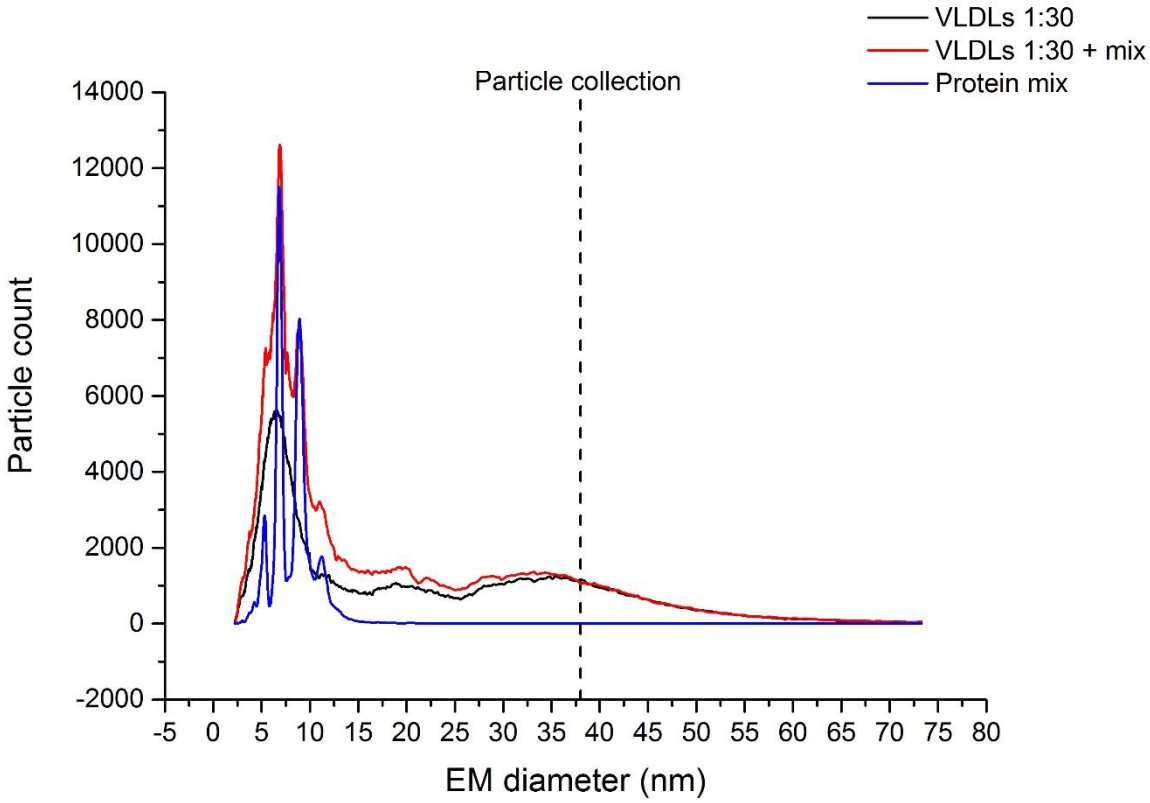

Figure 51: Size distribution for VLDLs, proteins and mixture of VLDLs with proteins. The EM collection diameter is also presented on the graph. The collection was carried out at 38 nm

9.2.2. nES GEMMA measurements for mixture of VLDLs and proteins

nES GEMMA measurements are described in Chapter 9.2.

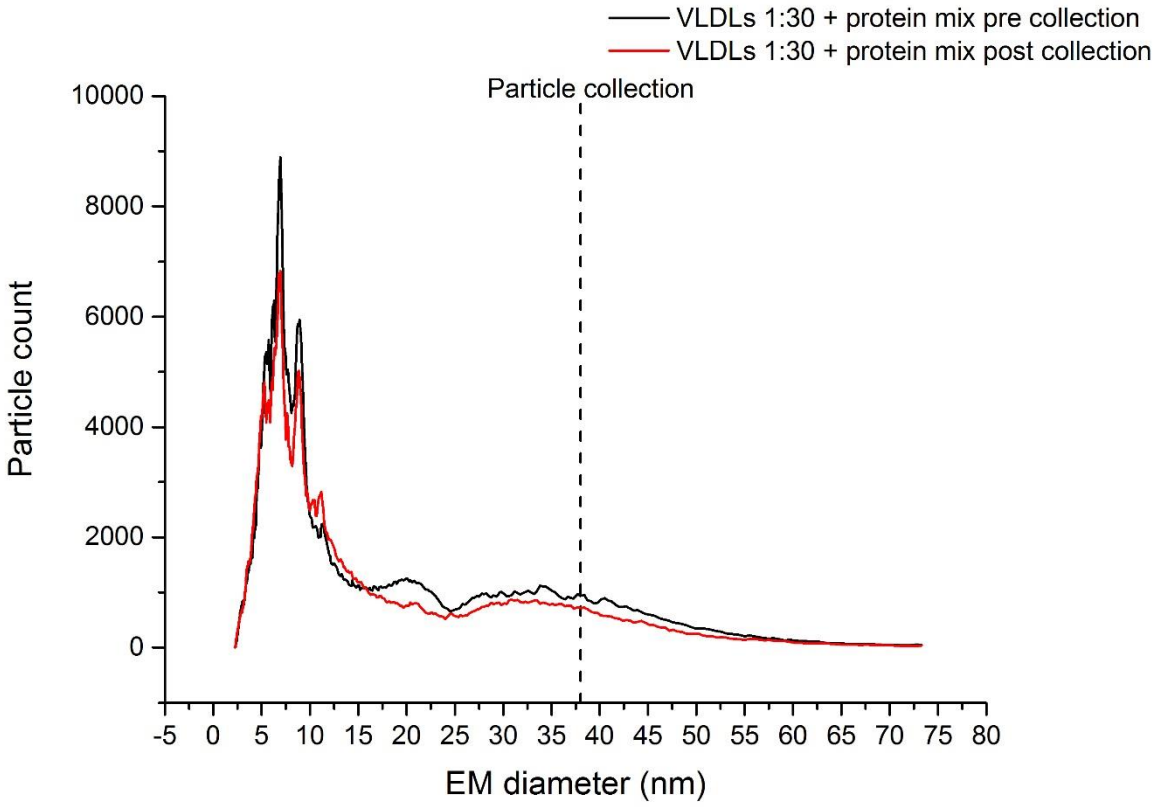

Figure 52: Size distribution for mixture of VLDLs with proteins before and after nES GEMMA collection. The EM collection diameter is also presented on the graph. The collection was carried out at 38 nm

9.2.3. Prior nES GEMMA collection MS spectrum VLDLs 1:30

Sample analysis described in Chapter 9.2.

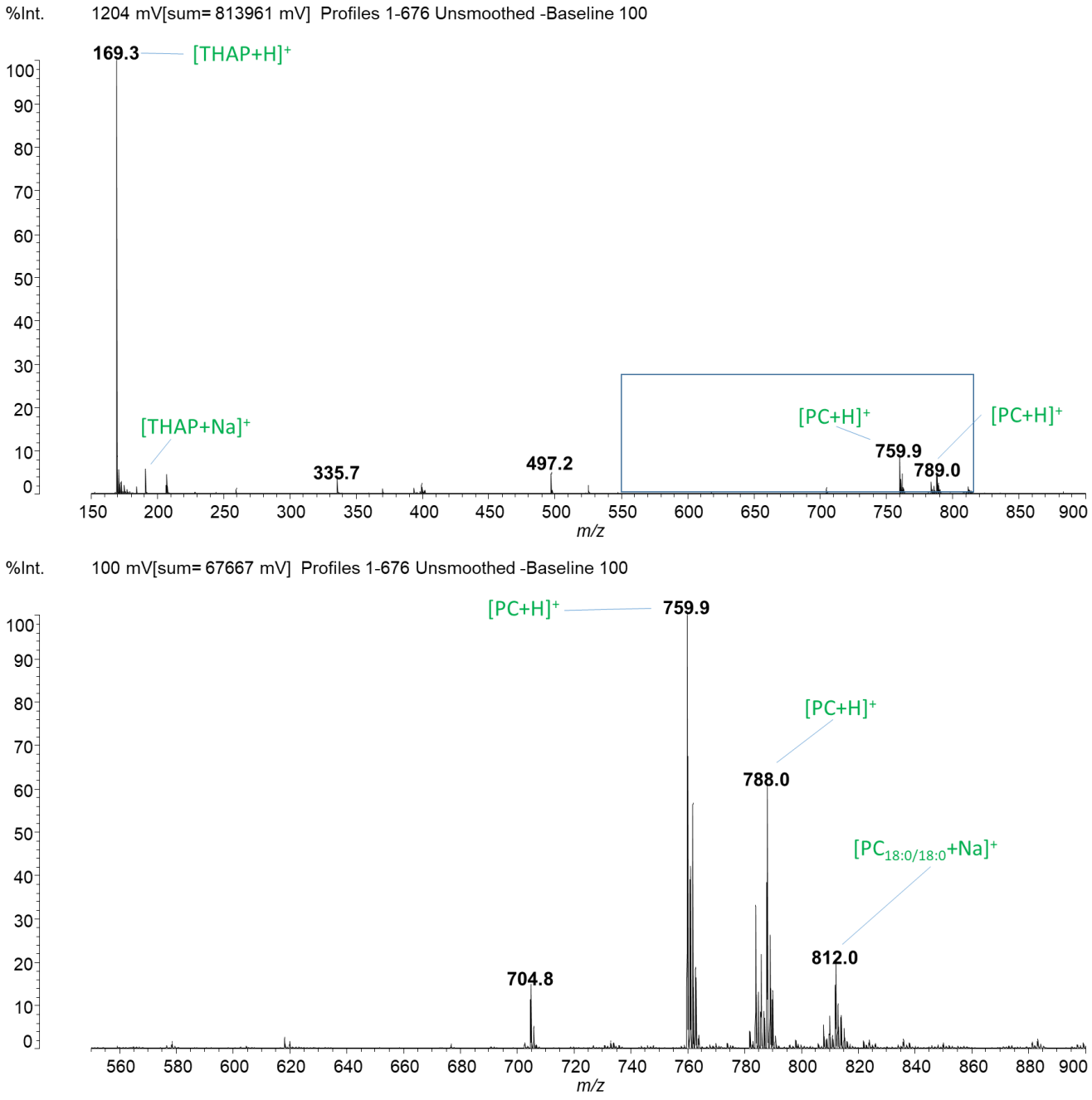

Figure 53: MS spectrum for VLDLs 1:30, before nES GEMMA collection. The upper panel shows the total mass range measured, the other panel represents enlarged m/z region (marked in blue in the upper panel) focussing on lipid peaks.

9.2.4. Prior nES GEMMA collection MS spectrum VLDLs 1:30 with protein mixture

Sample analysis described in Chapter 9.2.

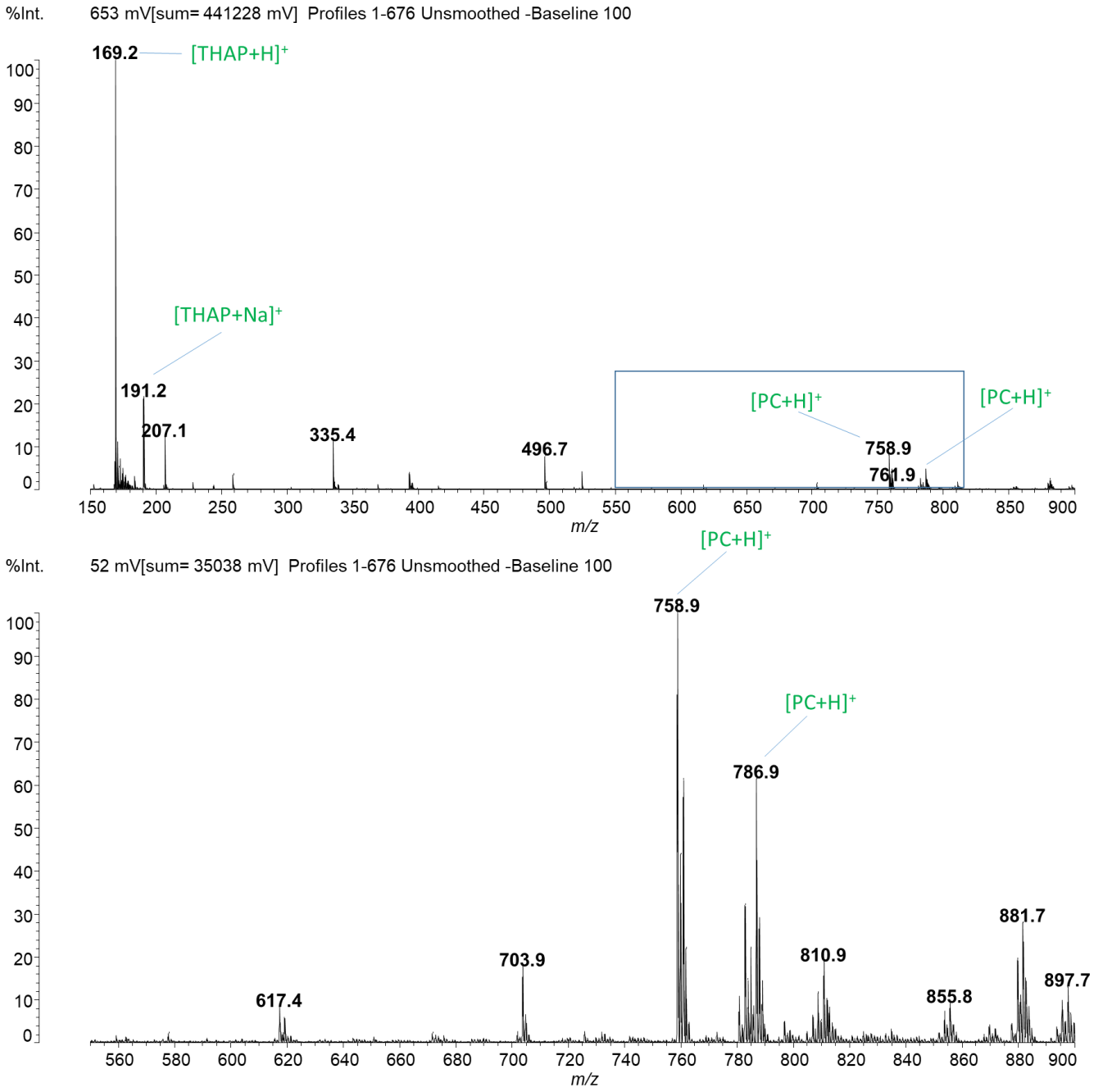

Figure 54: MS spectrum for VLDLs 1:30 with protein mixture, before nES GEMMA collection. The upper panel shows the total mass range measured, the other panel represents enlarged m/z region (marked in blue in the upper panel) focussing on lipid peaks.

9.2.5. After nES GEMMA collection MS spectrum VLDLs 1:30 with protein mixture

Sample analysis described in Chapter 9.2.

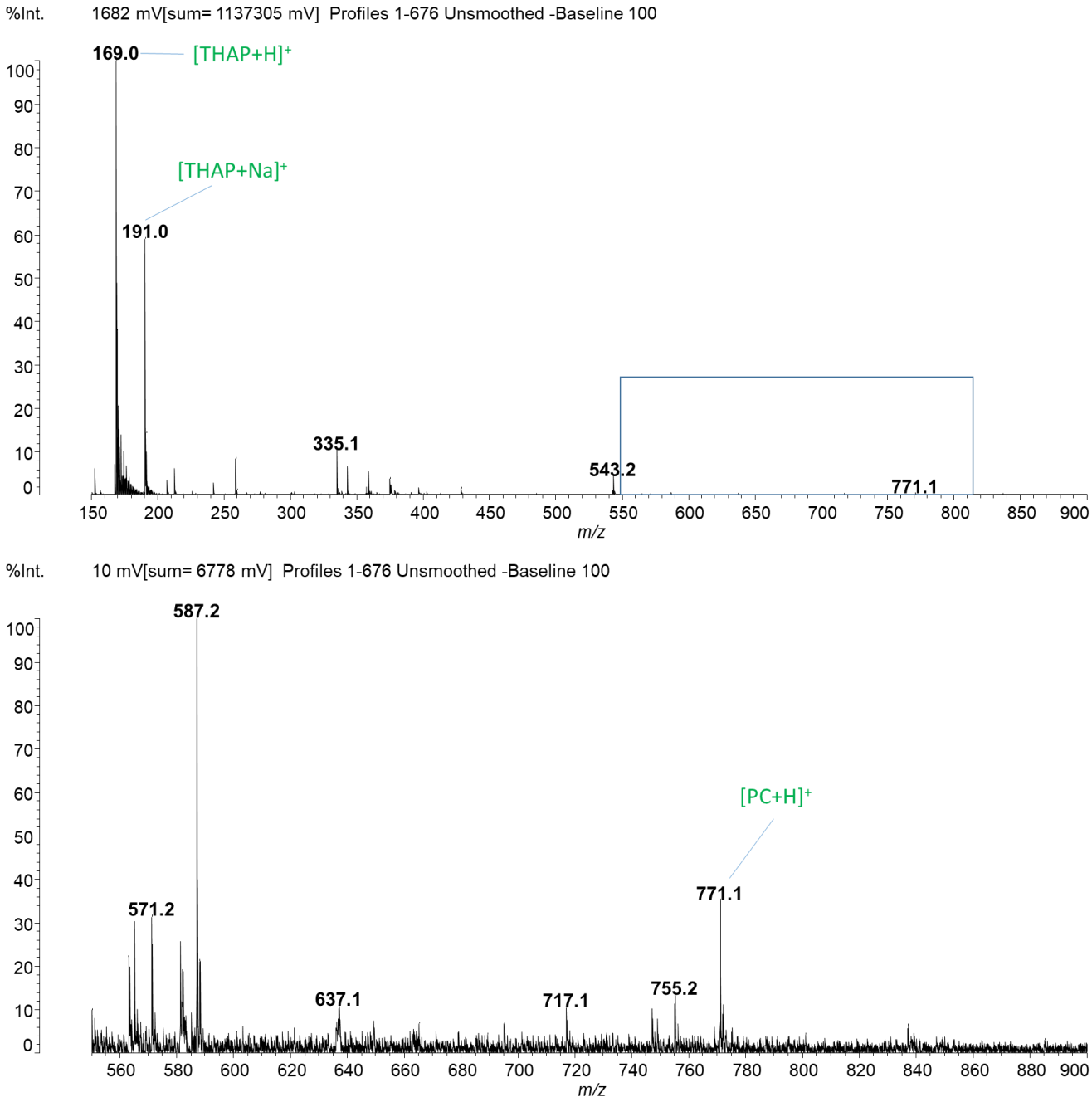

Figure 55: MS spectrum for VLDLs 1:30 with protein mixture, after nES GEMMA collection. The upper panel shows the total mass range measured, the other panel represents enlarged m/z region (marked in blue in the upper panel) focussing on lipid peaks.

9.3. MALDI mass spectrometry results of VLDLs at different particle size collection

VLDLs were analyzed with nES GEMMA and MALDI MS. The aim was to test if different EM collection diameters yield vesicles differing in their lipid species content. Hence, different lipid molecule patterns would be detected with MALDI MS prior and after nES GEMMA collection.

Firstly, VLDLs were subjected to buffer exchange and dilution to 1:20 via spin filtration. This process also removed small EM diameter material and salts present in the stock solution.

Firstly, the size distribution of the sample was acquired via nES GEMMA. Afterwards, analytes were collected on gold-coated silicon wafers at 28 nm, 33 nm, 38 nm and 43 nm EM particle diameter for approximately 5 hours (300 min), each. nES GEMMA spectra prior and after size-collection demonstrated the stability of the nES process during particle collection.

For MALDI MS measurements, 50 µl of each sample prior gas-phase electrophoretic fractionation were mixed with 50 µl of 20 mM THAP matrix solution and 0.9 µl of the mixture was applied to the MALDI MS target plate. For VLDL samples, different MALDI MS matrices were tested to obtain the optimal matrix compound and matrix concentration, which yields best results. Finally, 20 mM THAP matrix was chosen. Calibration was carried out with castor oil mixed with 5 mM NaCl in 20 mM THAP matrix.

After size separation and collection of the VLDLs at different collection EM diameters with nES GEMMA, the gold-coated silicon wafers were attached to the MS target plate and one spot of 20 mM THAP matrix was applied to the center of the wafer, respectively.

The aim was to acquire MS data for VLDLs prior and after offline hyphenation of nES GEMMA with MALDI MS. Results are presented in the following chapters.

MALDI MS spectra relate several peaks: usually the matrix peak can be seen as well as matrix adducts with sodium and peaks for lipid species. Lipid peaks are more abundant in mass spectra acquired prior to nES GEMMA size-collection. Peaks in the m/z range 150 – 900 m/z are presented. Subsequently, enlarged regions, corresponding to the m/z range 550-900 m/z with putative lipid peaks, are marked in blue.

Different lipid peak patterns were expected to be seen on MALDI MS spectra for different EM collection diameters. Therefore, size separation via nES GEMMA could be used to visualize different compounds, which are otherwise suppressed in a complex mixture. However, sadly MALDI MS spectra acquired did not show quantitative difference proving this hypothesis.

9.3.1. Prior nES GEMMA collection MS spectrum VLDLs 1:20

Sample analysis described in Chapter 9.3.

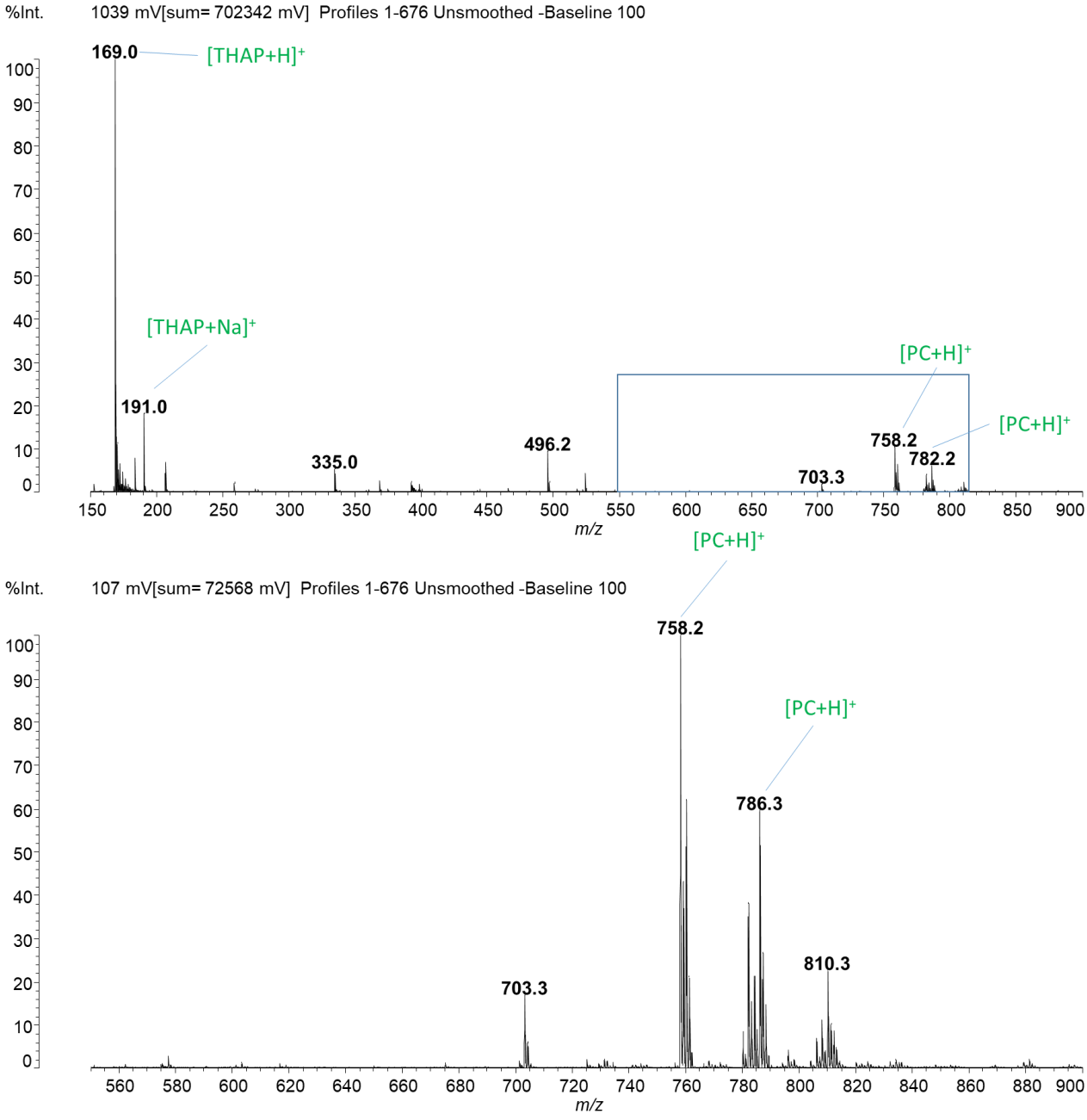

Figure 56: MS spectrum for VLDLs 1:20 before nES GEMMA collection. The upper panel shows the total mass range measured, the other panel represents enlarged m/z region (marked in blue in the upper panel) focussing on lipid peaks.

.

9.3.2. nES GEMMA measurements for VLDLs 1:20

nES GEMMA measurements are described in Chapter 9.3.

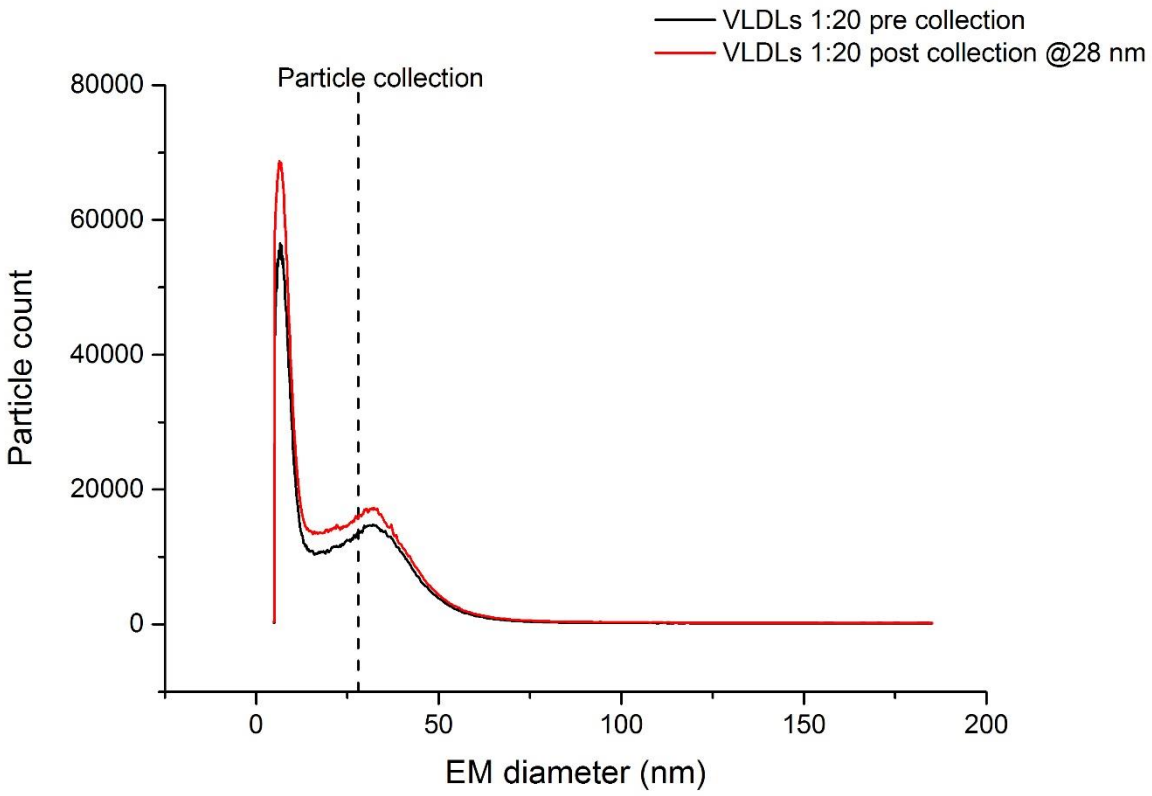

Figure 57: Size distribution for mixture of VLDLs 1:20, before and after nES GEMMA collection. The EM collection diameter is also presented on the graph. The collection was carried out at 28 nm.

9.3.3. After nES GEMMA collection MS spectrum VLDLs 1:20, collection @ 28 nm EM diameter

Sample analysis described in Chapter 9.3.

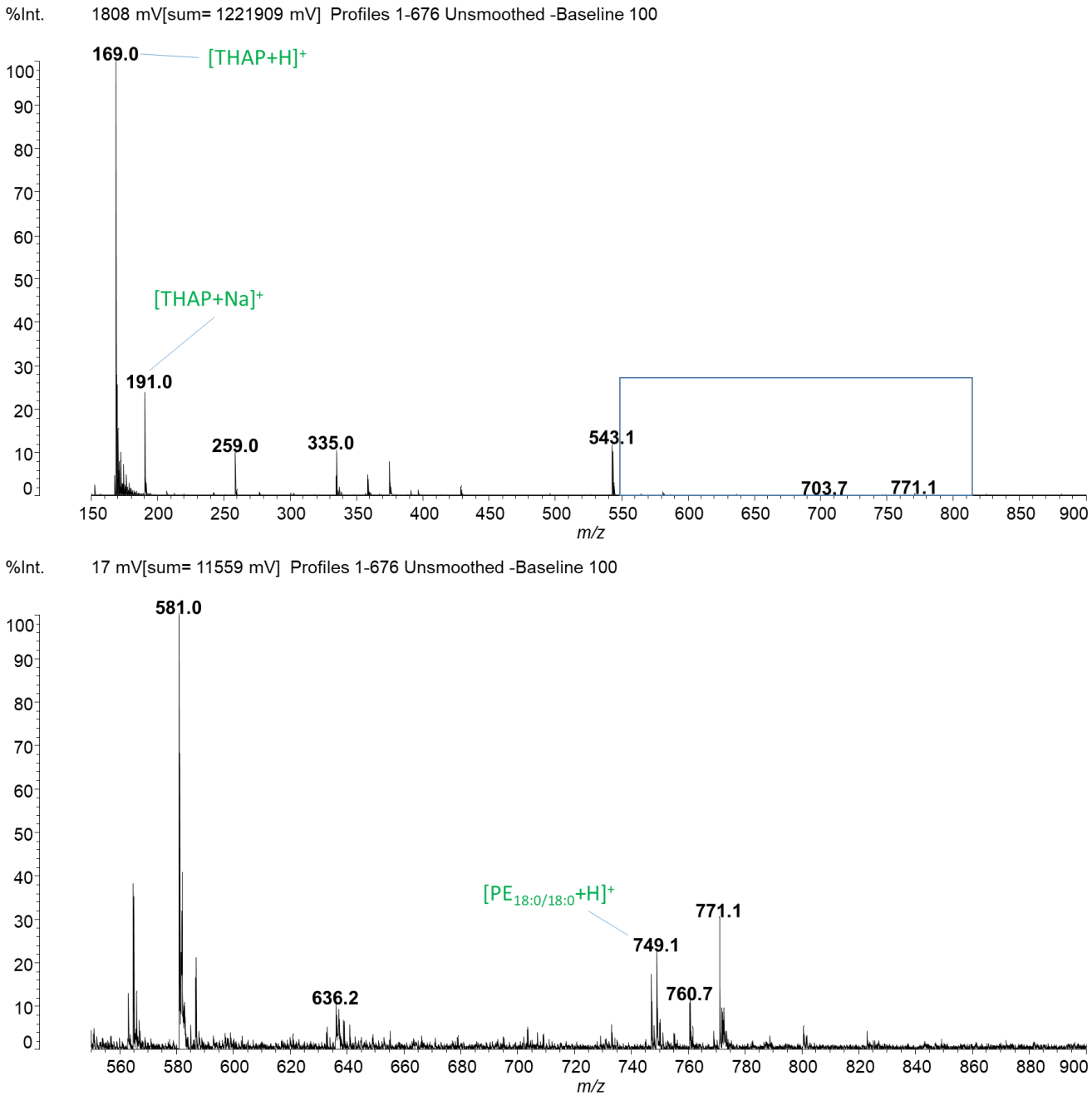

Figure 58: MS spectrum for VLDLs 1:20 after nES GEMMA collection @28 nm EM diameter. The upper panel shows the total mass range measured, the other panel represents enlarged m/z region (marked in blue in the upper panel) focussing on lipid peaks.

9.3.4. nES GEMMA measurements for VLDLs 1:20

nES GEMMA measurements are described in Chapter 9.3.

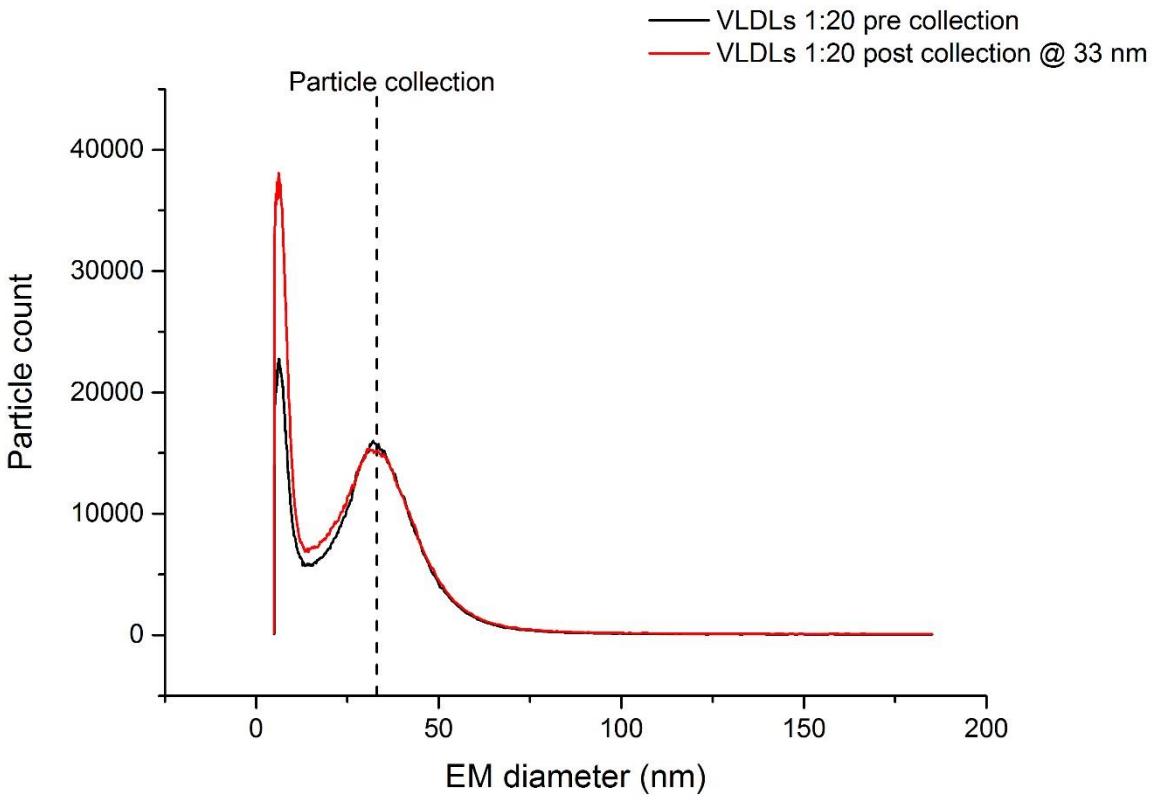

Figure 59: Size distribution for mixture of VLDLs 1:20, before and after nES GEMMA collection. The EM collection diameter is also presented on the graph. The collection was carried out at 33 nm.

9.3.5. After nES GEMMA collection MS spectrum VLDLs 1:20, collection @ 33 nm EM diameter

Sample analysis described in Chapter 9.3.

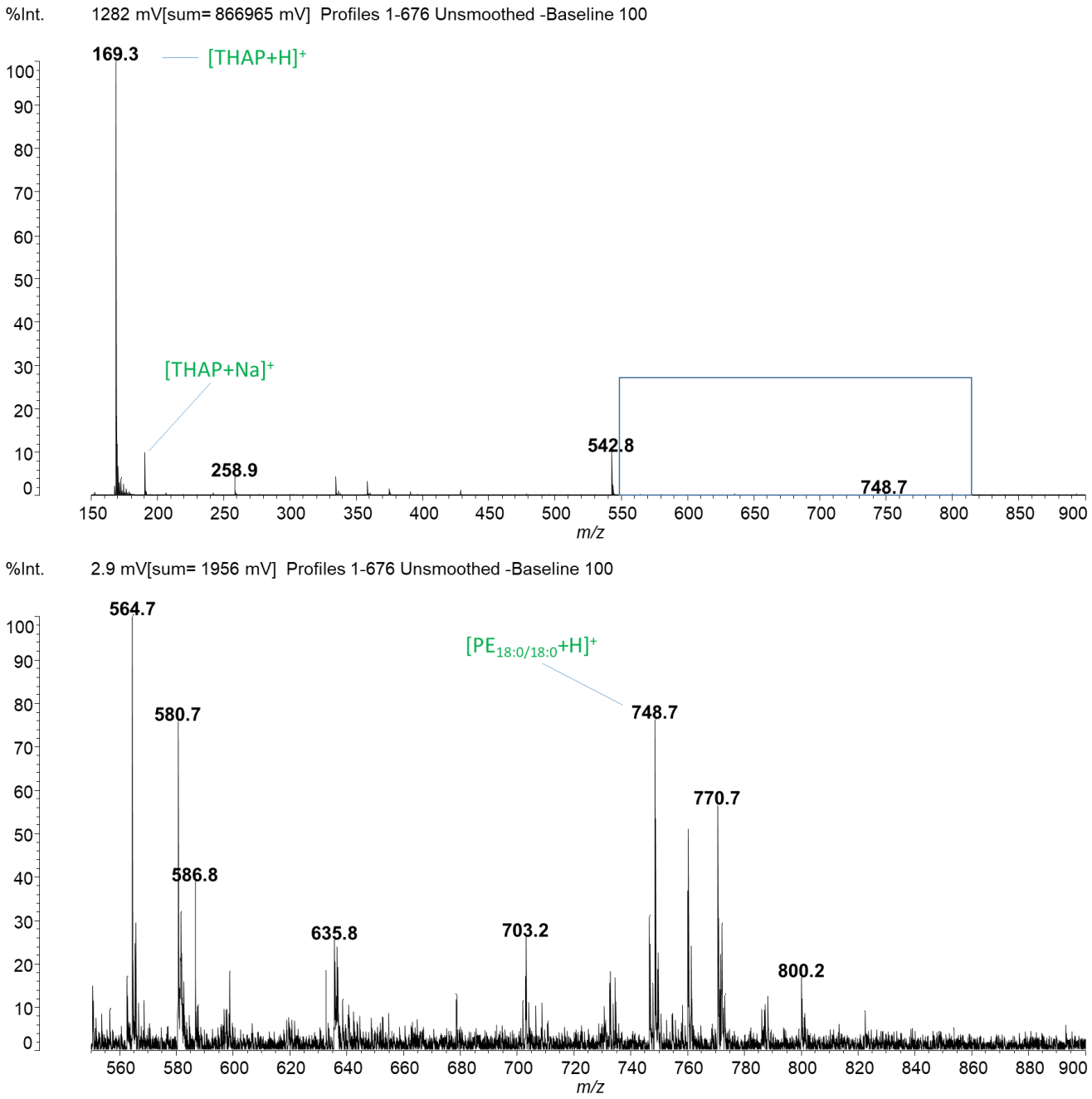

Figure 60: MS spectrum for VLDLs 1:20 after nES GEMMA collection @33 nm EM diameter. The upper panel shows the total mass range measured, the other panel represents enlarged m/z region (marked in blue in the upper panel) focussing on lipid peaks.

.

9.3.6. nES GEMMA measurements for VLDLs 1:20

nES GEMMA measurements are described in Chapter 9.3.

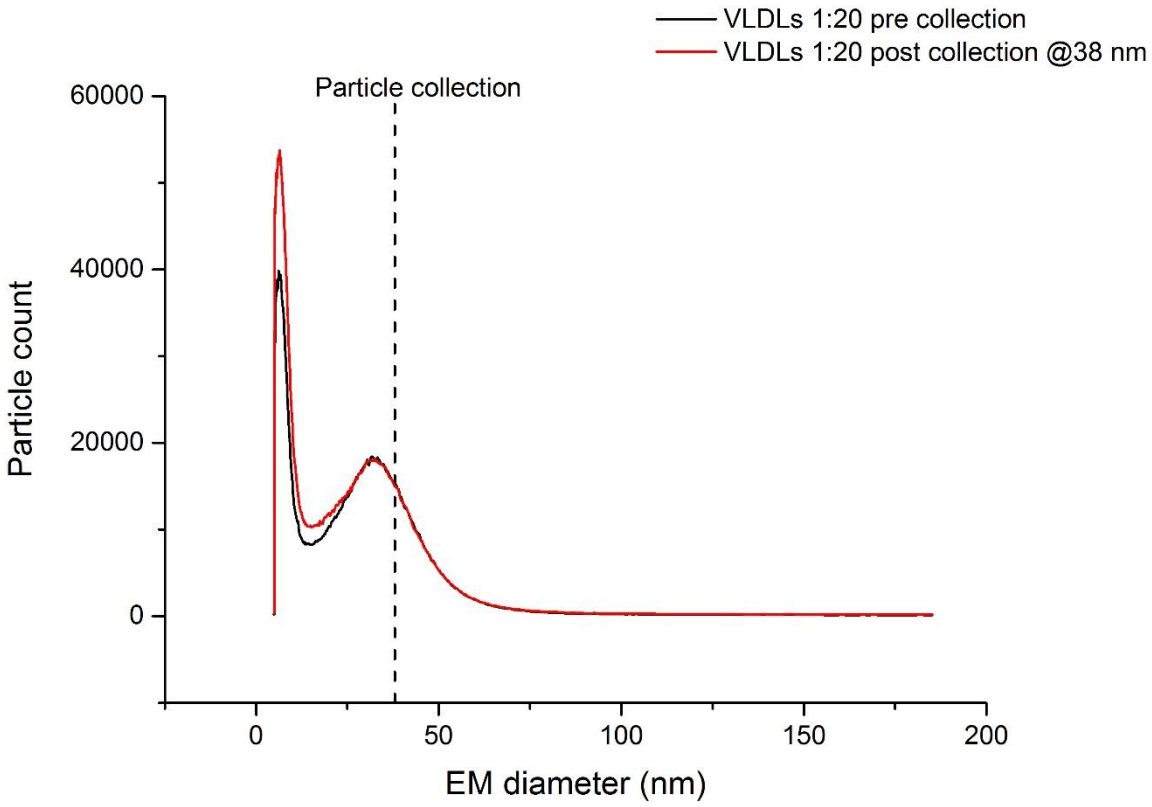

Figure 61: Size distribution for mixture of VLDLs 1:20, before and after nES GEMMA collection. The EM collection diameter is also presented on the graph. The collection was carried out at 38 nm.

9.3.7. After nES GEMMA collection MS spectrum VLDLs 1:20, collection @ 38 nm EM diameter

Sample analysis described in Chapter 9.3.

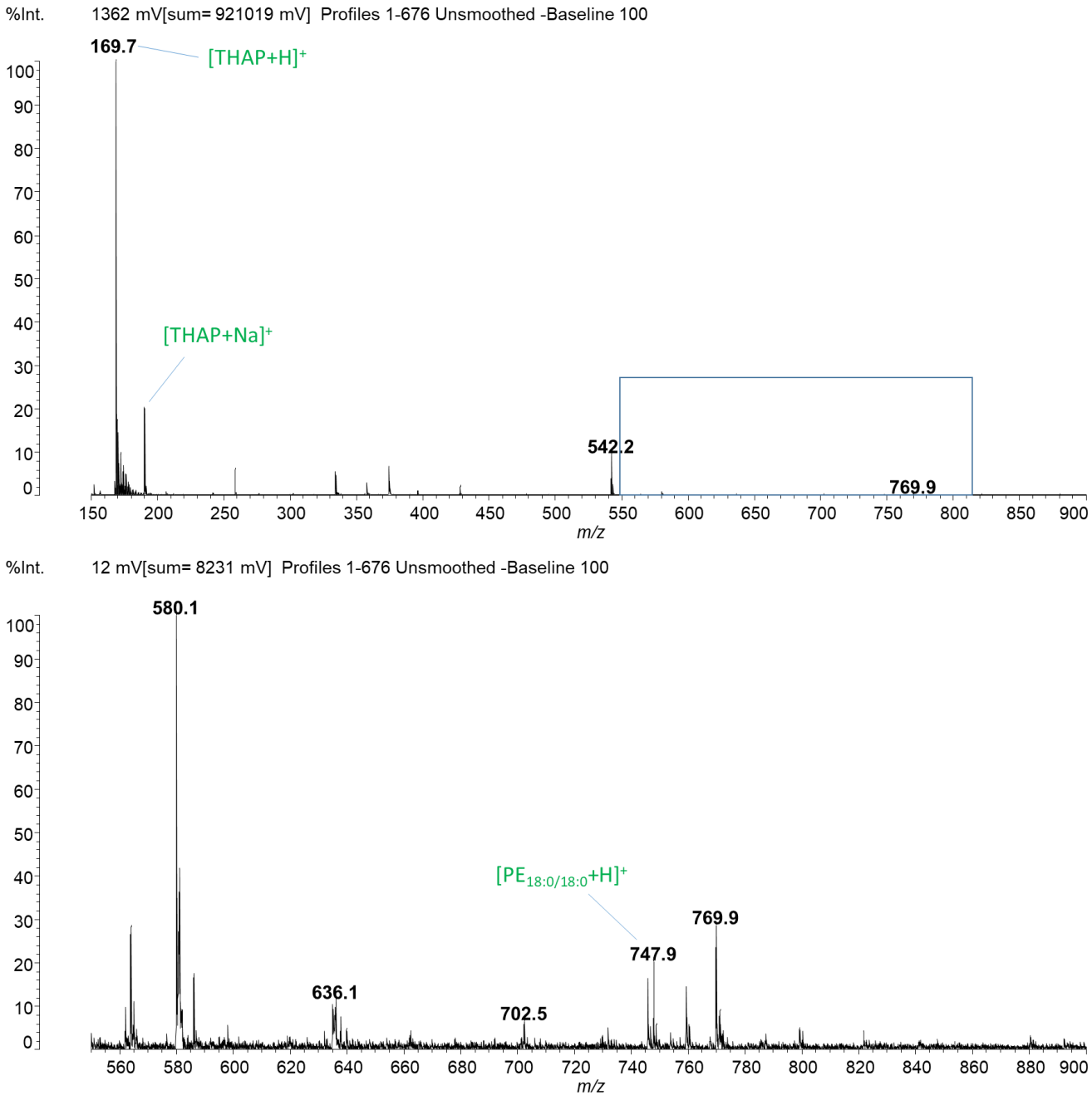

Figure 62: MS spectrum for VLDLs 1:20 after nES GEMMA collection @38 nm EM diameter. The upper panel shows the total mass range measured, the other panel represents enlarged m/z region (marked in blue in the upper panel) focussing on lipid peaks.

.

9.3.8. nES GEMMA measurements for VLDLs 1:20

nES GEMMA measurements are described in Chapter 9.3.

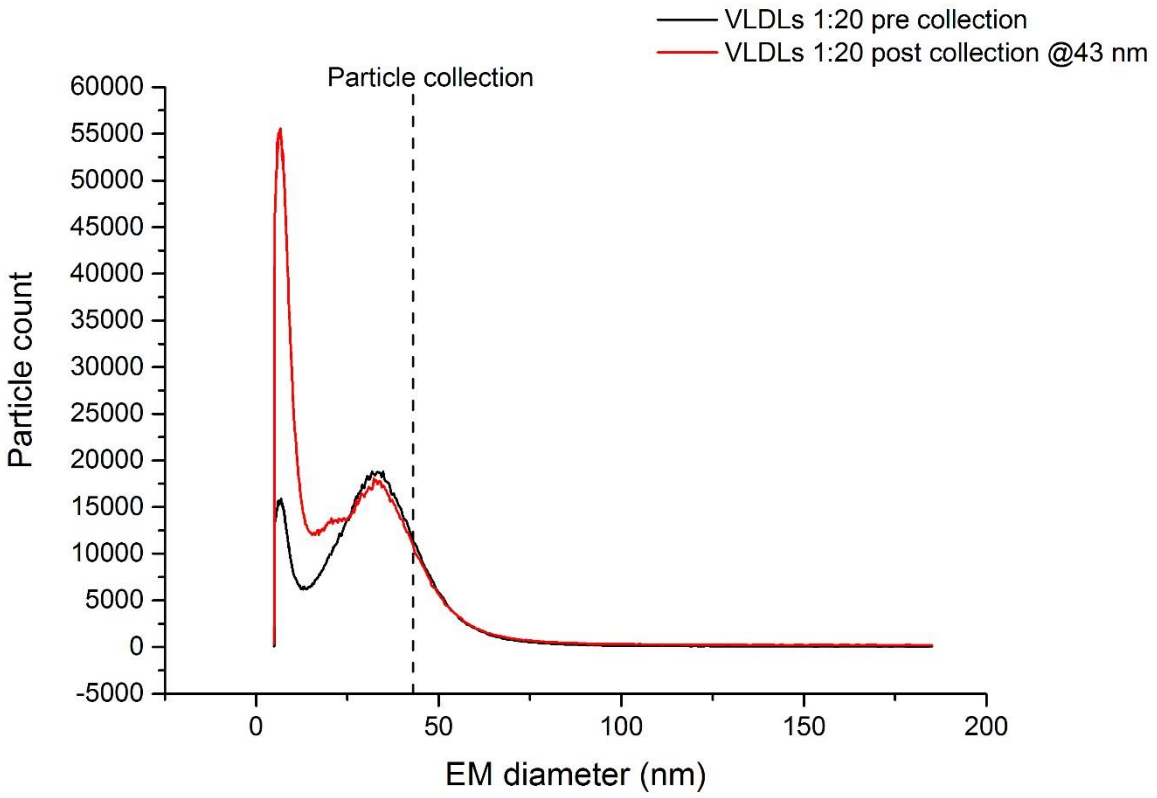

Figure 63: Size distribution for mixture of VLDLs 1:20, before and after nES GEMMA collection. The EM collection diameter is also presented on the graph. The collection was carried out at 43 nm.

9.3.9. After nES GEMMA collection MS spectrum VLDLs 1:20, collection @ 43 nm EM diameter

Sample analysis described in Chapter 9.3.

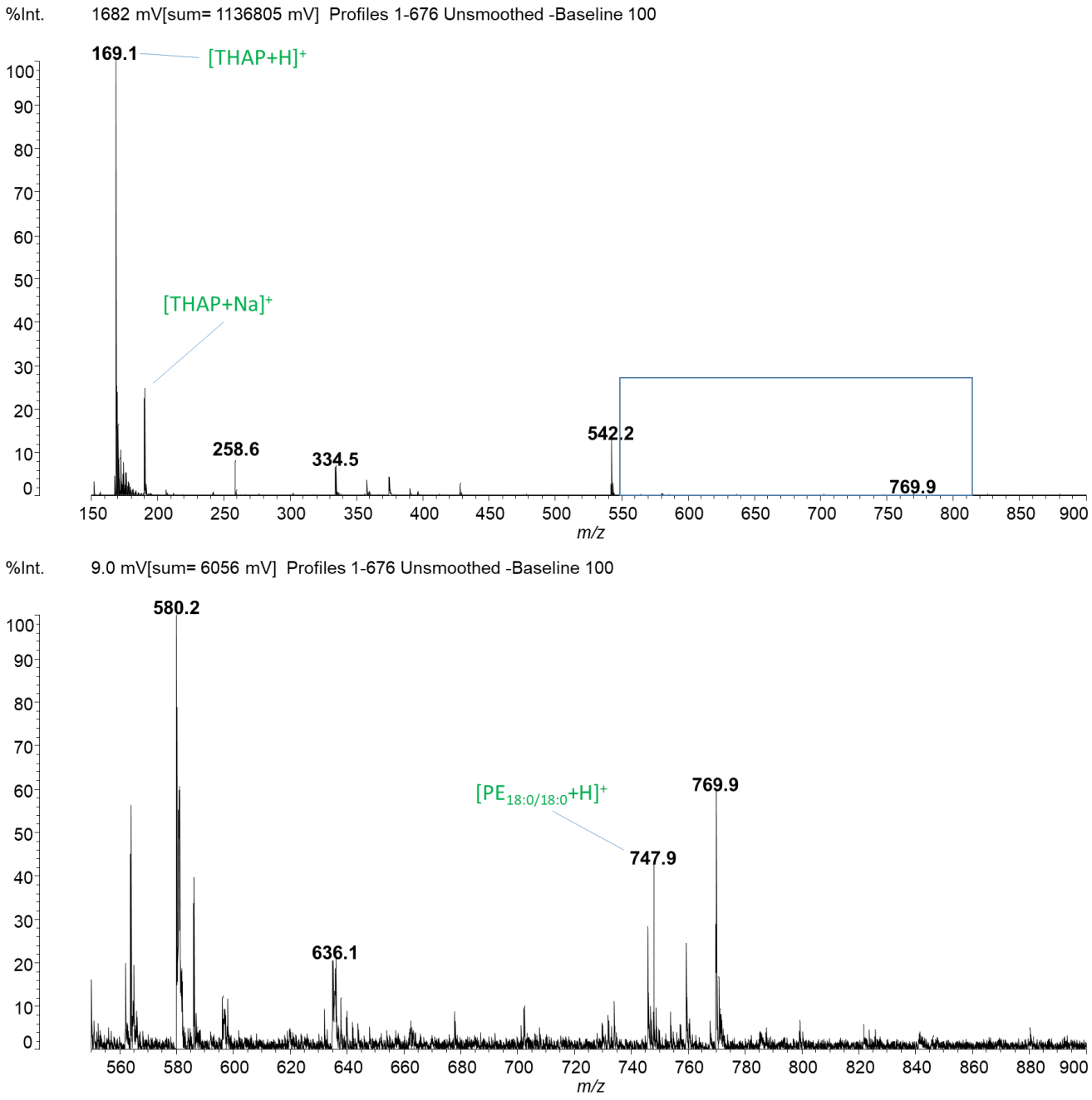

Figure 64: MS spectrum for VLDLs 1:20 after nES GEMMA collection @43 nm EM diameter. The upper panel shows the total mass range measured, the other panel represents enlarged m/z region (marked in blue in the upper panel) focussing on lipid peaks..

9.4. MALDI mass spectrometry with different MALDI MS matrices

Different MALDI MS matrix molecules are optimized for the MS measurements of different analytes. Usually a matrix compound is chosen by trial and error, however, some chemical properties exist which can be taken into consideration when choosing the right MALDI matrix for the sample.

MALDI MS was used to detect lipid molecules and organic cargo molecules, thus three different MALDI matrices were chosen: THAP, SA and CHCA respectively.

Different matrix concentrations were prepared with the corresponding matrix solvents:

Matrix compound	Matrix solvent	Concentrations
THAP	MeOH	5 mM, 10 mM, 15 mM
CHCA	H_2O:ACN = 1:1 (v:v) + 0.1% TFA	5 mM, 10 mM, 15 mM
SA	H_2O:ACN = 1:1 (v:v) + 0.1% TFA	5 mM, 10 mM, 15 mM

Table 33: Different MALDI matrix solutions

MALDI MS analysis was carried out for panthenol as a cargo molecule with THAP, SA and CHCA matrix. A stock solution of 20 mM panthenol in 40 mM NH_4OAc, pH 8.4 was further diluted to 1:10, 1:100 and 1:1000 to test the minimum amount of panthenol, which can still be detected via MALDI MS. 50 µl of panthenol sample was mixed with 50 µl of the corresponding matrix solution and approximately 1 µl of the mixture was applied to the MALDI target plate.

Likewise, MALDI MS analysis was carried out for melatonin as cargo molecule with THAP, SA and CHCA matrix. A stock solution of 4 mM melatonin in 40 mM NH_4OAc, pH 8.4 was further diluted to 1:10, 1:100 and 1:1000 to test the minimum amount of melatonin, which can still be detected via MALDI MS. 50 µl of melatonin sample was mixed with 50 µl of the corresponding matrix solution and approximately 1 µl of the mixture was applied to the MALDI target plate.

MALDI MS analysis was also carried out for VLDL samples with THAP, SA and CHCA matrix. Again, a stock solution was further diluted to 1:30. We wished to optimize the matrix compound to detect VLDL lipid molecules. 50 µl of VLDL sample was mixed with 50 µl of the corresponding matrix solution and approximately 0.9 µl of the mixture was applied to the MALDI target plate.

Images of the obtained crystals on the target plates with different matrix compounds mixed with analyte solution (mixture of liposomes and VLDLs in 10:3 volumetric ratio) are shown below:

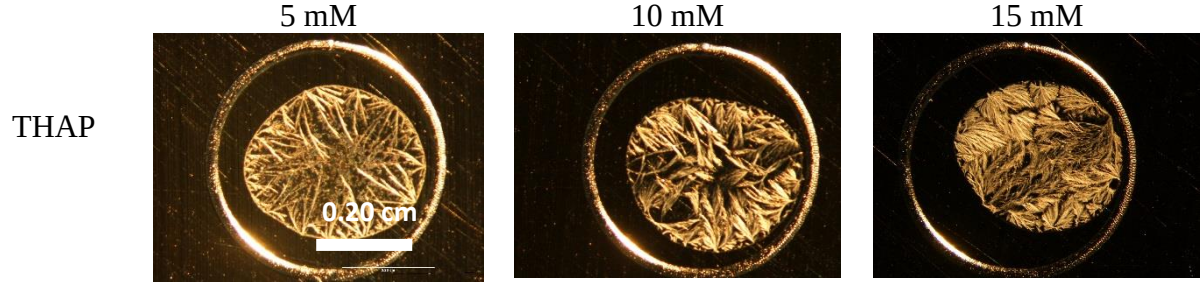

SA

CHCA

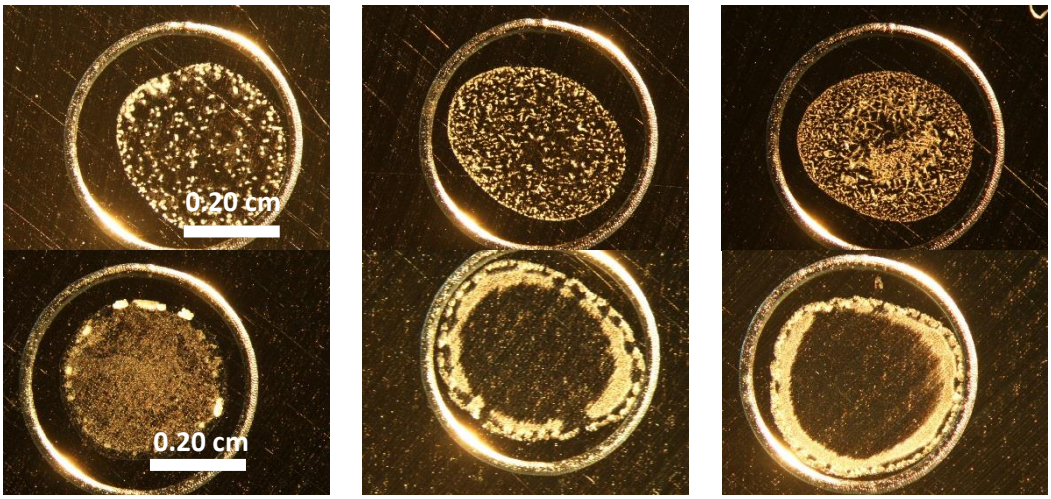

Figure 65: Images of matrix crystals for samples prior collection

9.4.1. MS spectrum for panthenol, 1:10 dilution with different matrices ([M] = $C_9H_{19}NO_4$, MW = 205,251 g/mol)

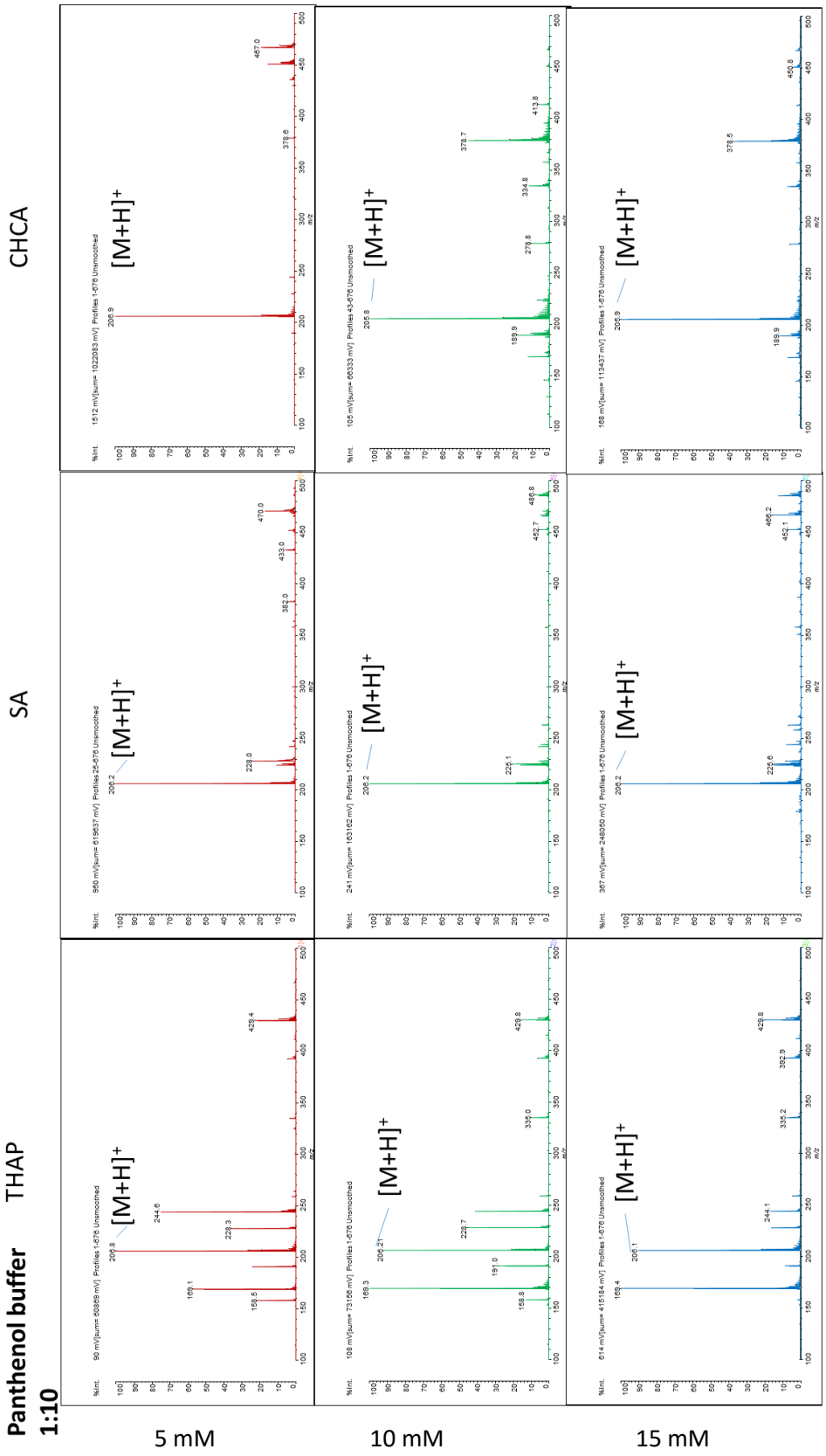

Figure 66: MALDI MS spectra for panthenol 1:10 with different matrices and different matrix concentrations

9.4.2. MS spectrum for panthenol, 1:100 dilution with different matrices ([M] = $C_9H_{19}NO_4$, MW = 205,251 g/mol)

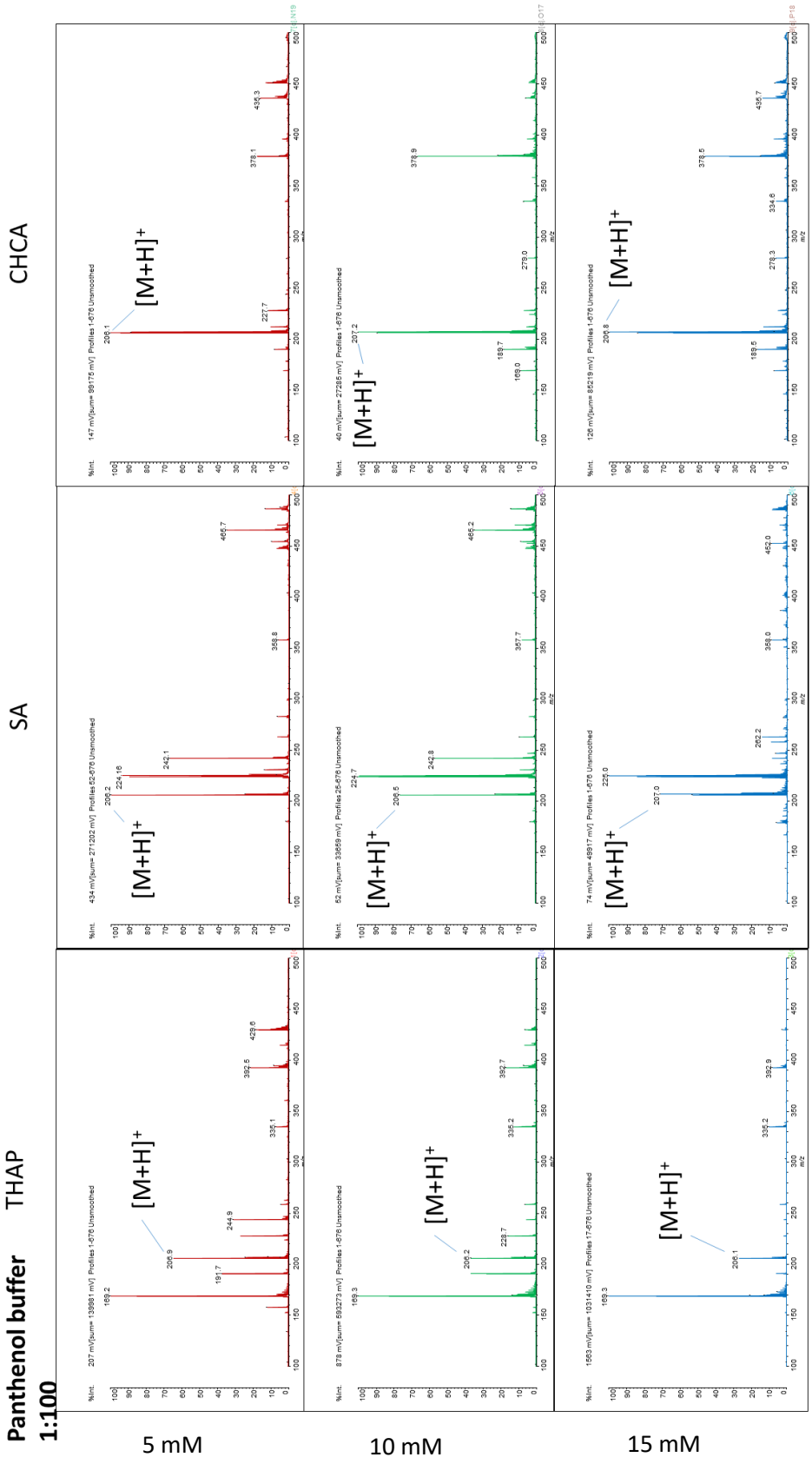

Figure 67: MALDI MS spectra for panthenol 1:100 with different matrices and different matrix concentrations

9.4.3. MS spectrum for panthenol, 1:1000 dilution with different matrices ([M] = $C_9H_{19}NO_4$, MW = 205,251 g/mol)

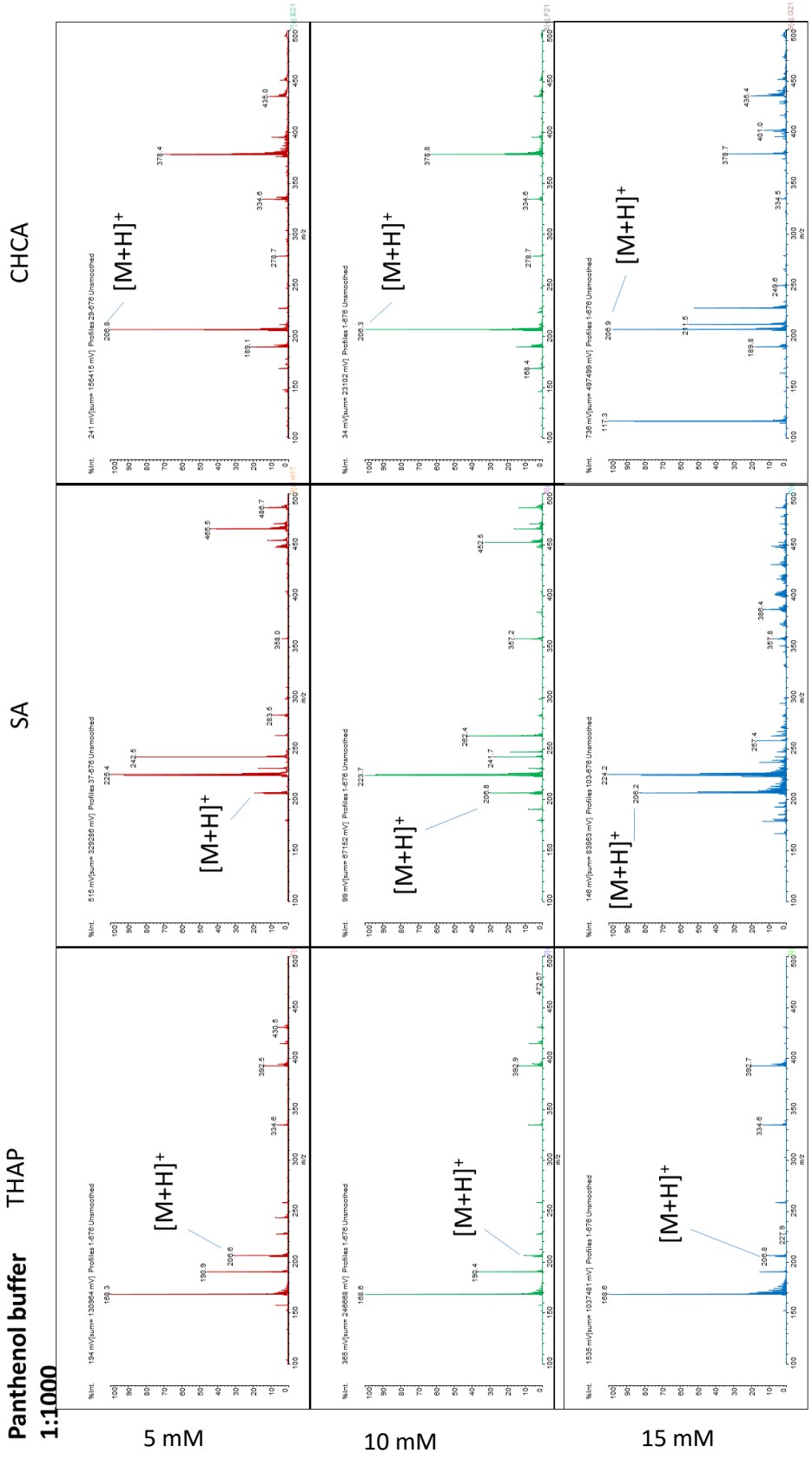

Figure 68: MALDI MS spectra for panthenol 1:100 with different matrices and different matrix concentrations

Intensities for the panthenol peak are presented below, measurements were performed automatically:

PANTHENOL 1:10	5 mM	10 mM	15 mM
THAP	90 mV	97 mV	**552 mV**
SA	**950 mV**	241 mV	367 mV
CHCA	**1512 mV**	105 mV	168 mV

PANTHENOL 1:100	5 mM	10 mM	15 mM
THAP	134 mV	351 mV	**468 mV**
SA	**434 mV**	41 mV	44 mV
CHCA	**147 mV**	40 mV	126 mV

PANTHENOL 1:1000	5 mM	10 mM	15 mM
THAP	58 mV	54 mV	**230 mV**
SA	103 mV	29 mV	**131 mV**
CHCA	241 mV	34 mV	**736 mV**

It can be seen that for different amounts of panthenol molecules present in the sample, different concentrations of the MALDI matrices give best results. For low quantities of panthenol, higher concentrations of matrix solutions should be used, i.e. the ratio between analyte and matrix molecules is crucial.

High concentration of THAP matrix always gives best results. This is not true for SA and CHCA matrix. As the concentration of the analyte is lower, the concentrations of the SA and CHCA matrices should be higher to obtain satisfactory results.

9.4.4. MS spectrum for melatonin, 1:10 dilution with different matrices ([M] = $C_{13}H_{16}N_2O_2$, MW = 232,28 g/mol)

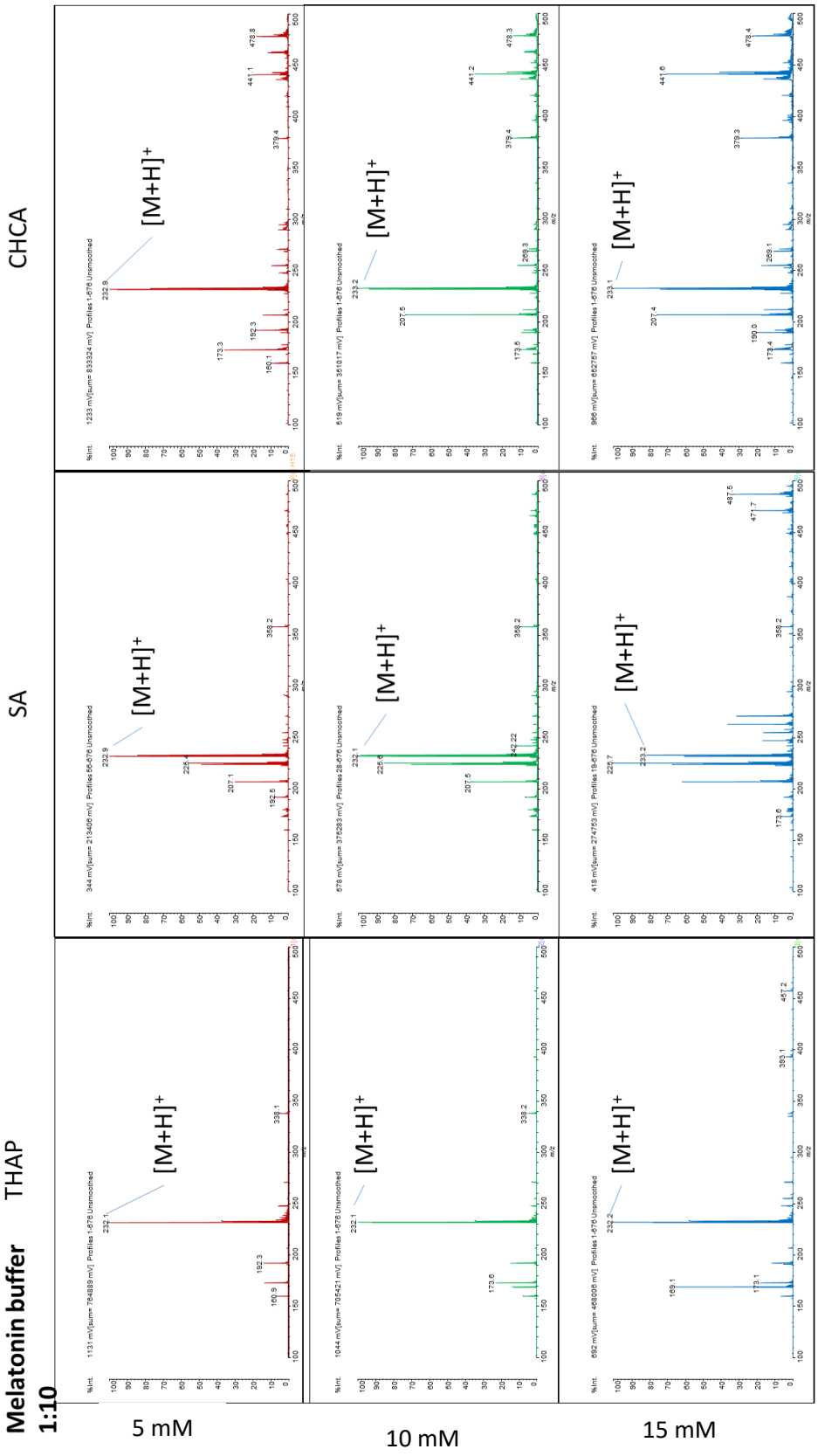

Figure 69: MALDI MS spectra for melatonin 1:10 with different matrices and different matrix concentrations

9.4.5. MS spectrum for melatonin, 1:100 dilution with different matrices ([M] = $C_{13}H_{16}N_2O_2$, MW = 232,28 g/mol)

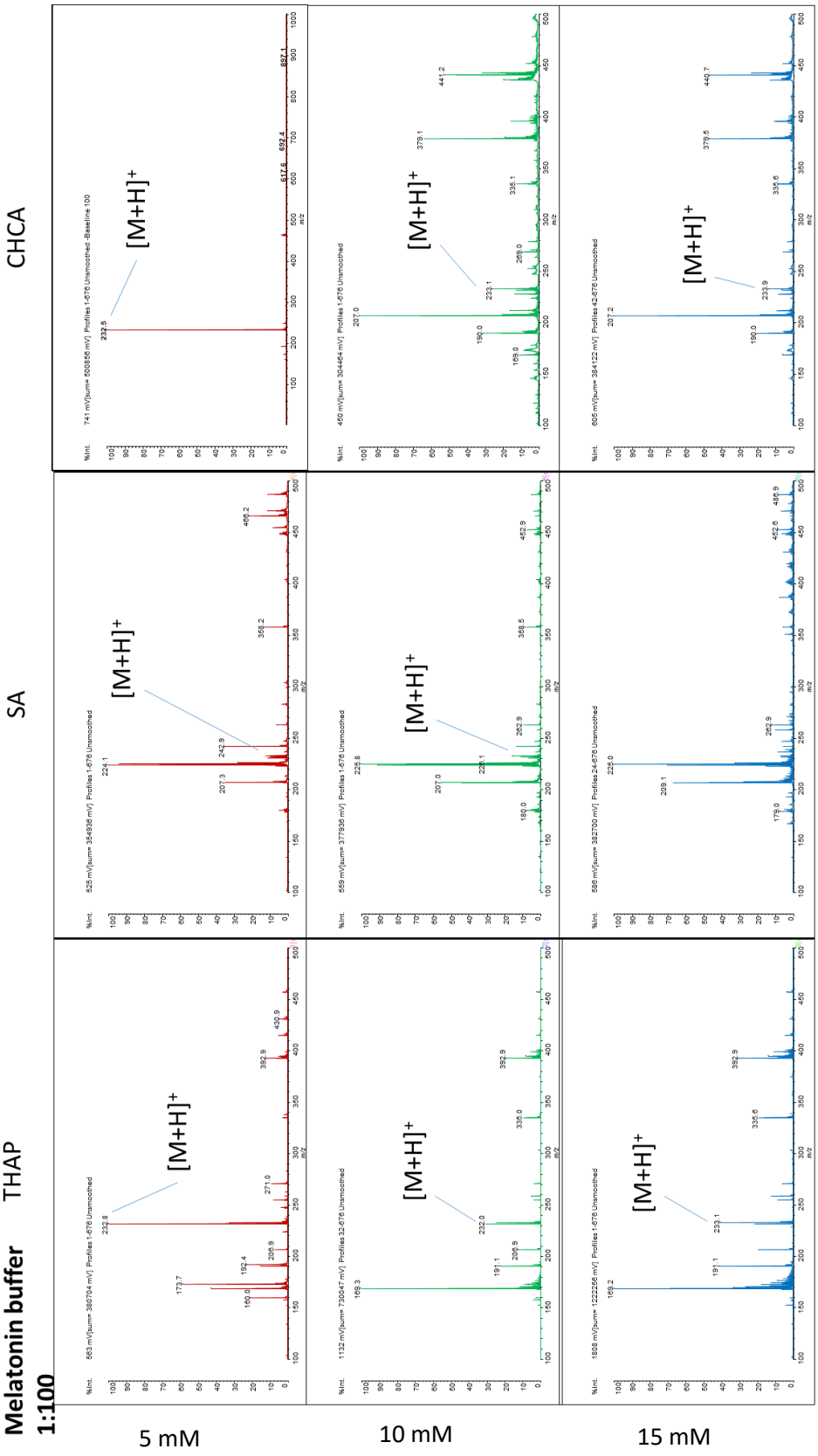

Figure 70: MALDI MS spectra for melatonin 1:100 with different matrices and different matrix concentrations

9.4.6. MS spectrum for melatonin, 1:1000 dilution with different matrices ([M] = $C_{13}H_{16}N_2O_2$, MW = 232,28 g/mol)

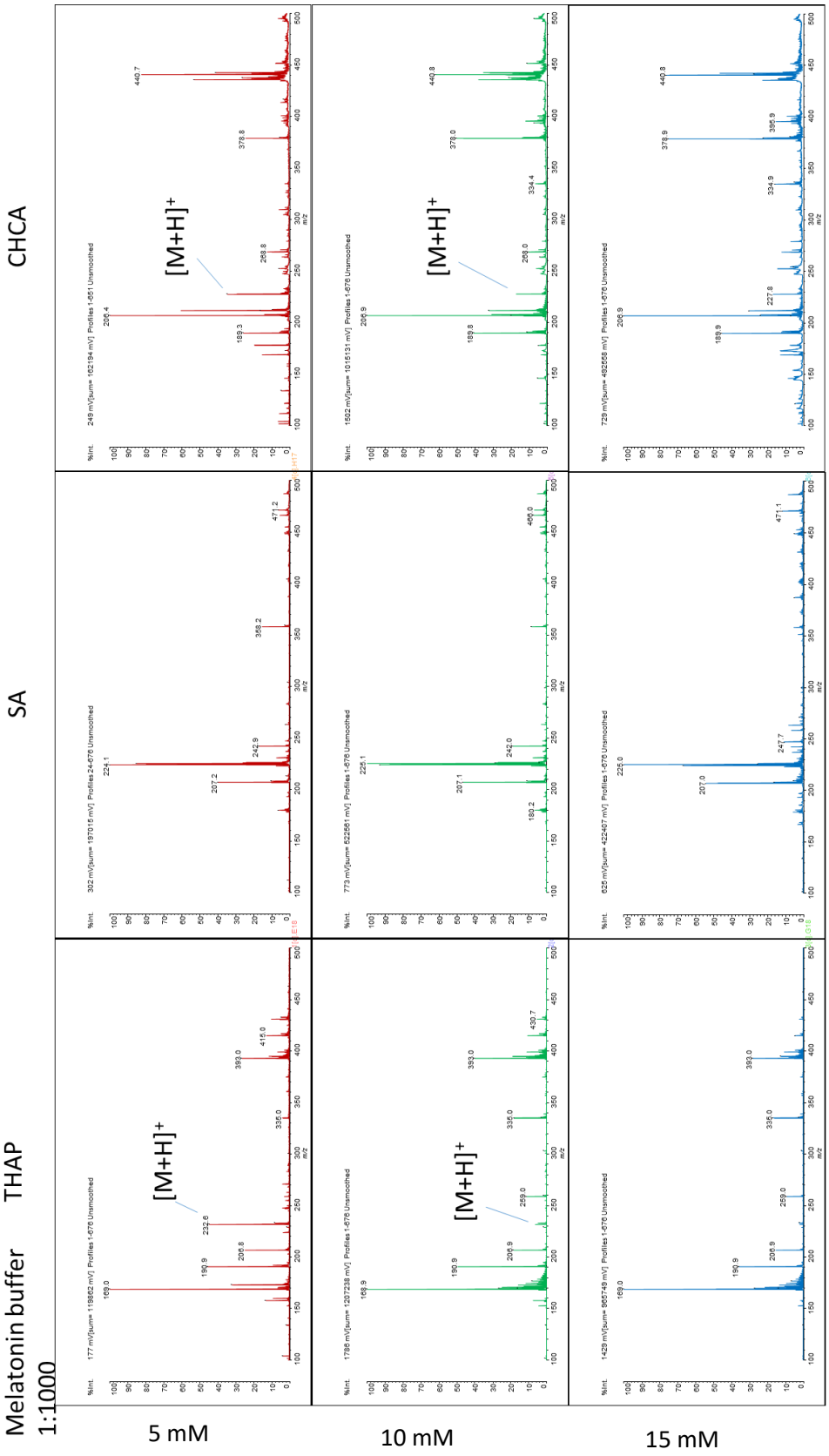

Figure 71: MALDI MS spectra for melatonin 1:1000 with different matrices and different matrix concentrations

Intensities for the melatonin peak are presented below, measurements were performed automatically:

MELATONIN 1:10	5 mM	10 mM	15 mM
THAP	**1131 mV**	1044 mV	692 mV
SA	344 mV	**578 mV**	376 mV
CHCA	**1233 mV**	519 mV	966 mV

MELATONIN 1:100	5 mM	10 mM	15 mM
THAP	563 mV	**1132 mV**	813 mV
SA	52 mV	**112 mV**	58 mV
CHCA	**741 mV**	121 mV	128 mV

MELATONIN 1:1000	5 mM	10 mM	15 mM
THAP	88 mV	**178 mV**	71 mV
SA	30 mV	**77 mV**	31 mV
CHCA	12 mV	**15 mV**	8 mV

For melatonin, MALDI MS matrices with 10 mM concentrations work best for low quantities of melatonin molecules. For higher concentrations of the melatonin, even lower concentrations of MALDI matrices give better results.

9.4.7. MS spectrum VLDLs 1:30 with different matrices

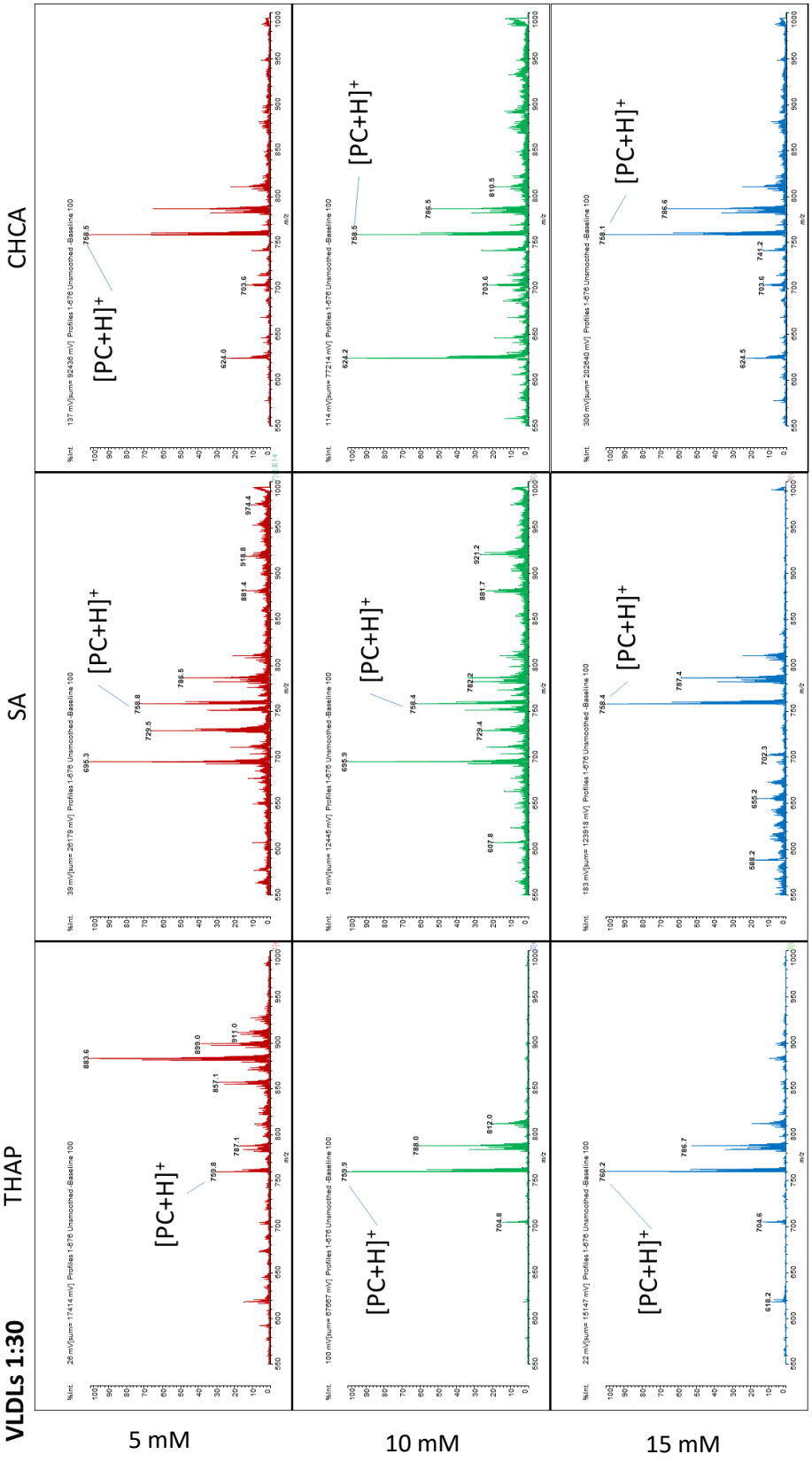

Figure 72: MALDI MS spectra for VLDLS with different matrices and different matrix concentrations

9.5. Different depositions of sample and MALDI MS matrix

To obtain better re-crystallization of the analyte and the MALDI MS matrix, different preparations of the sample-matrix solution were tested. Furthermore, different sample-matrix solution depositions to the target plate were analysed as well. 5 mM NaCl in 20 mM THAP was used for the matrix solution.

Liposomes with encapsulated panthenol were used as a sample compound. Different dilutions were used. Liposomes with melatonin in different dilutions were tested as well.

Firstly, 50 µl of sample and 50 µl of matrix solution was mixed together and approximately 1 µl of the mixture was applied to the target plate.

Secondly, one µl of the sample was applied directly to the target plate and let to dry. Afterwards 1µl of the matrix solution was applied over the sample depositions to the target plate.

Last but not least, one µl of the sample was applied directly to the target plate and let to dry. Afterwards one µl of the matrix solution was applied over the sample depositions and let to dry. Then one µl of 1:1 (v:v) H_2O:MeOH was applied over the sample and matrix depositions in order to dissolve both again and let them to dry to form new crystals.

To conclude, no significant differences between different preparation and sample deposition methods could be found. Therefore, the first preparation method, with the mixture of sample and the matrix deposited to the target plate, was used for further MALDI MS measurements.

9.5.1. MS spectrum liposomes with panthenol ([M] = $C_9H_{19}NO_4$, MW = 205,251 g/mol) – different sample preparation/deposition

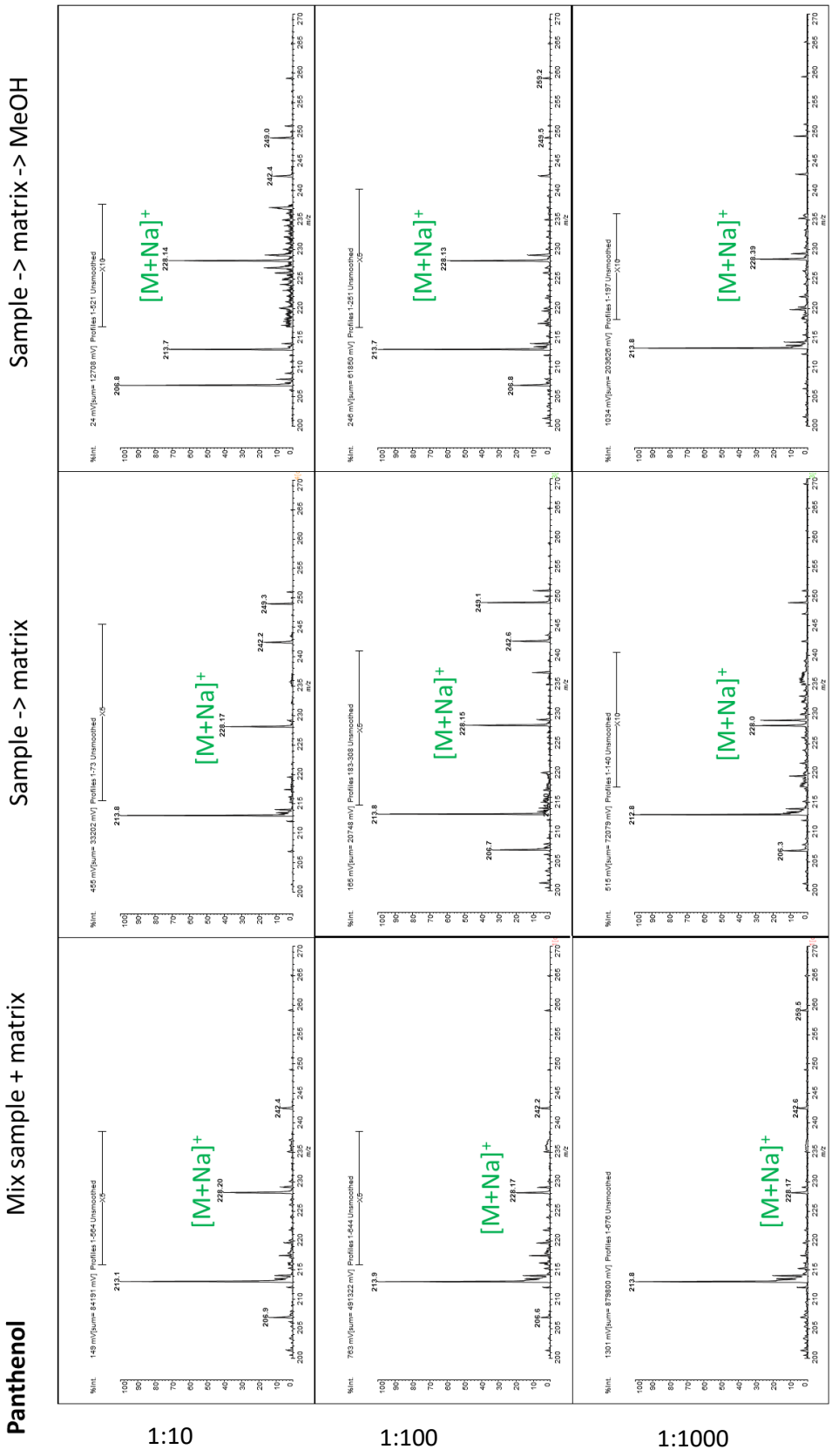

Figure 73: MALDI MS spectra for liposomes with panthenol, using different techniques to prepare and deposit the sample/matrix solution to the target plate

9.5.2. MS spectrum liposomes with melatonin ([M] = $C_{13}H_{16}N_2O_2$, MW = 232,28 g/mol) – different sample preparation/deposition

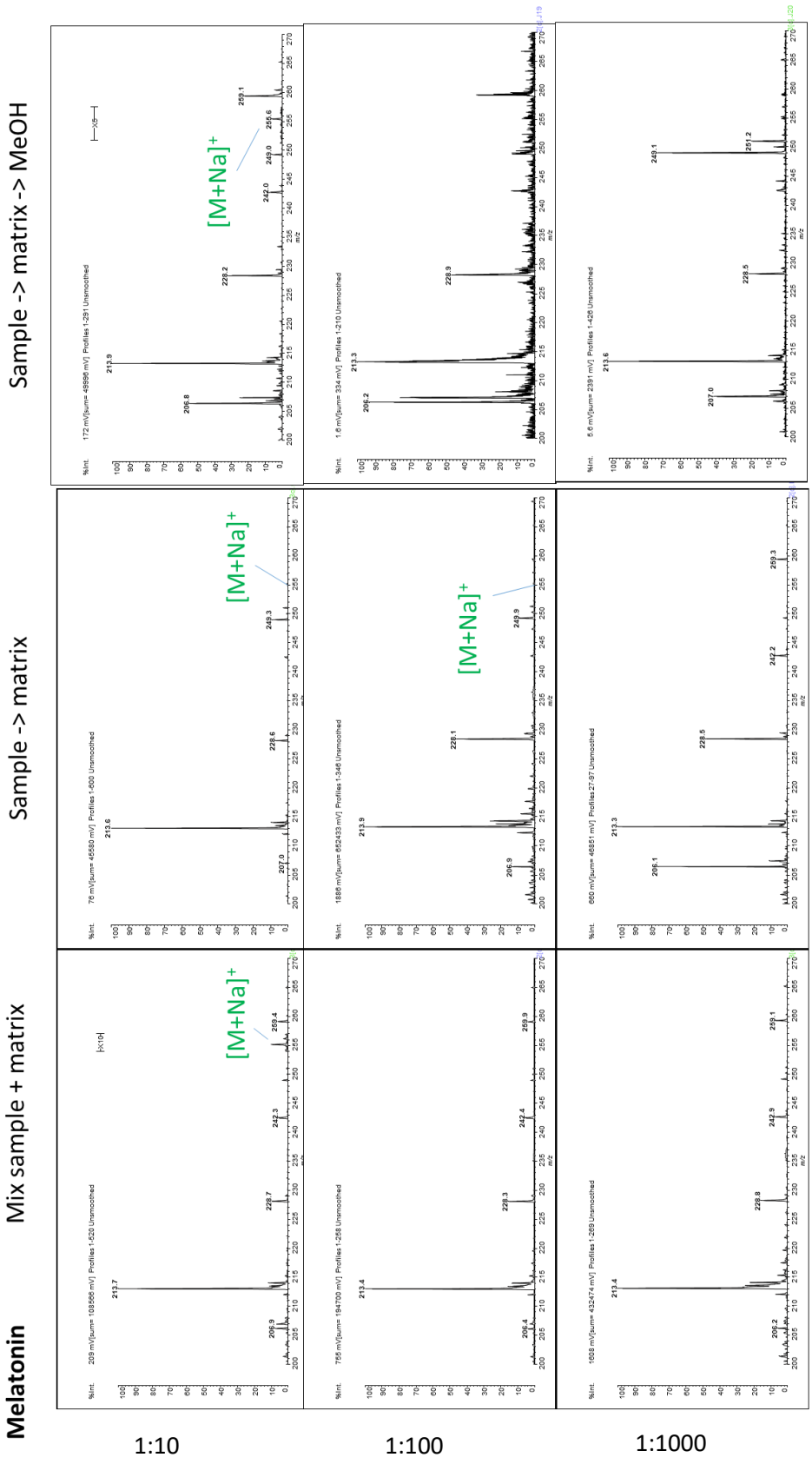

Figure 74: MALDI MS spectra for liposomes with melatonin, using different techniques to prepare and deposit the sample/matrix solution to the target plate